Biochemical and Structural Characterization of Cyclopropane Fatty Acid Synthase, and its Role in the Metabolism of *Pseudomonas aeruginosa*

Run Qi Shao

A thesis submitted to McGill University in partial fulfillment of the requirements of the degree of Master of Science

Department of Chemistry

McGill University

Montreal, Quebec, Canada

H3A 0B8

December 2022

Abstract:

Pseudomonas aeruginosa (P. aeruginosa) is a gram-negative opportunistic pathogen that is notorious for the acquisition of multidrug resistance (MDR). A major contributor to drug resistance in P. aeruginosa is the outer membrane (OM), which presents a permeability barrier to many drugs. An accumulation of cyclopropane fatty acids (CFAs) in the bacterial envelope is often observed in gram-negative bacteria as they enter stationary phase and begin to form biofilms. CFAs provide chemical and physical stability to the bacterial membrane and contribute to drug tolerance through poorlyunderstood mechanisms. CFAS is the cytosolic enzyme responsible for the biosynthesis CFAs. This enzyme installs cyclopropane rings into the unsaturated acyl chains of inner membrane (IM) phospholipids using S-adenosyl-L-methionine (SAM) as a methylene donor. The enzyme-catalyzed reaction is interesting in that the soluble CFAS enzyme must associate with the membrane surface where it cyclopropanates a very hydrophobic acyl chain using a very hydrophilic SAM co-substrate. To date, no biochemical or structural analysis has been performed on P. aeruginosa CFAS (PA-CFAS), and protein-membrane interactions are poorly understood in general. Thus, we have initiated a project to investigate the in vitro activity of PA-CFAS on phospholipid vesicles and to characterize the conformational dynamics of the enzyme using hydrogen-deuterium exchange MS (HDX-MS). We discovered that PA-CFAS functions in solution as a dimer similar to the Escherichia. coli- (EC-) and Lactobacillus acidophilus-CFAS (LA-CFAS). However, unlike its EC and LA counterparts, PA-CFAS is more active at a slightly acidic pH and has a stronger selectivity towards different lipid compositions. Using a mass spectrometry (MS) based approach, we have additionally investigated total proteome and lipidome changes in cfa knock out (KO) mutants of P. aeruginosa compared to wild type (WT). Several proteins related to OM underwent significant changes after the loss of cfa gene expression in a growth phase specific manner, providing clues as to how P. aeruginosa adapts to a lack of CFAs. The structural and functional insights into PA-CFAS gained from these studies could eventually facilitate future drug discovery efforts to treat P. aeruginosa related infections.

Résumé:

Pseudomonas aeruginosa (P. aeruginosa) est un pathogène opportuniste gram-négatif connu pour l'acquisition d'une résistance multiple aux médicaments (MDR). Un contributeur majeur à la résistance aux médicaments de P. aeruginosa provient de sa membrane externe (OM), qui présente une barrière de perméable à de nombreux médicaments. L'accumulation d'acides gras cyclopropanes (CFAs) dans l'enveloppe bactérienne est souvent observée chez les bactéries gram-négatives lorsqu'elles entrent en phase stationnaire et commencent à former des biofilms. Les CFAs assurent la stabilité chimique et physique de la membrane bactérienne et contribuent à la tolérance aux médicaments par des mécanismes jusqu'ici inconnu. La CFAS est un enzyme cytosolique responsable de la biosynthèse des CFAs. Cette enzyme permet l'addition de cycles cyclopropane aux chaînes insaturées des phospholipides de la membrane interne (IM) en utilisant la S-adénosyl-L-méthionine (SAM) comme donneur de méthylène. Cette réaction enzymatique implique une enzyme soluble devant s'associer à la surface membranaire où elle permettra l'ajout d'un cyclopropane sur une chaîne acyle très hydrophobe en utilisant un cofacteur SAM très hydrophile. À ce jour, aucune analyse biochimique ou structurale n'a été effectuée sur le P. aeruginosa CFAS (PA-CFAS) et les interactions protéine-membrane sont généralement mal comprises. Ainsi, nous avons initié un projet pour étudier l'activité in vitro du PA-CFAS sur les vésicules phospholipidiques et pour caractériser la dynamique conformationnelle de l'enzyme avec l'aide de la spectrométrie de masse par échange hydrogène-deutérium (HDX-MS). Nous avons découvert que le PA-CFAS fonctionne en solution comme un dimère similaire à Escherichia coli- (EC-) et Lactobacillus acidophilus-CFAS (LA-CFAS). Cependant, contrairement à ses homologues, le PA-CFAS est plus actif à un pH légèrement acide et a une plus grande sélectivité vis-à-vis la composition lipidique. En utilisant une approche basée sur la MS, nous avons étudié le changement global du protéome et du lipidome chez les mutants *cfa* knock-out (KO) de *P. aeruginosa* par rapport au type sauvage (WT). Plusieurs protéines liées à l'OM ont subi des changements significatifs après la perte de l'expression du gène *cfa* d'une manière spécifique à la phase de croissance, fournissant des indices sur la façon dont P. aeruginosa s'adapte à un manque de CFAs. Les

connaissances structurelles et fonctionnelles sur le PA-CFAS tirées de ces études pourraient éventuellement faciliter les futurs efforts de découverte de médicaments pour traiter les infections liées à *P. aeruginosa*.

Acknowledgement:

First and foremost, I would like to express my deepest gratitude to my graduate study supervisor, Dr. Christopher Thibodeaux, who gave me the key to explore the world of research and taught me valuable lessons on problem solving and critical thinking. He was always there to support me when I encountered challenges during my research journey and showed confidence in me when I had doubts in myself. Next, I would like to thank our collaborator, Dr. Dao Nguyen, who conducted preliminary *in vivo* study on *Pseudomonas aeruginosa* CFAS which led us to investigate the biochemical aspects of this interesting enzyme. Additionally, I wish to give special recognition to Nuwani Weerasinghe, who has assisted me greatly in conducting Native MS experiments.

Furthermore, I am grateful to all the members in Thibodeaux's group. They make me smile and laugh at all times and my research days are so delightful because of them. I want to especially thank Kevin Uggowitzer, who introduced me to the group when I was still an undergraduate student and was extremely helpful in countless occasions. I also want to thank my two special drinking friends, Jenaes Siva and Jingtan Han, with whom I can relieve my stress and have an enjoyable after work time.

In addition, I would like to acknowledge McGill university for giving me the opportunity to purse a Master of Science in chemistry, CRBS, FRQNT and CIHR for funding my research study which allowed me to accomplish what I always wished for. I would like to recognize Auclair lab to let me use the plate reader which made the colorimetric assay possible. I would also like to thank Julien Breault-Turcot for correcting my French abstract translation.

Lastly, I would like to thank my family and my partner, Nathan Wing Kwan Choi, who gave me unconditional love and support when I was at my lowest. Thank you for giving me strength at all times and I could not have undertaken this journey without you.

Table of content

Abstract:	1
Résumé:	2
Acknowledgement:	4
Table of content	5
List of Figures	8
List of Tables	. 10
Abbreviations	. 11
Contributions of Authors	. 15
1.0 Introduction:	. 16
1.1. What is <i>Pseudomonas aeruginosa</i> and why do we care:	. 16
1.2. <i>P. aeruginosa</i> biofilms:	. 17
1.3. Antibiotic tolerance in <i>P. aeruginosa</i> :	. 20
1.4. Bacterial cell envelope of <i>P. aeruginosa</i> :	. 23
1.4.1 Gram-negative bacterial cell envelope:	. 23
1.4.2. Outer membrane (OM):	. 24
1.4.3. <i>P. aeruginosa</i> outer membrane:	. 28
1.4.4. Cell envelope remodelling in gram-negative bacteria:	. 29
1.4.5. <i>P. aeruginosa</i> phospholipid profile:	
1.5. Cyclopropane fatty acids (CFAs):	. 33
1.5.1. Regulation of CFAs production in bacteria:	. 34
1.5.2. Anterograde transport of CFAs:	. 36
1.5.3. CFAs are associated with bacterial survival under different environmental	00
stressors:	. 38
1.5.4. CFAs are associated with membrane impermeability and tolerance in <i>P. aeruginosa</i>	39
1.6. Cyclopropane fatty acid synthase (CFAS):	
1.6.1. CFAS reaction mechanism:	. 41
1.6.2. CFAS structural analysis:	. 42
2.0. Thesis Statement:	
3.0. Results and Discussion:	. 46
3.1 Structure prediction of P. aeruginosa CEAS:	46

3.2. Expression and purification of PA-CFAS enzyme:	47
3.3. Biochemical analysis of <i>P. aeruginosa</i> CFAS activity:	49
3.3.1. Establish the 3-enzyme coupled colorimetric assay:	
3.3.2. CFAS activity depends on pH:	54
3.3.3. PA-CFAS stability test and assay optimization:	55
3.3.4. PA-CFAS activity depends on the lipid head groups:	60
3.3.5. Testing CFAS activity using <i>P. aeruginosa</i> lipid extracts:	63
3.3.6. Attempted optimization of PA-CFAS activity at pH 7.5:	65
3.3.7. Determination of kinetic parameters for PA-CFAS:	67
3.4. Structural analysis of <i>P. aeruginosa</i> CFAS:	71
3.4.1. Native mass spectrometry (Native MS):	71
3.4.2. Biophysical characterization of PA-CFAS using hydrogen-deuterium exchange mass spectrometry (HDX-MS):	73
3.5. Proteomics studies of <i>P. aeruginosa</i> :	82
3.6. Lipidomics studies of <i>P. aeruginosa</i> :	86
3.6.1. Fatty acid methyl esters (FAMEs) analysis using GC-MS:	86
3.6.2. Phospholipid profile analysis using LC-ESI-MS:	87
4.0. Conclusion and future perspective:	91
5.0. Methods:	93
5.1. Protein Expression:	93
5.1.1. Expression of <i>P. aeruginosa</i> and <i>E. coli</i> CFAS enzyme:	93
5.1.2. Expression of <i>E. coli</i> SAH nucleosidase enzyme:	93
5.1.3. Expression of <i>E. coli</i> LuxS enzyme:	93
5.2. Protein Purification:	94
5.2.1. Purification of <i>P. aeruginosa</i> (Uniprot: Q9HT28) and <i>E. coli</i> CFAS enzy (Uniprot: P0A9H7):	-
5.2.2. Purification of <i>E. coli</i> SAH nucleosidase enzyme:	94
5.2.3. Purification of <i>E. coli</i> LuxS enzyme:	94
5.2.4. Verification of protein mass using LC-ESI-MS:	95
5.3. CFAS activity assay:	95
5.3.1. Liposome preparation:	95
5.3.2. <i>P. aeruginosa</i> membrane lipid extraction:	96
5.3.3. <i>P. aeruginosa</i> cell lysate preparation:	96

5.3.4. Standard spectrophotometric assay for CFAS:	96
5.3.5. Steady state kinetic analysis:	97
5.3.6. Cysteine calibration curve:	97
5.3.7. SAH nucleosidase and LuxS activity assay:	98
5.3.8. Assays to ensure that coupled enzymes are not limiting the CFAS re	eaction:98
5.4. Hydrogen-Deuterium exchange (HDX) assays:	98
5.4.1. Standard HDX assays preparation:	98
5.4.2. LC-MS conditions for HDX:	99
5.4.3. HDX-MS data analysis:	100
5.5. Native Mass Spectrometry (native MS):	100
5.5.1. Native MS sample preparation:	100
5.5.2. Native MS conditions:	100
5.5.3. Native MS data analysis:	101
5.6. Proteomics studies:	102
5.6.1. Proteomics sample preparation:	102
5.6.2. LC-MS conditions for proteomics:	103
5.6.3. Proteomics data processing and analysis:	104
5.7. Lipidomics studies:	104
5.7.1. Preparation of Fatty acid methyl esters (FAMEs):	104
5.7.2. GC-MS conditions for FAMEs analysis and data processing:	105
5.7.3. Lipid extraction and preparation for lipidomics studies:	105
5.7.4. LC-MS conditions for lipidomics analysis and data processing:	105
6.0. References:	107

List of Figures

Figure 1.1. The original five-step biofilm development1
Figure 1.2. The three main events involved in biofilm formation
Figure 1.3. Differences in MIC, disk diffusion and TD test results between susceptible tolerant and resistant bacteria.
Figure 1.4. Gram-negative bacterial cell wall organization2
Figure 1.5. Lipopolysaccharide (LPS) structure in the outer membrane (OM) of gram negative bacteria2
Figure 1.6. murein lipoprotein (Lpp) structure2
Figure 1.7. The three main types of fatty acyl chain modification are desaturation isomerization and cyclopropanation3
Figure 1.8. <i>cfa</i> gene is regulated transcriptionally3
Figure 1.9. Proposed lipid trafficking mechanisms in gram-negative bacteria3
Figure 1.10. EC-CFAS detailed reaction mechanism4
Figure 1.11. SAM, bicarbonate ion (BCI) and lipid (EPH) in the active site of LA-CFAS4
Figure 3.1. EC- and PA-CFAS structural comparison4
Figure 3.2. Liquid chromatography electrospray ionization mass spectrometry (LC-ES MS) analysis of His ₆ -PA-CFAS4
Figure 3.3. Schematic illustration of the colorimetric, coupled enzyme activity assay for CFAS5
Figure 3.4. LC-ESI-MS spectrum of SAH nucleosidase and LuxS5
Figure 3.5. Cysteine calibration curve with slope, y-intercept and R-square valuindicated5
Figure 3.6. LuxS assay shows that nearly all SAH was converted to Hcy within a 10 mi derivatization time frame.
Figure 3.7. Production of Hcy depends on the PA-CFAS concentration5
Figure 3.8. The concentrations of SAH nucleosidase and LuxS are not the limitin factors.
Figure 3.9. Testing the stability of PA-CFAS at 37 °C and pH 6.5 6
Figure 3.10. PA-CFAS activity depends on POPE:POPG ratio
Figure 3.11. PA-CFAS activity assay using <i>P. aeruginosa</i> extracted lipid from exponential phase vs. using 50:50 POPE:POPG.
Figure 3.12. Attempted optimization of PA-CFAS activity at pH 7.5 6

Figure 3.13. Michaelis-Menten kinetics and the corresponding Lineweaver-Burk process (inset) for EC-CFAS with varied SAM concentrations.	
Figure 3.14. Michaelis-Menten kinetics and the corresponding Lineweaver-Burk plot PA-CFAS with varied SAM concentrations.	
Figure 3.15. Native mass spectrometry studies of the PA-CFAS dimer	72
Figure 3.16. Deuterium exchange with backbone amide hydrogen	74
Figure 3.17. General scheme for a bottom-up HDX-MS workflow.	75
Figure 3.18. Solvent deuterium exchange properties of PA-CFAS.	77
Figure 3.19. Solvent deuterium exchange properties of PA-CFAS at pD 6.1	78
Figure 3.20. Wood plot for PA-CFAS HDX peptides that undergo significant changes value <0.01) in deuterium uptake after 4 h of pre-incubation at 37 °C.	٠.
Figure 3.21. Total ion chromatograms of HDX-MS samples containing 0.05% (w/v) DD showing the decrease in signal intensity after many injections.	
Figure 3.22. Volcano plot of protein expression changes between WT and <i>cfa</i> KO <i>aeruginosa</i> during stationary growth.	
Figure 3.23. Volcano plot of protein expression changes between WT and <i>cfa</i> KO <i>aeruginosa</i> during exponential growth.	
Figure 3.24. Example of an extracted ion chromatogram for 744.48 m/z	88

List of Tables

Table 3.1. Catalytic activity of PA-CFAS depends on pH	55
Table 3.2. Kinetic parameters of EC- and PA-CFAS with SAM.	69
Table 3.3. Effect of quench buffer conditions on PA-CFAS-liposome precipitation	. 80
Table 3.4. Abundance of various fatty acids in WT and <i>cfa</i> KO <i>P. aeruginosa</i> cells detected by GC-MS analysis.	
Table 3.5. Abundance of PC and PE with various lengths in WT and <i>cfa</i> KO <i>P. aerugino</i> cells.	

Abbreviations

(p)ppGpp Guanosine 3',5'-bisdiphosphate or -bistriphosphate

°C Degree Celcius

μL Microliterμm MicrometerμM MicromolarÅ Angstrom

ABC Ammonium bicarbonate

ACN Acetonitrile

Ala Alanine
Arg Arginine
Asp Aspartate

B. subtilisCFCystic fibrosis

CFA Cyclopropane fatty acid

CFAS Cyclopropane fatty acid synthase

CmaA Mycolic acid cyclopropane synthase

CTD C-terminal domain

Cys Cysteine
Da Dalton

DCA Deoxycholic acid
DDM Dodecyl maltoside
DDS Dodecanoyl sucrose

Des Desaturase

DOPE Dioleoyl-phosphatidylethanolamine
DPPG Dipalmitoyl-phosphatidylglycerol
DTNB 5,5'-dithiobis-(2-nitrobenzoic acid)

DTT Dithiothreitol
EA Ethyl acetate

EC, E. coli Escherichia coli

EPS Extracellular polymeric substance

FAME Fatty acid methyl ester

FPLC Fast protein liquid chromatography

GC-MS Gas chromatography mass spectrometry

GdmHCl Guanidine hydrochloride

Glu Glutamate

GluFib [Glu-1]-fibrinopeptide B

h Hour

H. pylori Helicobacter pylori

HAQ 4-hydroxy-2-alkylquinoline

Hcy L-homocysteine

HDX-MS Hydrogen/deuterium exchange coupled to mass spectrometry

His Histidine

His_{6x} Hexa-histidine

HIV Human immunodeficiency virus

IC₅₀ Inhibitory concentration

IM Inner membrane

IPTG β -D-1-thiogalactopyranoside

kDa Kilodalton
KO Knock out

LA, L. acidophilus Lactobacillus acidophilus

LC-ESI-MS Liquid Chromatography Electrospray Ionization Mass

Spectrometry

Lpp Murein lipoprotein

LPS Lipopolysaccharides

LuxS S-ribosylhomocysteinase

Lys Lysine Molar

M. tuberculosis Mycobacterium tuberculosis

mDAP Diaminopimelic acid

MDR Multi-drug resistant

MFP Membrane fusion protein

mg Milligram

MIC Minimum inhibitory concentration

min Minute
mL Milliliter
mM Millimolar

mRNA Messenger RNA

MS Mass spectrometry

nanoESI Nanoelectrospray ionization

NEM N-ethylmaleimide

Ni-NTA Nickel-nitrilotriacetic acid

NTD N-terminal domain
OM Outer membrane

OMP Outer membrane proteins

P. putida Pseudomonas putida

PA, P. aeruginosa Pseudomonas aeruginosa

PE Phosphatidylethanolamine

PG Phosphatidylglycerol

PL Phospholipid

PLGS ProteinLynx Global Server

PMF Proton motive force

PML Polymorphonuclear leukocytes

POPE 1-palmitoyl-2-oleoyl-phosphatidylethanolamine

POPG 1-palmitoyl-2-oleoyl-phosphatidylglycerol

PQ Paraquat

QS Quorum-sensing

RMSD Root mean square deviation

S. Typhimurium Salmonella enterica serovar Typhimurium 14028s

SAH S-adenosyl-L-homocysteine

SAM S-adenosyl-L-methionine

Ser Serine

SFA Saturated fatty acids
SHX Serine hydroxamate
SOD Superoxide dismutase

SOPG 1-stearoyl-2-oleoyl-phosphatidylglycerol

SR Stringent response

SRH S-ribosylhomocysteine sRNA Small regulatory RNAs

TCEP Tris(2-carboxyethyl)phosphine

TD test Tolerance detection test

TFA Trifluoroacetic acid

TNB 2-nitro-5-thiobenzoate

TWIM Travelling wave ion mobility

Tyr Tyrosine

UFA Unsaturated fatty acids
UTR Untranslated region

v Volt

VAP Ventilator-associated pneumonia

WHO World Health Organization σ^{70} General sigma factor 70

 σ^{S} Alternative sigma factor

Contributions of Authors

This thesis is written as one chapter. All work done in this chapter was conducted by the author with the following exceptions. In Sections 3.2. and 3.3.1., recombinant plasmids containing EC-, PA-CFAS, SAH nucleosidase and LuxS were kindly provided by Dr. Dao Nguyen. In Sections 3.5 and 3.6., the *cfa* KO *P. aeruginosa* strain was constructed by Dr. Nguyen's group, and both the WT and *cfa* KO samples used for the proteomics and lipidomics studies were sent as frozen cell pellets by the same group.

1.0 Introduction:

1.1. What is *Pseudomonas aeruginosa* and why do we care:

Pseudomonas aeruginosa (P. aeruginosa) is a gram-negative, rod-shaped, aerobic bacterium which can cause a variety of blood and lung infections [1]. It is very commonly found in the environment such as freshwater and soil. In urban settings, hot tubs and swimming pools can be carriers of this bacterium and without precautions, it can cause a wide-range of infections. Some of the most common community-acquired infections originating from this bacterium include folliculitis, inflammation in hair follicles also known as hot tub rash, and osteomyelitis in puncture wounds [1-3]. Although sporadic P. aeruginosa infections can occur in the community, the large majority of severe diseases caused by these bacteria remain in the healthcare setting. P. aeruginosa is an opportunistic pathogen that mainly targets patients with a compromised immune system such as those with cancer, infected by human immunodeficiency virus (HIV) and also those who are receiving intensive care [1]. P. aeruginosa takes advantage of the human host's disabled immune system and causes a variety of detrimental diseases. Some concrete examples of very common nosocomial diseases caused by P. aeruginosa would be ventilator-associated pneumonia (VAP) and catheter-associated urinary tract infections [4, 5]. In particular, VAP caused by P. aeruginosa has a prevalence of 4% and a high mortality rate of 13.5% [6, 7]. An important finding shows that patients who had previously been infected by this bacterium have a significantly higher rate of reinfection compared to those who had no prior encounter with *P. aeruginosa* [6]. This phenomenon can be explained by resistance exhibited by this bacterium. In fact, P. aeruginosa is known to be a multi-drug resistant (MDR) pathogen due to its very advanced resistance mechanism. Treatments and management of chronic infections have become increasingly more difficult due to these MDR strains, which render killing by antibiotics ineffective. Patients infected by MDR strains also have a significantly higher mortality rate [8]. P. aeruginosa has been identified as one of the most life-threatening bacteria in 2017 by the World Health Organization (WHO) due to its resistance to carbapenem, and new drugs and treatment strategies are urgently needed in order to overcome the limited repertoire of effective antibiotics [9].

1.2. P. aeruginosa biofilms:

It has been estimated that 40-80% of bacteria on earth can form biofilms [10, 11]. A bacterial biofilm is defined as a collection of bacterial cells that grow as a community. In general, biofilms are dynamic structures, where the bacterial cells can reversibly attach to a surface. If environmental conditions change and are no longer advantageous for survival, the biofilm can break down and individual cells can colonize other more favorable niches. In general, the microbial cells in a biofilm are surrounded by a matrix of extracellular polymeric substance (EPS) that is comprised of polysaccharides, proteins and extracellular DNA [12]. Biofilms can consist of a single bacterial strain or of a combination of multiple different microbial (bacterial and/or fungal) species.

Some of the earliest work on the formation of biofilms was performed on *P. aeruginosa* in 2002 [13]. They described the formation of bacterial biofilm as a complex system that can be divided into five main stages (Figure 1.1.). The process is initiated by non-specific reversible attachment of planktonic (i.e. single) bacterial cells to a surface. The transient attachment of bacteria to the surface is typically achieved by flagella or other types of bacterial cell-surface appendages. Next, cells begin to cluster on the surface where they begin the process of more permanent attachment. This step is characterized by the activation of the Las quorum-sensing (QS) system which enables a cell densitydependent regulation of gene expression in bacteria [14, 15]. When the cells accumulate to a certain threshold, the autoinducer produced by Lasl binds to LasR which, in turn, activates the transcription of many genes [16]. Among these changes in gene expression, genes involved in flagellar biogenesis are deactivated as cells become less motile and genes conferring the production of EPS components are initiated. Drug tolerance can also start to be observed in cells at this stage suggesting a change in bacterial physiology. Drug tolerance will be discussed further in the next section. The first maturation stage is indicated by the formation of a layer of cells with a thickness >10 µm, and the second maturation stage is characterized by the formation of microcolonies where the biofilm reaches its maximum thickness (up to 100 µm). Dispersion is the final stage of biofilm development. Bacterial cells in this stage regain their mobility and break through the matrix while the matrix components start to degrade and the cycle restarts.

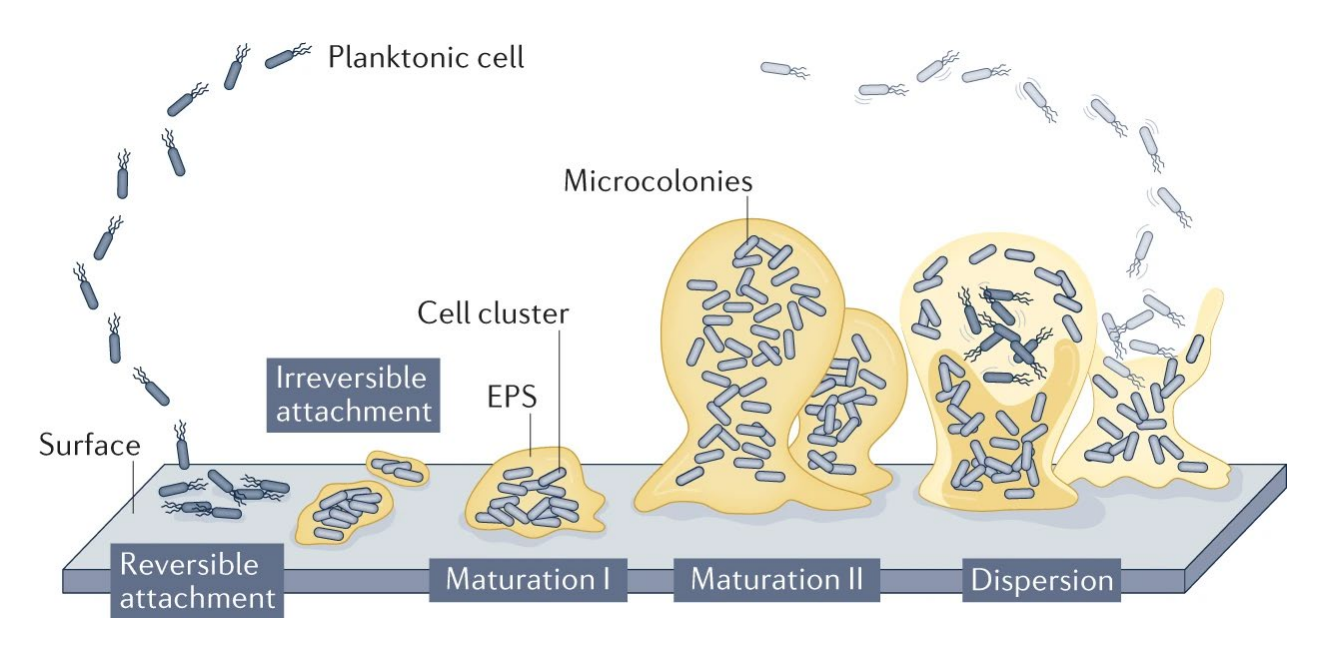


Figure 1.1. The original five stages of biofilm development. *Adapted with permission* [17].

Up to date, further research has been done on the development of biofilm and reveals that this original five-step model has its limitations. For instance, this laboratory model oversimplifies the condition where biofilm forms naturally and does not capture the complexity of a real-world system such as in an industrial or a healthcare setting. Hostassociated biofilms rely on the local environment of the host and the interactions between host and microorganisms can vary considerably [17, 18]. Under different environment conditions, the formation of biofilms does not always follow the five steps in a sequential manner and biofilm morphology can be very diverse [19]. Furthermore, a surface for attachment is also not always required for establishing a biofilm. For example, in soft tissue infections, bacteria form aggregates rather than attaching to surfaces in patients. In a cystic fibrosis lung infected by P. aeruginosa, bacterial aggregates are surrounded by polymorphonuclear leukocytes (PMLs), a type of white blood cells, and are embedded by mucus with no obvious surface present [20]. In biological wastewater treatment, biofilms formed by a diverse consortium of microbial species can exist in both free-floating aggregates and surface-attached forms. For these reasons, the updated model suggests that in surface-absent biofilms, cellular aggregates can be formed by the following mechanisms: 1) small parts of aggregates can detach from surface-associated biofilm

through sloughing [21]; 2) planktonic bacteria can aggregate when daughter cells remain with mother cells during division – a process that can be aided by secreted EPS or surface adhesion molecules [22]; 3) even in the absence of cell division, auto-aggregation can occur in stationary phase planktonic bacteria; 4) host extracellular polymers can aid the formation of aggregates in liquid phase either by polymer depletion, where the polymers pushes bacterial cells together and promotes aggregation [23-25], or by polymer bridging, where polymers links individual bacterial cells and bring them together to form aggregates [25, 26]. In summary, the current proposed model for general biofilm formation involves three main events where microorganisms of diverse species can enter at any stage: aggregation, growth and disaggregation [17] (Figure 1.2.).

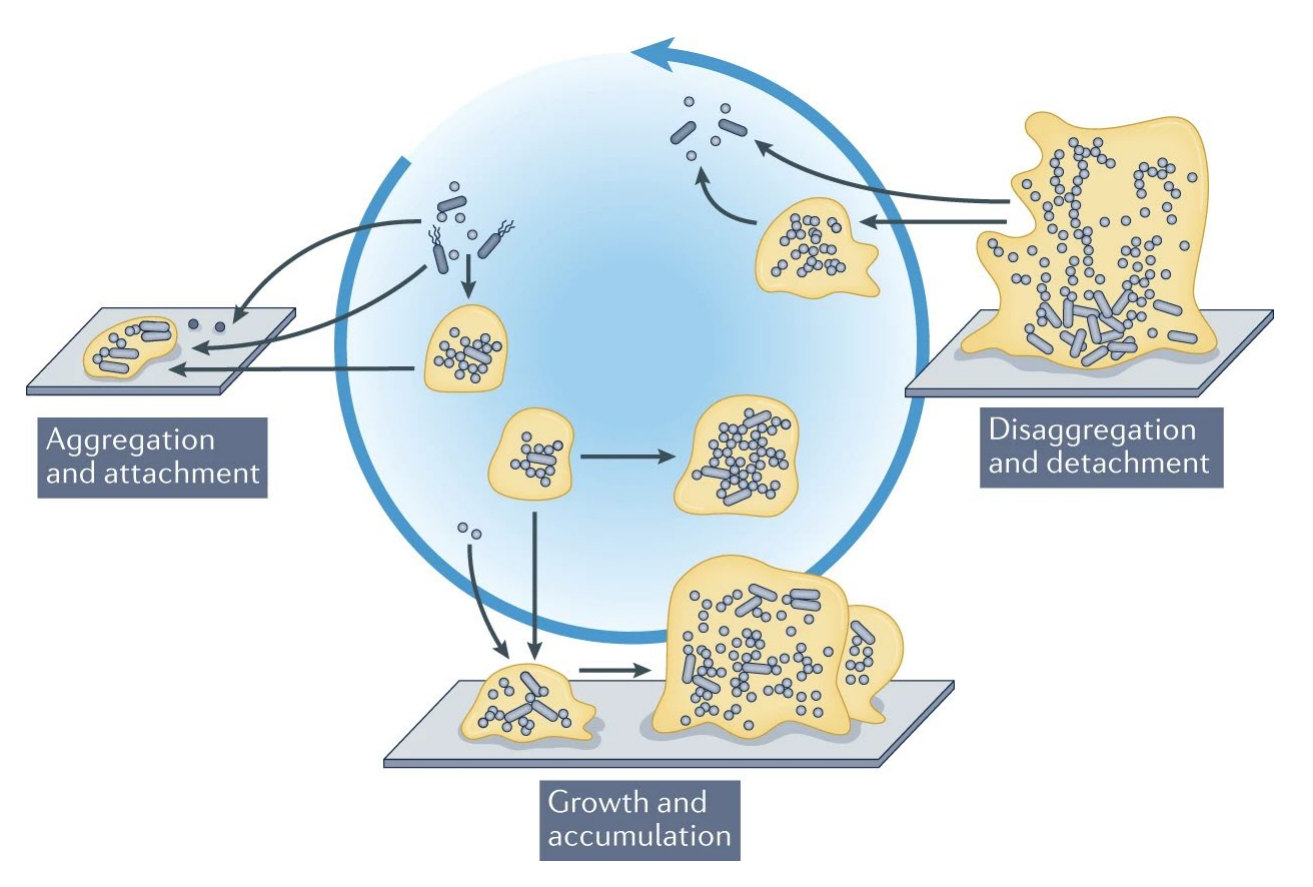


Figure 1.2. The three main events involved in biofilm formation. *Adapted with permission* [17].

As mentioned above, *P. aeruginosa* has demonstrated its ability to form biofilms – a process that is associated with increased drug tolerance [27, 28]. Biofilm formation

protects bacteria from environmental stress, enhances their long-term persistence, and makes them tolerant to many antibiotics.

1.3. Antibiotic tolerance in *P. aeruginosa*:

Antibiotic resistance is a term that we hear repeatedly when we talk about hard-to-treat bacterial infections. Despite the duration of treatment, resistant bacteria can grow in the presence of antibiotics. Resistance can be achieved by several mechanisms including by modification of the drug target, by inactivation of the drug and/or by upregulating the efflux of the drug. Overall, these mechanisms are mediated by enzymes and are inherited and acquired from progenitor cells that had previously experienced antibiotic exposure[29]. Drug tolerance, on the other hand, is a non-inherited mode of antibiotic resistance. Tolerance occurs when a homogeneous bacterial population that is normally susceptible to antibiotics becomes less sensitive to drug treatment and have a prolonged survival. Tolerance is mostly observed in non-dividing stationary phase bacterial cells such as those found in biofilms. Tolerance is often induced by a variety of physiological and environmental stressors such as starvation in a nutrient-limited condition [30], ATP depletion [31] and in hypoxic environments [32]. Tolerance and resistance can be distinguished by the minimum inhibitory concentration (MIC) which measures the concentration of antibiotic at which bacteria stop growing. For a given antimicrobial compound, tolerant bacteria will have the same MIC as wild type (WT) cells, whereas resistant strains will have a significantly higher MIC. Furthermore, because tolerant and wild-type bacteria have the same MIC, normal disk-diffusion assays (a common method to detect antimicrobial susceptibility) will not enable detection of drug tolerance (Figure 1.3.). A tolerance detection test (TD test, Figure 1.3) was developed in 2017 which helps to measure the survival of bacteria after antibiotic treatment by promoting growth to the inhibition zone after the drug has diffused away [33]. Only tolerant bacteria will be able to grow because they survived previous antibiotic killing through different mechanisms such as being dormant [34].

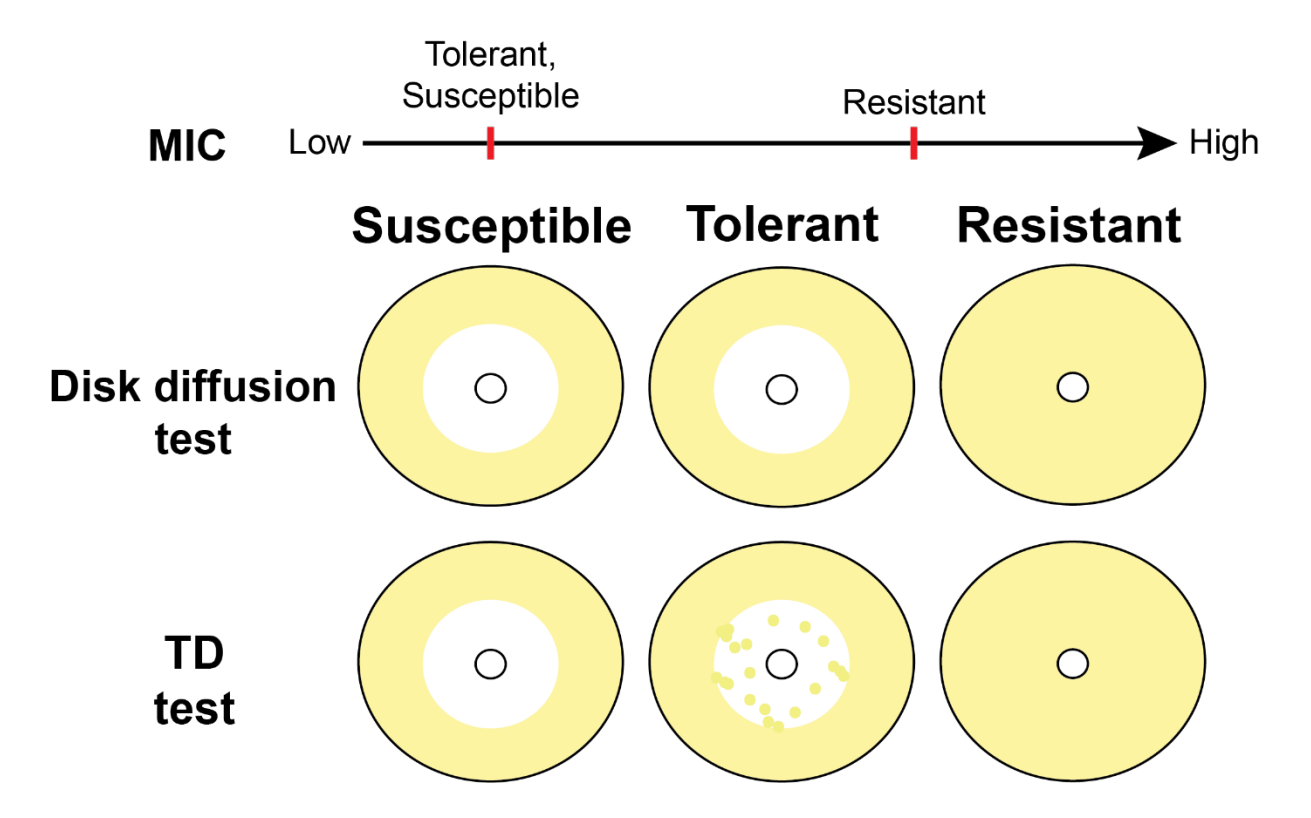


Figure 1.3. Differences in MIC, disk diffusion and TD test results between susceptible, tolerant and resistant bacteria.

In biofilms, bacterial cells located closer to the periphery were found to consume most of the nutrients, leaving the rest of cells to starve. Interestingly, this starvation also led to the development of tolerance [35]. In a study conducted in 2011 [36], researchers found that the activation of starvation-signaling stringent response (SR) through guanosine 3',5'-bisdiphosphate or -bistriphosphate (e.g. (p)ppGpp) signaling in *P. aeruginosa* is responsible for the development of tolerance. When bacteria experience limited sources of nutrients such as carbon, amino acids and iron, the *relA* and *spoT* genes are activated. The RelA and SpoT enzymes catalyze the formation of the second messenger, (p)ppGpp, which leads to a cascade of signaling events and alters the expression of numerous genes. Inactivation of the *relA* and *spoT* genes result in inactivation of the SR. Upon starvation induced by serine hydroxamate (SHX), WT bacteria are shown to be more tolerant to ofloxacin killing compared to the $\Delta relA$ *spoT* mutants. They also grew WT and $\Delta relA$ *spoT* mutant of *P. aeruginosa* to stationary phase and biofilms which mimics the natural environment where starvation occurs. Similar trends are observed as the mutants

are more susceptible to ofloxacin in both stationary phase and in biofilms compared to the WT counterpart. When the mutants are complemented by functional copies of the *relA* and *spoT* genes, resistance to ofloxacin is restored to WT levels.

One of the consequences of (p)ppGpp signaling involved in drug tolerance includes upregulation of superoxide dismutase (SOD) [37] – an enzyme that quickly removes superoxide by breaking it into molecular oxygen and hydrogen peroxide. Catalases and peroxidases can break down hydrogen peroxide to effectively deplete reactive oxygen species in cells [37]. 4-hydroxy-2-alkylquinolines (HAQs) are important signaling molecules in cell-cell communication. Yet an overproduction of HAQs can also have prooxidant effects which causes oxidative damage to bacteria resulting in higher susceptibility to antibiotics [38]. Indeed, when the SR genes are inactivated, a higher level of HAQ production is observed in these $\Delta relA$ spoT mutants. Similarly, the removal of SOD genes sodAB can also efficiently sensitize these bacteria to antibiotics. Interestingly, drug tolerance can be restored in $\Delta relA$ spoT mutants by complementing them with SOD genes, suggesting that the primary mechanism of sensitization involves reactive oxygen species that are normally detoxified by SOD activity.

Oxidative stress can render bacteria more susceptible to antibiotics through oxidative damage leading to cell death. However, a sublethal level of superoxide can actually stimulate the development of drug tolerance in stationary phase *P. aeruginosa* by increasing SOD activity via (p)ppGpp or RpoS signaling [37, 39]. It was observed that, by inactivating the SR and/or SOD genes, superoxide-generating compounds such as paraquat (PQ) can no longer stimulate drug tolerance against ofloxacin. The advantage of the SOD defect does not stop there. Another effect of SOD impairment is an increase in membrane permeability in *P. aeruginosa* which also contributes to enhanced antibiotic killing. When stringent response and/or SOD genes are disrupted, bacteria have a higher drug uptake and a leakier outer membrane while their efflux activity remained unchanged. In contrast, WT cells already have a much less permeable membrane compared to the mutants. They become even more impermeable to antibiotics when they are pre-treated with a sublethal level of PQ, which is not seen in their mutant counterparts [37].

In addition, when mice were infected with $\Delta relA\ spoT$ mutants of stationary phase P. aeruginosa, they have a higher survival rate after treating with antibiotics compared to those infected by WT. In short, this study demonstrates that (p)ppGpp signalling is crucial for mediating antibiotic tolerance in P. aeruginosa through an impaired defense mechanism against reactive oxygen species under nutrient limited conditions such as those found in stationary phase and biofilms.

Aside from changes in gene expression that contribute to tolerance, the physical properties of biofilm itself also limits drug penetration. As mentioned above, starvation in biofilm cells has been attributed to difficult diffusion of nutrients through the polysaccharide-rich EPS matrix. With a similar idea, when a drug is administered, this characteristic of biofilm can also limit the diffusion of these small molecules which results in lower accessibility to the drug and failed antibiotic killing [40].

Moreover, despite being mechanistically distinct, tolerance was proven to play a critical role in the development of resistance [41]. For this reason, targeting unique molecular features of tolerant bacteria can, in theory, improve antibiotic treatment by decreasing the likelihood of drug resistance.

1.4. Bacterial cell envelope of *P. aeruginosa*:

1.4.1 Gram-negative bacterial cell envelope:

There are three main components in the gram-negative bacterial cell envelope. Starting with the layer closest to the cytosol, the inner membrane (IM) is a phospholipid bilayer which keeps all the cytosolic components enclosed. For example in *E. coli*, the IM is mainly composed of phosphatidylethanolamine (PE) and phosphatidylglycerol (PG) with minor lipids include phosphatidylserine and cardiolipin [42]. The second layer is a peptidoglycan cell wall which gives bacteria their shape and rigidity and can protect the cytosol from experiencing high turgor pressure from the environment which can result in cell lysis [43]. It is composed of multiple units of the disaccharide *N*-acetyl glucosamine-*N*-acetyl muramic acid crosslinking via short peptides [44]. Unlike the gram-positive bacteria, which contain a thick peptidoglycan layer, gram-negative bacteria possess only a very thin layer of peptidoglycan [45]. Finally, surrounding the peptidoglycan is the outer

membrane (OM), which is the first line of defense of bacteria to outside stress and antibiotics [46].

a Gram-negative bacteria

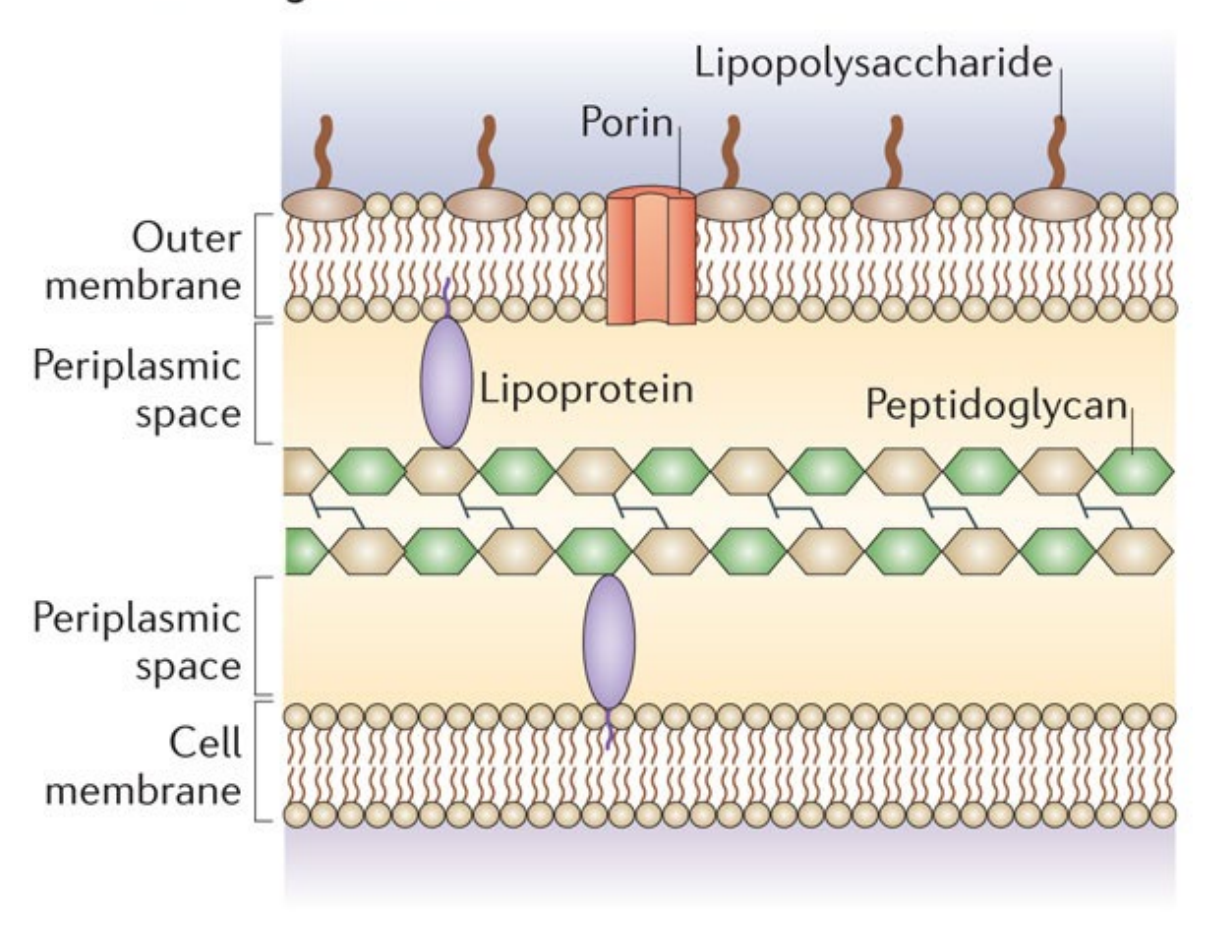


Figure 1.4. Gram-negative bacterial cell wall organization. Adapted with permission [47].

1.4.2. Outer membrane (OM):

The OM is an asymmetric lipid bilayer with different components in the outer and inner leaflets. The outer leaflet is mainly composed of lipopolysaccharides (LPS) while the inner leaflet is largely composed of phospholipids. LPSs are composed of a hydrophilic polysaccharide, also known as the O-antigen, attached to a hydrophobic endotoxin called lipid A, which is embedded in the outer leaflet of the OM. Because the LPSs are located on the surface of the cell, they are often directly involved in the pathology of gramnegative bacterial infections [48].

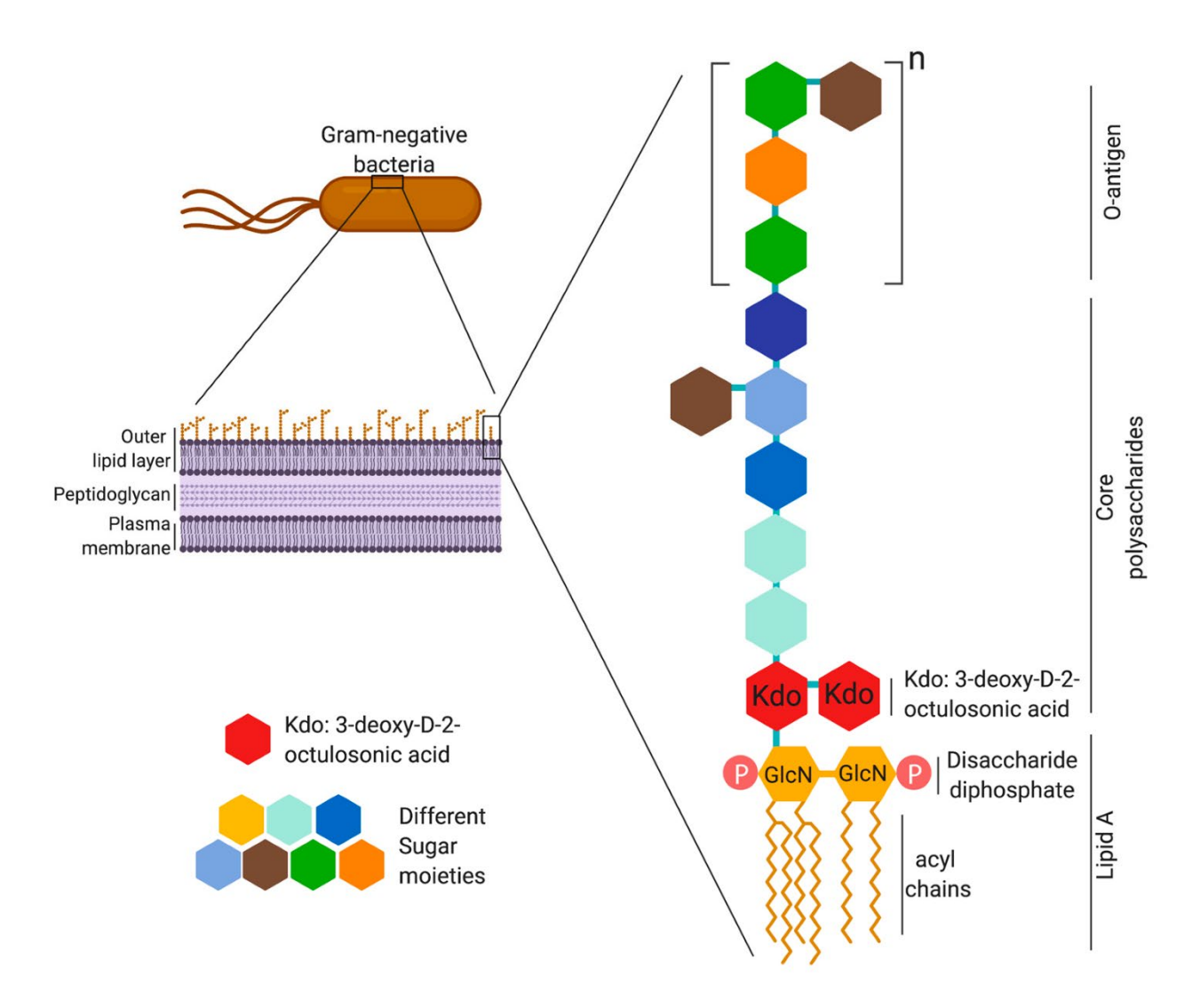


Figure 1.5. Lipopolysaccharide (LPS) structure in the outer membrane (OM) of gramnegative bacteria. *Adapted with permission* [48].

The OM also contains many embedded proteins which can be largely categorized into two classes: transporter proteins and lipoproteins. The most abundant lipoprotein in the OM is murein lipoprotein (Lpp) which forms a peptide bond between its C-terminal Lysine (Lys) side chain and diaminopimelic acid (mDAP) moieties in the peptidoglycan layer. The *N*-terminal cysteine of Lpp is attached to a lipid that is embedded in the OM [49]. Lpp has an important role in maintaining the integrity of the bacterial cell envelope by crosslinking the OM to the peptidoglycan cell wall. Similar to LPS, Lpp is an antigen that is known to cause an inflammatory response in many bacterial infections [50].

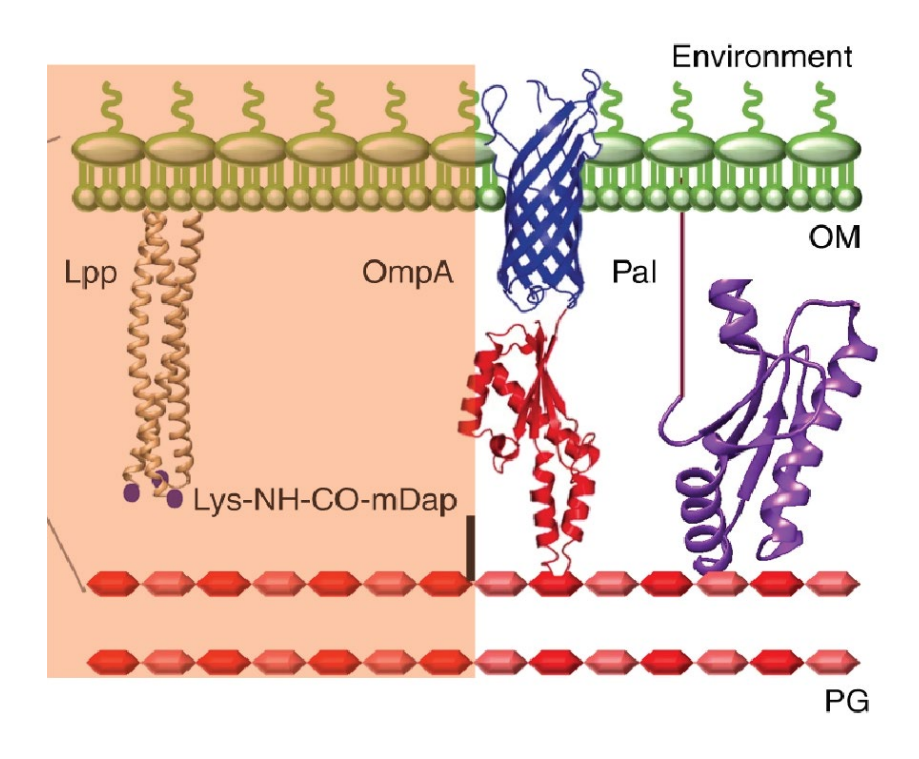


Figure 1.6. Murein lipoprotein (Lpp) structure (highlighted in red box). Lpp keeps cell integrity by crosslinking outer membrane (OM) to the peptidoglycan layer (PG) [49].

The second major category of OM proteins are the β -barrel proteins. The name of β -barrel comes from their protein structure which is formed by β -sheets that fold into a cylindrical barrel shape. These majority of outer membrane proteins (OMPs) are fall within the porin class of proteins, which collectively serve to mediate and regulate the transport of metabolites across the OM.

In *E. coli*, the porins OmpF and OmpC have been extensively studied. They are the most abundant OMPs and are responsible for passive diffusion of small molecules such as essential sugars and amino acids across the OM. Antibiotic penetration is an important factor for efficient antimicrobial activity and these general diffusion porins are often believed to be the major point of entry of many drugs. OmpF and OmpC are often used to study small molecule permeability and to gain insight for downstream drug design. These porins act as a functional trimer and each monomer is a β -barrel composed of 16 anti-parallel β -strands [51]. These strands are connected by longer, flexible loops on the extracellular side and shorter turns in the periplasm. The loops on the cell surface serve as a filter to allow diffusion of molecules with selective size and charge. Taking OmpF as

an example, the longest loop of this porin, L3, folds into the transmembrane pore and its acidic residues Glu117 and Asp113 create a constriction zone with the basic residues on the opposing side of the pore. These electrostatic interactions can further limit the passing of unfavourable molecules. Comparing OmpF to OmpC, the latter has a more negatively charged pore which makes it more selective for cations that OmpF [52]. For example, negatively charged β -lactam antibiotics can cross the OM by diffusing through these porins and it has a lower permeability to OmpC than OmpF due to the selectivity. Bacteria can develop resistance to drugs by downregulating the expression of these general diffusion porins and by modifying the size or the selectivity of the pore through mutations in the extracellular loops [53]. LamB and PhoE are other examples of abundant OMPs that allow for transport of more specific molecules such as phosphates. OmpA is a rather unusual OMP because it has two different conformations. Its minor conformation serves as a porin, but its major role is a structural protein which contributes to the integrity of the OM through interactions between its periplasmic domain and peptidoglycan [54].

Bacteria can also develop resistance by pumping antibiotics out the periplasm and cytoplasm through efflux pumps. Efflux pumps can either be single-component or multicomponent. Single component efflux systems are usually IM transporters which can pump out the unwanted small molecule from the cytosol and IM into the periplasm. The IM transporters either use ATP as energy source (such as the abundant ATP-binding cassette transporters) or they use the influx of H⁺ or Na⁺ to pump drugs across the membrane (H⁺ or Na⁺/drug antiporter) [55]. Multi-component efflux systems, on the other hand, are usually huge protein complexes that span the IM to OM and which create a tunnel that passes harmful compounds from the cytosol, IM and periplasm all the way to the extracellular space. It should be noted that there is no energy source (ATP) in the bacterial periplasmic space. Thus, the active transport of materials within and across the gram-negative cell envelope typically requires similar multicomponent enzymatic machines with an ATP-dependent motor protein embedded in the inner membrane. ATP hydrolysis by this motor protein provides the energy source to trigger conformational changes that ultimate bind to and export the target molecule from the cell. These protein complexes usually consist of three essential parts: an IM transporter (motor protein), a periplasmic adaptor protein (membrane fusion protein, MFP) and an OM channel (outer membrane factor). After the drug is pumped into the periplasm, it can then travel through the MFP and OMF to be ejected to the extracellular space. Examples of well-studied efflux systems in $E.\ coli$ would be AcrAB-TolC and AcrAD-TolC complexes. AcrB is the IM transporter motor protein which is known to be very flexible as it can pump out most of the unfavorable molecules with diverse properties. However, it has a hard time to remove aminoglycosides and some of the more polar β -lactams. For these compounds, the AcrAD-TolC system is used [56, 57].

1.4.3. *P. aeruginosa* outer membrane:

As a member of the gram-negative bacteria, *P. aeruginosa* share many similarities with E. coli in their overall cell envelope structure. However, P. aeruginosa lacks the large general diffusion porins such as OmpC and OmpF present in E. coli which contribute to higher tolerance of *P. aeruginosa* to antibiotics as the OM is generally less permeable [58]. Instead, P. aeruginosa has a variety of substrate-specific porins. For instance, OprD is a major OM porin in P. aeruginosa which is responsible for transporting basic amino acids, peptides and the carbapenem class of antibiotics such as meropenem [59]. Drug resistance in P. aeruginosa often involves a downregulation of OprD expression which results in less permeability for antibiotic entrance [60]. The crystal structure of OprD shows high resemblance to OmpC and OmpF from E. coli, except that OprD contains an18 strand β-barrel instead of a16 strand barrel [61]. OprD has two long loops folded into its pore (L3 and L7) which form the constriction zone with β -strands S17 and S18. The residues within the constriction zone are largely negatively charged. However, several arginine and lysine residues are scattered across funnel from the extracellular to the periplasmic side, giving the porin an asymmetric charge distribution in the pore. These characteristics of OprD suggest that acidic compounds are likely to be preferentially accepted for transport.

Another abundant OMP in P. aeruginosa is the fascinating, conformationally dynamic OprF, which is a homolog of E. coli OmpA. Just like the latter, OprF is a complex porin with two existing conformations. The large majority of the porin exists in a closed conformation with an 8-stranded β -barrel N-terminal domain (NTD) linked to a periplasmic C-terminal domain (CTD). The NTD is embedded in the OM while the CTD interacts with

peptidoglycans and OM lipoproteins such as Oprl which helps to maintain the OM structural integrity through intracellular interactions [62, 63]. Aside from forming intracellular interactions, OprF can also interact with extracellular components of the biofilm EPS matrix. It was shown that OprF has opposing effects in aerobic and anaerobic environments on the production of the second messenger, cyclic-di-GMP, which is known to upregulate biofilm related gene expression. It is believed that OprF plays a role in biofilm development and the effect may be oxygen-dependent [64, 65]. This closed OprF conformation also plays a role in bacterial virulence through host-pathogen interactions[63]. OprF contributes to virulence by attaching to host cells and by triggering host immune responses. For example, it is known that OprF can adhere to human alveolar epithelial cells and induce lung infections [66].

The minor open conformation of OprF is folded into a large β -barrel with over 14 strands and with different pore sizes. OprF can also oligomerize into transient multiprotein complexes. It was proposed that the closed conformation is a thermodynamically stable folding intermediate while the open conformer could be the final structure of the protein [67]. And only a small portion of the open conformers, dubbed sub-conformations, give OprF a role in transporting small molecules and even larger solutes of up to 3 kDa [67, 68]. It was found that the switch in OprF conformation is related to environmental stress. Higher temperature appears to favor the open conformation while lower temperatures induce the shift towards the closed conformer [69].

Due to the highly impermeable OM and the expression of efflux pumps, antibiotic killing of gram-negative bacteria can often be very challenging compared to gram-positive counterparts. Combining with the rapid evolving resistance mechanism and the natural occurrence of bacterial tolerance, we are in need to find new strategies to overcome these obstacles.

1.4.4. Cell envelope remodelling in gram-negative bacteria:

Gram-negative bacteria can modify their existing membrane phospholipids (PLs) in response to adverse environmental conditions. For instance, by attaching an aminoacyl group such as Lys or Ala to the PG headgroup, the anionic PL can be transformed into a cationic or neutral lipid, respectively. In *P. aeurignosa*, the formation of alanyl-PG is

observed when cells are exposed to acidic growth conditions [70]. This modification is dependent on the MprF enzyme which has been suggested to be associated with resistance [71]. On the other hand, membrane fluidity is mostly achieved by chemical modification of fatty acyl chains. There are three main modifications that can be performed on the fatty acids: desaturation of a saturated lipid, cis-trans isomerization of unsaturated fatty acids (UFA), and cyclopropanation of unsaturated acyl chains [72].

Figure 1.7. The three main types of fatty acyl chain modification are desaturation, isomerization and cyclopropanation.

UFAs can be generated either from the anaerobic FabAB-mediated pathway where the double bond is introduced into the growing acyl chain during fatty acid biosynthesis, or from aerobic desaturase (Des)-mediated pathway [73, 74]. In the latter pathway, desaturation of fully saturated lipids is a post-synthetic modification which generates UFA

tails strictly in the *cis* configuration. Higher level of UFAs can make the bacterial membrane significantly more fluid. For instance, in *Bacillus subtilis* (*B. subtilis*), the production of UFAs is activated by a membrane embedded sensor, DesK, which can detect the physical properties of the bacterial membrane. Once DesK detects senses the decreased membrane fluidity, it phosphorylates the transcription factor DesR which activates expression of desaturase enzymes. When UFA production is no longer required, the high level of UFAs act as a signalling molecule to activate a negative feedback to cease the activity of desaturase [74]. Another interesting type of desaturase is found in *P. aeruginosa* which can introduce double bonds into acyl-CoAs from exogenous fatty acids [75]. The expression of desaturase genes in this system is controlled by the transcription regulator, DesT. When levels of unsaturated acyl-CoA are high, DesT represses *desCB* expression by binding tightly to its promoter. The release of DesT from the promoter is induced by low levels of unsaturated acyl-CoA, which favours the expression of the desaturases [75].

Isomerization of a UFA by a *cis-trans* isomerase change the configuration between Z and E without changing the location of the double bond. The Z-conformer (cis UFA) is characterized by having hydrogen atoms located on the same side of the bond and Econformer (or *trans* UFA) is indicated by the opposite trend. Although the great majority of UFAs in bacteria adapt the cis configuration, certain species contain trans UFAs including *Pseudomonas* and *E. coli* [76]. The structural difference between the two conformers is the space occupied by the kink of the double bond. The *E*-conformer has a smaller kink compared to Z-conformer, allowing for tighter packing of acyl chains in the lipid bilayer and a subsequently higher lipid-phase transition temperature. On the other hand, the E-conformer is still more fluid than fully saturated lipids because of its double bond[76]. Due to these unique characteristics of the E-conformer, bacteria are able to use UFA isomerization to control the membrane in response to environmental conditions. In fact, an increasing level of isomerization to the E-conformer via isomerases is observed during environmental stress in *Pseudomonas putida (P. putida)* [77]. Upon shifting to higher temperature, the Z-conformer causes the membrane to become overly fluid. The conversion of Z- to E-conformer provides better acyl chain packing resulting in a decrease

in membrane fluidity and permeability which allows better bacterial growth at the new temperature.

Finally, bacteria can incorporate cyclopropane rings into fatty acid tails by adding a methylene group to an unsaturated lipid in the cis(Z) acyl chain. The enzyme responsible for this reaction is named cyclopropane fatty acid synthase (CFAS). The detailed effects of cyclopropanation on bacteria will be discussed in the next section.

1.4.5. *P. aeruginosa* phospholipid profile:

Under environmental stress signals, bacteria can modify the composition of their membrane lipids in order to improve survival. And due to the physiological differences between planktonic and sessile bacteria, researchers are curious to study the change of lipid profile in both the IM and OM of *P. aeruginosa* from non-attached form to biofilms. A study in 2011 uncovered the impact of biofilm growth on the IM phospholipid (PL) composition. Their results showed that, compared to planktonic bacteria, those in biofilms have a significant decrease in PLs containing uneven numbered acyl chains and a small increase of phosphatidylethanolamine (PE) with longer acyl tails [78].

A study in 2014 compared the difference of the change of PL composition in both IM and OM as the biofilm develops [79]. The most detected lipids are PE and PG which are the two major classes of lipids in the *P. aeruginosa* membrane. It was shown that PL with shorter chains (total number of carbon below 32) are enhanced in sessile bacteria throughout the development of biofilms. In addition, longer chained PL (total number of carbon above 37) shows a significant increase in early biofilm and their proportion gradually decreases as biofilm matures. Interestingly, the overall PL profile in mature biofilm appears to be closer to planktonic bacteria. However, there are still some remarkable differences. In both IM and OM enriched samples, the proportion of cyclopropanated phospholipids increases as the biofilm ages. In brief, they conclude that the change in PL profile is biofilm growth dependent and that the difference in lipid composition is the greatest between planktonic bacteria and young biofilms. As the biofilm matures, these sessile bacteria start to have a PL profile similar to their free-floating counterparts which may indicate that detachment is starting to occur.

Compared to biofilm development, the different phases of bacterial growth (planktonic vs. sessile) appears to have a bigger role in the total PL profile change. Le Sénéchal et al. investigated the difference in PL profile between attached and non-attached P. aeruginosa over a 24 h incubation period [80]. Curiously, PL profiles in both attached and non-attached bacteria appear to follow the same evolution pattern during the incubation time. It was discovered that the evolution pattern of PLs can be classified into two profiles. First profile implies a remarkable decrease in its proportion during the 3 to 6 h of incubation, followed by increase at the end of 24 h. The second profile shows an opposite trend compared to the first profile, where a significant increase in PL proportion is observed between 3 to 6 h of incubation and followed by a smaller decrease until the end of the experiment. In accordance with previous studies, most of the PLs containing uneven numbered acyl chains are following the first profile and PLs with even numbered acyl chains have the second profile. Furthermore, saturated fatty acids (SFAs) have a preference to follow the second profile while UFAs can be seen in both profiles. This may indicate that there is a decrease in membrane fluidity during the transition from exponential to stationary growing phase in planktonic bacteria and during the formation of microcolonies in biofilm development.

To add more complexity to the PL profile change in *P. aeruginosa*, a more recent study from the same group compared PL profiles of the reference PAO1 strain to several clinically relevant strains of *P. aeruginosa* involved in cystic fibrosis (CF). It was revealed that there is indeed a variability of PL profile between PAO1 and clinical strains. Even among the CF group, the PL profile can be unique to specific strains. This study shows that biofilm PL compositions are highly heterogeneous and that the PL profiles are shaped by growth conditions, growth state (planktonic vs. biofilm), and also environmental factors unique to the origin of the strain [81].

1.5. Cyclopropane fatty acids (CFAs):

The existence of cyclopropane fatty acids (CFAs) was discovered few decades ago. More curiously, the accumulation of CFAs is often observed in gram-negative bacteria when the cells enter slow or non-growing phases as found in biofilms and under stress. The

production of a large number of CFAs is metabolically expensive for the bacterial cells, and has attracted the attention of researchers to study the potential effects of CFA biosynthesis on membrane stability in these bacteria [82].

1.5.1. Regulation of CFAs production in bacteria:

The synthesis of CFAs is carried out by the *cfa* gene. The timing of the activation of this locus is tightly regulated as the production of CFAs only occurs during the transition from log to stationary phase. The mechanism of cfa activation was first studied in E. coli. It was found that the cfa gene (which encodes cyclopropane fatty acid synthase, CFAS) is transcribed from two promoters. The more distal promoter, activated by the general sigma factor 70 (σ^{70}), is constitutively active. Meanwhile, the proximal promoter is activated only during the phase transition window, and this promoter is regulated by RpoS - the alternative sigma factor (σ^{S}) for RNA polymerase [83]. RpoS is often involved in the transcription of genes induced by stress or the transition into stationary phase [84]. Both of these processes require large scale changes to cell metabolism. On the other hand, the distal promoter is constantly activated to express a basal level of CFAS. In addition, from in vivo studies, CFAS has a high instability with a short half-life. It is believed that the production of CFAs is due to a large burst of CFAS expression controlled by RpoS. As bacteria fully enter stationary phase (Figure 1.8 A), CFAS is quickly degraded and maintains a basal level of activity. Transcription of the rpoS gene depends on the signaling of (p)ppGpp, which is produced by the RelA and SpoT enzymes (vide supra) [85]. Overall, CFA production can be explained by the following signaling pathway: during the phase transition or upon stress stimuli such as starvation, the RelA and SpoT enzymes synthesize (p)ppGpp, which subsequently accumulates and activates the transcription of the *rpoS* gene. The RpoS (σ ^S) transcription factor in turns binds to the proximal cfa promoter and activates the transcription and expression of CFAS to initiate CFA synthesis.

Aside from transcriptional regulation of the *cfa* gene, a second level of control is regulated post-transcriptionally by small regulatory RNAs (sRNAs) [86]. After mRNAs are transcribed, different sRNA can either help to positively regulate protein expression or to supress protein expression via mechanisms such as hindering mRNA-ribosome binding

or by promoting mRNA degradation. The mRNA encoding cfa is regulated by multiple small RNAs, which respond to various environmental signals. Three siRNAs have been identified in recent years which have distinct regulatory effect on cfa gene. The RydC and ArrS sRNAs share an overlapping binding site and activate the production of the CFAS protein by masking an RNase E cleavage site in the mRNA 5'-untranslated region (UTR) of the cfa gene. On the other hand, the CpxQ sRNA binds at the 5'-UTR upstream of RydC and ArrS, and promotes cfa mRNA degradation by RNase E, resulting in a decrease in CFAS production (Figure 1.8. B). Furthermore, the post-transcriptional regulation of cfa mRNA by sRNAs is isoform specific. As described previously, the cfa gene can be transcribed from two different promoters, the σ^{70} -dependent distal promoter results in a longer cfa mRNA while the RpoS-dependent proximal promoter generates a shorter mRNA. It has been shown that only the longer isoform is regulated by sRNAs consistent with the necessity of tight regulation of CFA levels during exponential phase and non-stressed conditions. In brief, the *cfa* gene is subject to extensive regulation at the genetic level through RpoS-dependent signaling, and at the post-transcriptional level by a set of sRNAs in response to different environmental signals. This exquisite, multitiered regulation suggest that control of CFA production is critical for cell survival under different conditions. Finally, it is interesting to note that the RpoS and (p)ppGpp signaling pathways are also involved in the development of drug tolerance in P. aeruginosa as described above. Thus, it is likely that the activation of phospholipid cyclopropanation contributes in some form to this observed drug tolerance. Further evidence for this claim will be presented in Section 1.5.3 and 1.5.4.

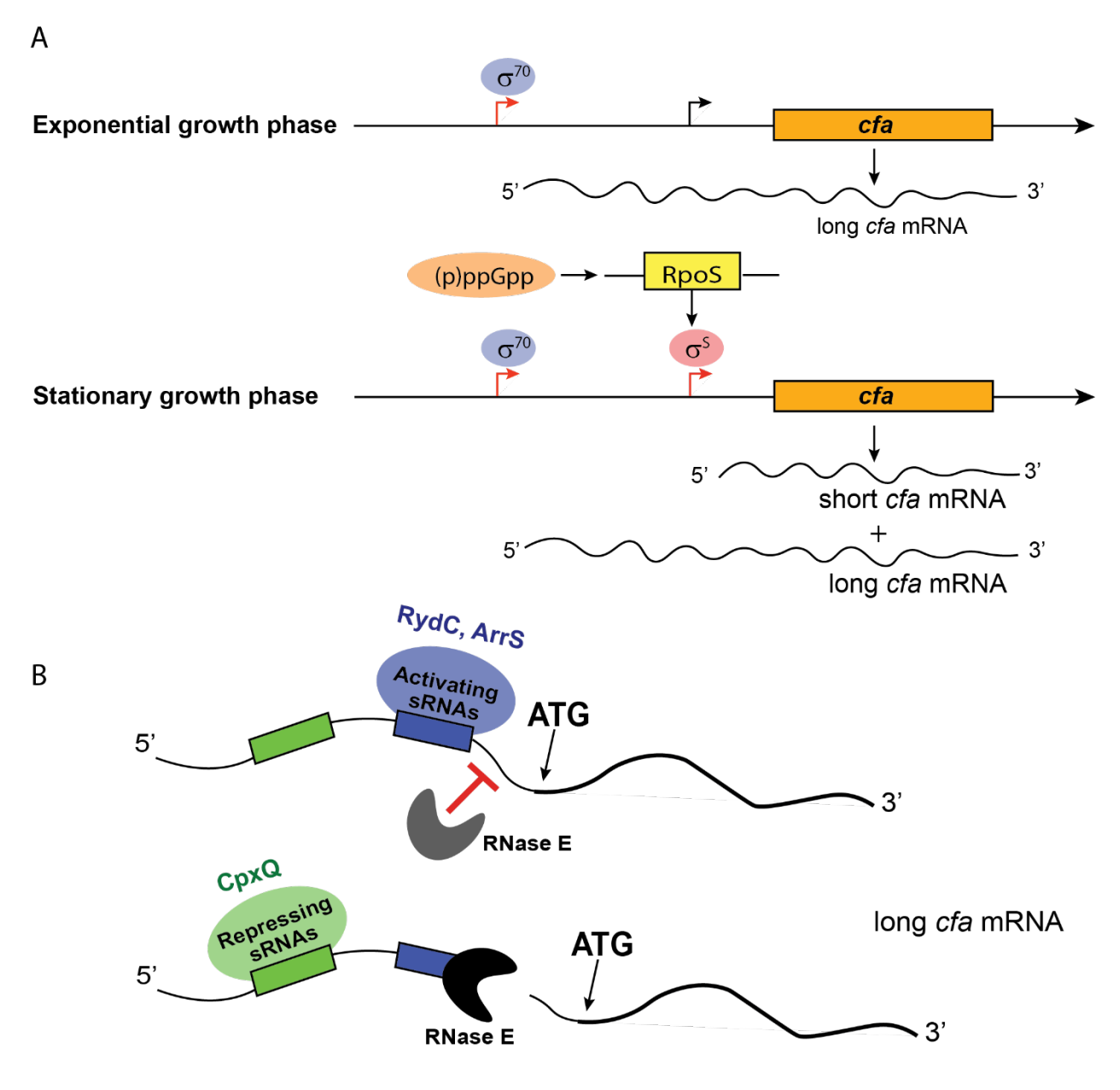


Figure 1.8. *cfa* gene is regulated transcriptionally **A)** via RpoS gene activation, and **B)** via sRNAs CpxQ, RydC and ArrS.

1.5.2. Anterograde transport of CFAs:

CFAS is a cytosolic enzyme and CFAs are synthesized in the inner leaflet of the IM. It is still not clear how CFAs are transported from the IM to the OM because there is a lack of energy source such as ATP in the periplasmic space [87]. Currently, there are a few plausible theories to explain lipid trafficking between IM and OM. Starting off with protein-mediated transport, the fatty acyl chain would be protected from the aqueous environment

of the periplasm by a chaperone protein. Two pathways are proposed for this mechanism: a soluble protein can bind to the lipid from the IM and travel through periplasm to deposit the lipid to the OM, or a large protein or complex which physically connects the two membranes creates a hydrophobic passage for lipid trafficking[88, 89]. A few transport systems such as the Tol-Pal complex and OmpC-Mla pathway have been shown to mediate retrograde lipid transport from the OM to IM, but their role in anterograde transport (from IM to OM) has not been established[90, 91]. The second theory of lipid trafficking is suggested to occur through direct exchange of lipids between the two membranes via either vesicle budding or fusion of the IM and OM to form a bridge for free lipid diffusion. However, there is little evidence to support this theory and the peptidoglycan layer in the periplasm would be expected to hinder the vesicle budding [87].

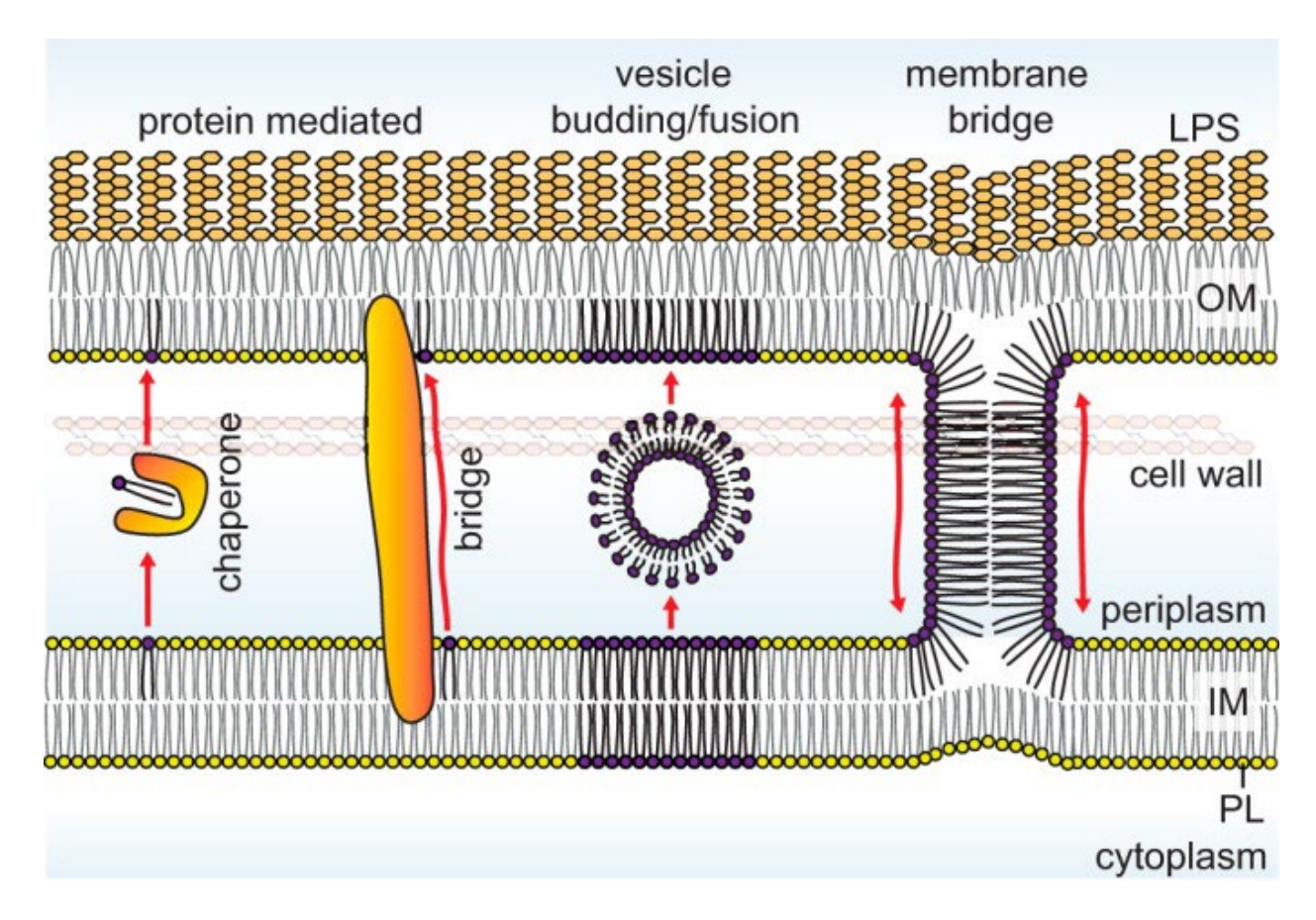


Figure 1.9. Proposed lipid trafficking mechanisms in gram-negative bacteria [87].

1.5.3. CFAs are associated with bacterial survival under different environmental stressors:

There is much evidence showing the association of CFA with bacterial survival under stress conditions and upon the administration of antibiotics. For example, *E. coli* shows CFA-dependent acid resistance during acid shock. *E. coli* has a higher sensitivity to the drop in pH when the *cfa* gene is knocked out, and acid resistance is restored when a plasmid containing the *cfa* gene is introduced to the bacteria [82]. The presence of CFAs in both the IM and OM can potentially reduce membrane permeability to protons which in turn keeps the bacteria viable [92].

There are also similar findings in other species of bacteria. In *P. putida*, disruption of the cfa gene has been shown to promote susceptibility to organic solvent stress compared to WT. However, in this strain of bacteria, removal of CFAs do not increase sensitivity to acid shock and antibiotics [93]. A study done in 2019 has identified a *cfa* locus (HP0416) in Helicobacter pylori (H. pylori) [94]. H. pylori is also a MDR pathogen similar to P. aeruginosa that causes severe gastric diseases and cancer. As the only known bacterial strain which can survive the strongly acidic gastric environment, the authors found that CFAs played an important role in acid tolerance in *H. pylori*. The deletion of the *cfa* gene showed a reduced gastric colonization as well as reduced antibiotic resistance in both in vitro and in vivo assays. Studies using a mouse model suggested that the Δcfa strain of H. pylori failed to colonize mice compared to the wild-type H. pylori. From the same study, the authors successfully identified an inhibitor for CFAS, dioctylamine, which is a substrate mimetic with a moderate inhibitory concentration (IC₅₀). Furthermore, in a 2022 study on Salmonella enterica serovar Typhimurium 14028s (S. Typhimurium), CFAs were also shown to be involved in virulence [95]. Supporting the E. coli and H. pylori model, the cfa mutant of S. Typhimurium experienced decreased survival at extremely acidic conditions (pH 3). In addition to differential pH susceptibility, other stressors such as oxidative stress and disruption of the bacterial proton motive force (PMF) also showed a detrimental effect on the viability of the cfa mutant compared to wild-type. These data suggest that CFAs likely serve a broad role in keeping bacterial cells alive. *In vivo* studies revealed that mice infected by the S. Typhimurium cfa mutant had an increased survival

compared to those infected by wild-type bacteria, presumably because the mutant pathogen was more susceptible to host defense systems.

1.5.4. CFAs are associated with membrane impermeability and tolerance in *P. aeruginosa*.

With the mounting evidence that CFAs affect the survival of different gram-negative bacteria under stress conditions, our collaborator, Dr. Dao Nguyen and her group have investigated the effect of CFAs in P. aeruginosa. As described in the section 1.4.3, P. aeruginosa has an outstandingly impermeable OM, lacks the large general diffusion porins, and possesses complex enzymatic efflux systems. These characteristics make antibiotic penetration exceptionally difficult and results in poor antibacterial activity. Dr. Nguyen's group has recently discovered an association between the level of CFAs produced in *P. aeruginosa* and the permeability of the cells to antibiotics. Using plasmid constructs in *cfa* knockout cells that enabled tight regulation of exogenous *cfa* expression, they observed a trend where higher cfa expression leads to lower membrane permeability. They also measured the association between the level of CFAs and susceptibility to antibiotics. Their results show a positive correlation between the level of CFAs in the cells and the survival of the bacteria. At a lower percentage of CFAs, bacteria are more sensitive to antibiotics such as ofloxacin and meropenem, whereas tolerance is observed in bacteria with higher CFA levels. Similar to the studies mentioned above, in vivo studies showed that mice infected with a cfa knock out (KO) strain of P. aeruginosa have a higher survival rate after ofloxacin treatment compared to mice infected by a wild type (WT) P. aeruginosa strain.

With this evidence supporting that CFAs are indeed correlated with bacterial tolerance against antibiotics and adverse environmental conditions, it is curious to know how they actually affect the membrane permeability and fluidity. It was proposed that the formation of CFAs can prevent UFA oxidation, in turn protecting cells from oxidative stress [96]. Another speculation suggests that CFAs can reduce membrane fluidity, thus resulting in a more rigid and impermeable membrane to small molecules such as drugs [97]. The effect of CFAs on membrane fluidity is intermediate between the effects of *cis* and *trans* UFAs. Interestingly, a study conducted in 2015 investigated the effect of CFAs on the

fluidity of lipid bilayers using molecular dynamics [98]. They found that CFAs may help bacteria to maintain membrane stability by the following methods. First, CFAs can promote membrane fluidity by affecting lipid packing. The lateral area occupied by a lipid molecule in the leaflet was used to estimate the effectiveness of lipid packing. The results revealed that the addition of cyclopropane rings into UFAs increases the lateral area of the lipid [98], leading to less dense acyl chain packing in the membrane and enhancing membrane fluidity. As a consequence of lipid packing defects, there is a higher chance for lipids to move laterally in membranes that are rich in CFAs, and this enhanced lipid diffusion can promote membrane fluidity. In addition, they investigated the effect of CFAs on the thickness of lipid bilayers [98] and discovered that the presence of CFAs do not change bilayer thickness. In contrast, cis UFAs have a thinning effect on the lipid bilayer. Thus, cis UFAs and CFAs likely promote membrane flexibility through different mechanisms. cis UFAs bend the fatty acid tails, which increases the flexibility between lipid chains, thins the bilayer thickness, and results in a fluid membrane. In CFAcontaining membranes, the acyl chains are more ordered and fluidity is achieved by steric restraint induced by the presence of methylene bridges which has no membrane thinning effect [98]. The cyclopropane ring also limits free rotation of the CFA acyl chains, which could contribute to the relative impermeability of CFA-containing membranes. Overall, the study by Poger and co-workers suggests that the unique features of CFAs can both enhance membrane fluidity while maintaining stability. These seemingly contradictory properties effectively allow bacteria to have an impermeable lipid bilayer against adverse conditions without over rigidifying their membrane [98].

1.6. Cyclopropane fatty acid synthase (CFAS):

Cyclopropane fatty acid synthase (CFAS) is the enzyme responsible for the production of CFAs when bacteria enter stationary (non-growing) phase. CFAS uses S-adenosyl-L-methionine (SAM) as a methyl donor to cyclopropanate the alkene of an unsaturated fatty acyl chain. The interesting aspect of the mechanism of the enzyme that distinguishes CFAS from most other SAM-dependent methyltransferases is that the reaction does not end with methyl transfer. A deprotonation step is required to form the final cyclopropane

ring on the fatty acid substrate. In brief, instead of a methyl group, CFAS adds a methylene group to its substrate. The side product generated from this reaction is S-adenosyl-L-homocysteine (SAH) which exhibits strong product inhibition towards CFAS with a K_i of 30 μ M [99].

1.6.1. CFAS reaction mechanism:

The mechanism of action of this enzyme was proposed to have the double bond of the unsaturated fatty acyl chain serving as a nucleophile to attack the methyl group of SAM to generate a protonated carbocation intermediate. The second step is to deprotonate the methyl group of this carbocation by an active site bound bicarbonate ion (HCO₃-) to release the final cyclopropane ring (Figure 1.10.). Support for a rate-limiting methyl transfer was provided by kinetic studies using the Se- or Te-containing chalcogen analogues of SAM. In this study, the elemental effects on the rate of the CFAS-catalyzed reaction paralleled the electrophilicity of the onium congener of the chalcogen, suggesting cleavage of the chalcogen-Me bond in the transition state. Enzymatic removal of bicarbonate from the reaction mixture reduced CFAS activity, suggesting a role for the bicarbonate ion in catalysis. The methyl transfer step was originally thought to be ratelimiting [100]; however, in a more recent study, the deprotonation step was shown to be at least partially rate-limiting through measurement of a primary tritium kinetic isotope effect on the cyclopropanation reactions [101]. In addition, the same study has demonstrated that no exchange of the cyclopropane methylene protons with the solvent was observed which suggests the enzyme adapts a closed conformation during catalysis. Cumulatively, these data are most consistent with a concerted insertion of a methylene into the double bond via a protonated cyclopropane-like transition state.

SAM SAH + H+

CFAS

$$Glu_{239} O^{-}-H-O O^{-}$$

$$CH_{3} CH_{3} CH_{3}$$

$$CH_{3} CH_{3} CH_{3}$$

Figure 1.10. EC-CFAS detailed reaction mechanism.

1.6.2. CFAS structural analysis:

The first crystal structures of enzymes in the CFAS family were the mycolic acid cyclopropane synthases (CmaAs) from *Mycobacterium tuberculosis* (*M. tuberculosis*) [102]. These studies revealed a monomeric enzyme consisting of a Rossmann fold of seven-stranded β-sheet and α-helices similar to other SAM-dependent methyltransferases [103]. However, the cell walls of mycobacteria differ from gramnegative bacteria such as E. coli and P. aeruginosa in that they have a waxy coating of long chained mycolic acids on the cell surface. Like the phospholipid substrates of CFAS, mycolic acids contain long unsaturated hydrocarbon chains that serve as the substrates for the CmaA enzymes. In 2018, a crystal structure of the E. coli CFAS (EC-CFAS, PDB: 6BQC) was solved by Sauer and co-workers to a resolution of 2.07 Å and revealed that the EC-CFAS exists as a dimer in the crystal [104]. Sedimentation velocity centrifugation and gel filtration chromatography confirmed that EC-CFAS forms a dimer in solution. Each monomer of EC-CFAS has a bi-domain structure, with a small α -helical NTD attached via a flexible linker to the catalytic CTD, the latter of which has high structural

homology to the *M. tuberculosis* CmaA enzymes. Electron density consistent with a glycerophospholipid was also observed in the structure. The phosphate head group of this lipid (which co-purified with the enzyme and could not be conclusively identified) was bound to the N-terminal domain by a small positively charged patch consisting of Lys48 and Arg18. Likewise, one of the two acyl chains was bound to the NTD, whereas the second acyl group extended across the domain interface into the active site of the catalytic domain. The dimer interface is formed by antiparallel pairing of β-strands located near the C-terminus of the catalytic domain. A bicarbonate ion was again observed in the active site, where it interacted with the side chains of His266, Tyr317 and Glu239. Through site-specific mutations, the authors discovered some interesting aspects of this enzyme. First, mutations to the dimerization interface revealed that monomeric EC-CFAS exhibits a 150-fold lower catalytic efficiency compared to the wild-type (WT) enzyme which suggests that the dimerization is crucial to CFAS activity. Also, the flexible, unstructured linker between the N- and C-terminal domains is proved to be important for enzyme function. Enzyme activity significantly dropped when the N- and C-terminal domains were split into separate proteins and when the linker was modified in length. These data suggest that protein-protein interactions (both intramolecular and intermolecular) are likely important for proper function. The authors also suggested that EC-CFAS functions as an asymmetric dimer with one monomer helps to bind to the lipid membrane while the other monomer catalyzes the reaction.

Another crystal structure of the *Lactobacillus acidophilus* CFAS (LA-CFAS, PDB:5Z9O) in complex with a phospholipid was solved to a resolution of 2.7 Å [105] . Their results revealed the same dimeric structure of CFAS which supports the EC-CFAS model. LA-CFAS also consists of two domains with an N-terminal lipid binding domain and a Cterminal catalysis domain. The co-crystallized lipid was modeled phosphatidylethanolamine (PE). The 18-carbon acyl chain at the sn1 position binds to the C-terminal domain and the 16-carbon acyl chain at sn2 position binds to the Nterminal domain. Similar to EC-CFAS, the linker region between the two domains (residues Lys97 to Ser113) has very poor electron density, suggesting that the linker might be flexible in order to help the N-domain guide the lipid from the membrane to the active site in the catalytic domain. Through computational methods, SAM was successfully docked into the active site in the catalytic domain. An important observation from the docking experiment is that the methyl group of SAM points in the direction of the lipid substrate (Figure 1.11.). Similar to EC-CFAS and rest of the CFAS family, a bicarbonate ion sits in the active site and hydrogen bonds with five highly conserved amino acids: Ser134, Cys135, Glu242, His269 and Tyr320. Kinetic studies of LA-CFAS also show that the reaction rate indeed depends on bicarbonate. Tyr133 in LA-CFAS and Tyr137 in EC-CFAS are suggested to stabilize the carbocation through π -cation interaction after methyl transfer in order to facilitate the following deprotonation step [101, 105].

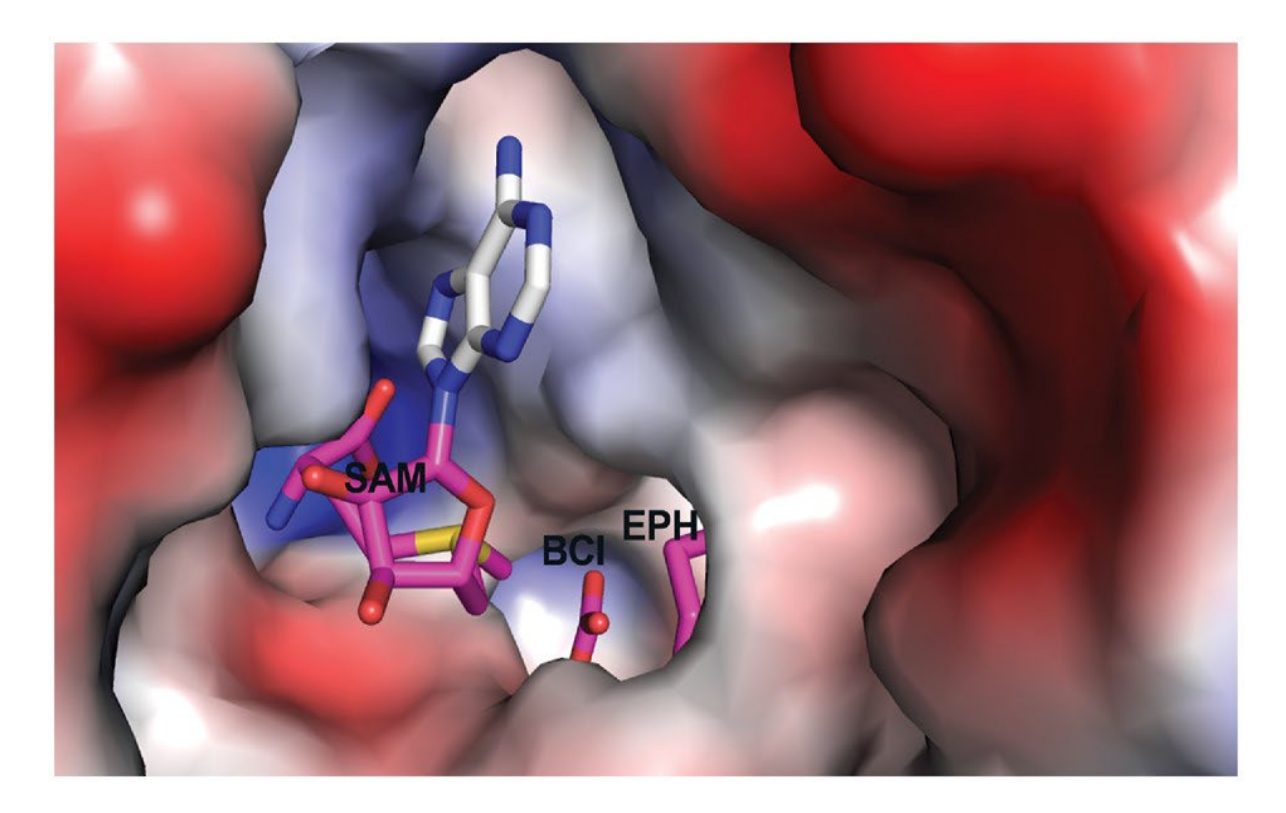


Figure 1.11. SAM, bicarbonate ion (BCI) and lipid (EPH) in the active site of LA-CFAS. The methyl group of SAM is pointing at the double bond of lipid ready to be modified. *Adapted with permission* [105].

2.0. Thesis Statement:

Due to the strong correlation between the loss of CFAs and the increase in membrane permeability of *P. aeruginosa*, CFAS is suggested to be a potential drug target to treat *P.*

aeruginosa related infections by restricting tolerance and improve the overall drug entry. In this thesis, we aim to investigate the biochemical properties of *P. aeruginosa* CFAS (PA-CFAS) using in vitro enzymatic assays as no prior in vitro studies have been reported on this enzyme. Furthermore, crystal structures of EC-CFAS and LA-CFAS revealed that these enzymes function as a dimer and have distinct N- and C-domains which work together to form the active site. Although the lipid binding pocket is resolved in the crystal structure, the conformational changes involved in substrate binding and catalysis are still poorly understood. We aim to establish a workflow utilizing hydrogen-deuterium exchange mass spectrometry (HDX-MS) to investigate the important changes in conformational dynamics of PA-CFAS upon lipid binding and cyclopropanation catalysis. These structural insights will allow us to identify important regions which can potentially serve as allosteric sites for future drug discovery. Lastly, CFAS is largely expressed during entry to stationary phase and cfa gene expression is tightly controlled transcriptionally. cfa knock out (KO) mutants of P. aeruginosa are also observed to have a greater membrane permeability compared to WT. We aim to understand this phenotype by studying the changes in proteome and lipidome in cfa KO mutants using mass spectrometry (MS) based approach.

3.0. Results and Discussion:

3.1. Structure prediction of *P. aeruginosa* CFAS:

To properly study and investigate the structural details of PA-CFAS, we generated a structural model of the PA-CFAS enzyme using the AlphaFold network on the Google Colab server [106, 107]. EC-CFAS has been previously crystallized, and its structure was reported as a functional dimer (Figure 3.1. A). Therefore, we generated a dimer of PA-CFAS using AlphaFold to predict the possible protein-protein interactions. The structure of the best-scoring AlphaFold model revealed a similar structure to the EC-CFAS dimer, with an N-terminal lipid binding domain and a C-terminal catalytic domain. Alignment of these two structures provided a root mean square deviation (RMSD) of 1.91 Å. (Figure 3.1. B). RMSD measures the average distance between the atoms of the two proteins and the smaller the RMSD value, the more similar the two structures [108]. Taking a closer look at the active site of PA-CFAS, the putative bicarbonate binding site consists of Glu237, His264 and Tyr321 which are conserved in EC-CFAS and LA-CFAS. Tyr128 is in close proximity to the lipid binding site which can serve to stabilize the cation intermediate as proposed previously (Figure 3.1. C). Due to the high sequence identity (41%) and structural similarity, we hypothesized that PA-CFAS would behave similarly to its *E. coli* counterpart.

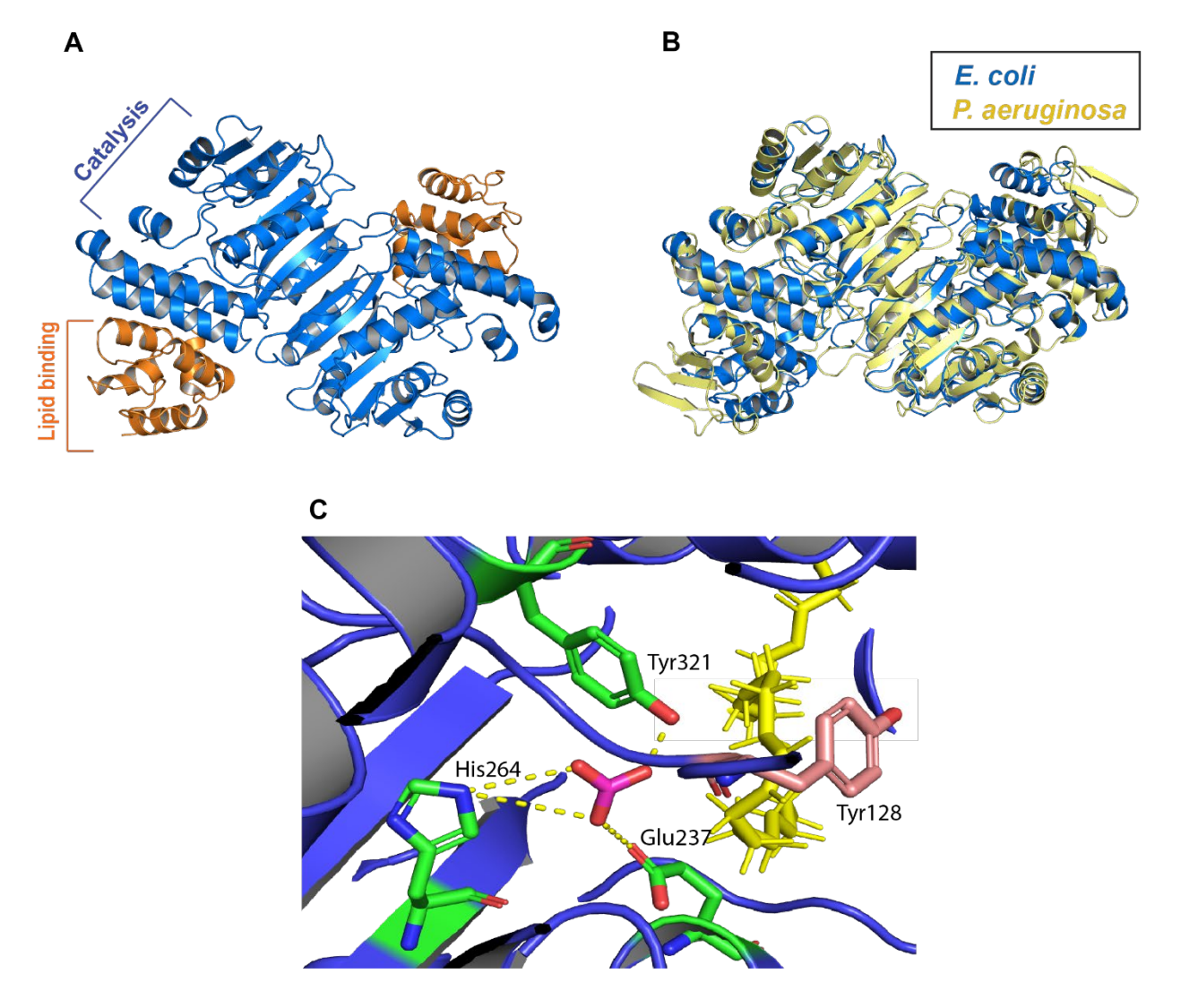


Figure 3.1. EC- and PA-CFAS structural comparison. **A)** Crystal structure of EC-CFAS dimer (PDB: 6BQC). The lipid binding domain is colored in orange and the catalytic domain is colored in blue. The dimer interface is formed by pairing of a β -stranded region near the C-terminus of the catalytic domain. **B)** Structural alignment of the *E. coli* (blue) and *P. aeruginosa* (yellow) CFAS dimers. An RMSD of 1.91 Å was calculated using PyMol. **C)** Active site of PA-CFAS with the docked bicarbonate ion (magenta) and lipid chains (yellow) obtained from the EC-CFAS structure. The bicarbonate ion is coordinated by His264, Tyr321 and Glu237 (green) and is similarly docked in the X-ray crystal structures of the EC- and LA-CFAS enzymes. Hydrogen bonds are indicated by dashed lines. Tyr128 (salmon) is in close proximity of the docked lipid.

3.2. Expression and purification of PA-CFAS enzyme:

The PA-CFAS enzyme was heterologously expressed as a His_{6x}-fusion protein in *E. coli* and was purified using a method reported previously for the EC-CFAS enzyme [104].

After protein expression, His6-PA-CFAS was first purified using Ni-NTA affinity chromatography. To further separate the protein from aggregated forms, fractions collected from the Ni-NTA purification were concentrated and injected into a fast protein liquid chromatography (FPLC) instrument for size exclusion chromatography. This second purification also serves as a buffer exchange step, allowing us to remove the high concentration of imidazole needed for elution of the His-tagged protein from the Ni-NTA column. This purification procedure yielded approximately 5 mL of 70 µM protein from 3 L of cell culture, with no obvious precipitation. To verify whether the protein was successfully expressed and purified without any unexpected truncation, the mass of the protein was verified by liquid chromatography electrospray ionization mass spectrometry (LC-ESI-MS). The chromatogram (Figure 3.2. A) shows a single peak with a retention window of 11.5-13 min, suggesting that the protein is indeed pure. The mass spectrum revealed a broad charge state distribution (40⁺-70⁺ ions, Figure 3.2.B), from which the deconvoluted m/z value for the [M+H]+ molecular ion was determined 46486 Da (Figure 3.2.C). This observed molecular weight corresponds exactly to the value expected for the PA-CFAS monomer.

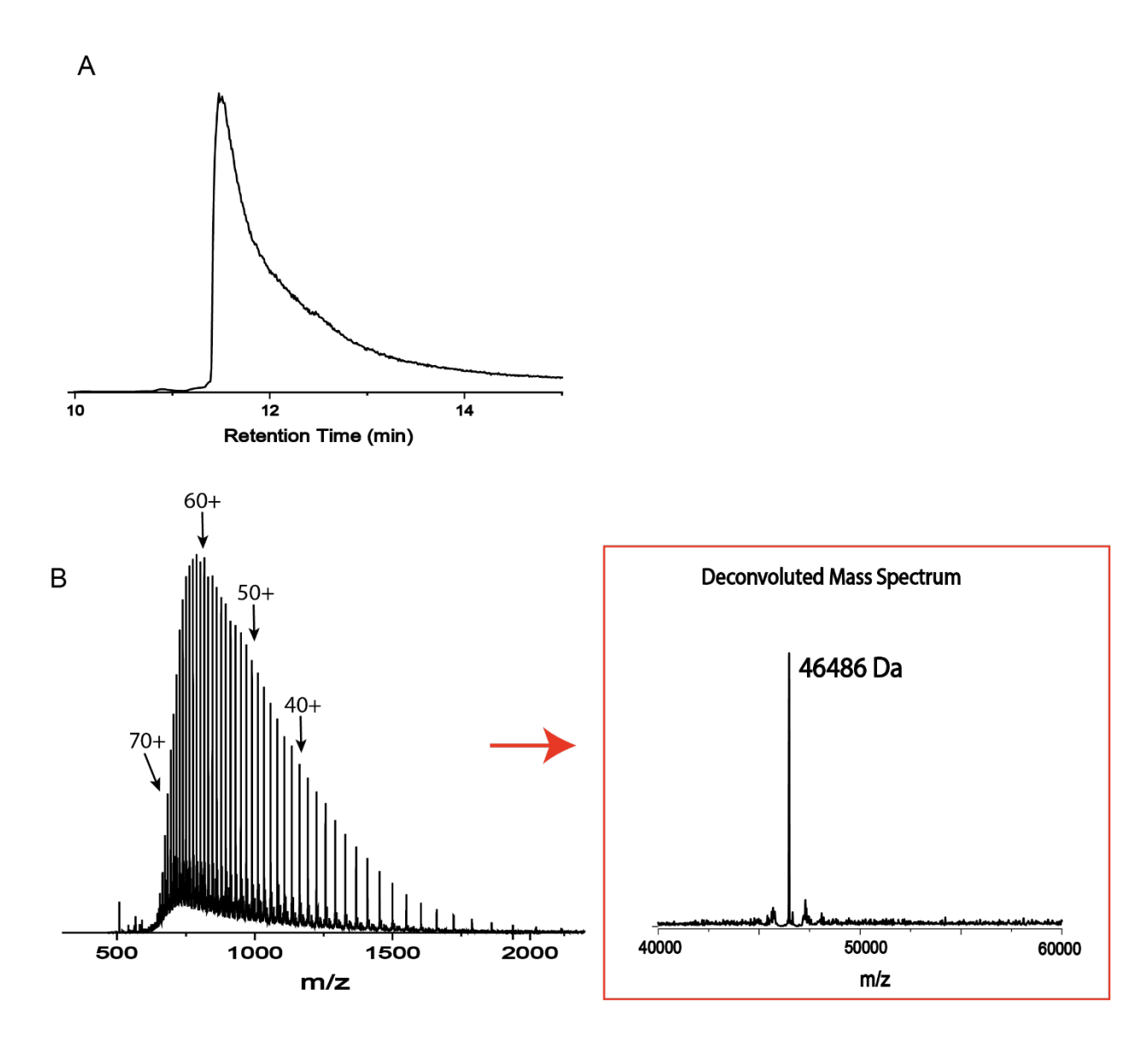


Figure 3.2. Liquid chromatography electrospray ionization mass spectrometry (LC-ESI-MS) analysis of His₆-PA-CFAS. **A**) Chromatogram of His₆-PA-CFAS resolved on a protein C4-reverse phase liquid chromatography column. **B**) The mass spectrum of His₆-PA-CFAS integrated over the chromatographic peak (from 11-12 min) showing a charge state distribution ranging from the 40+ ion to the 70+ ion.

3.3. Biochemical analysis of *P. aeruginosa* CFAS activity:

3.3.1. Establish the 3-enzyme coupled colorimetric assay:

To study the kinetic properties of PA-CFAS, we adapted a colorimetric assay developed previously for EC-CFAS by Guianvarc'h (Figure 3.3) [109]. This 3-enzyme coupled assay utilizes a plate reader which allows robust and high-throughput analysis of the enzymatic

activity. In this assay, the *S*-adenosyl-L-homocysteine (SAH) product of the CFAS-catalyzed reaction is first hydrolyzed by SAH nucleosidase into *S*-ribosylhomocysteine (SRH) and adenine. This step is crucial because SAH is known to be a product inhibitor which binds tightly to CFAS and inhibits its activity [99]. SRH is then cleaved further by a third enzyme, *S*-ribosylhomocysteinase (LuxS), into L-homocysteine (Hcy) and 4,5-dihydroxy-2,3-pentanedione [110]. Hcy contains a free thiol group which reacts rapidly with 5,5'-dithiobis-(2-nitrobenzoic acid) (DTNB) by cleaving the disulfide bond and releasing 2-nitro-5-thiobenzoate (TNB-). TNB- can ionize in water in neutral or alkaline pH to reveal a yellow-colored TNB²-dianion which absorbs at a wavelength of 412 nm [111]. The absorbance can be quantified using a plate reader and it reflects the concentration of Hcy in the coupled reaction, which in turn corresponds to the concentration of SAH produced by CFAS.

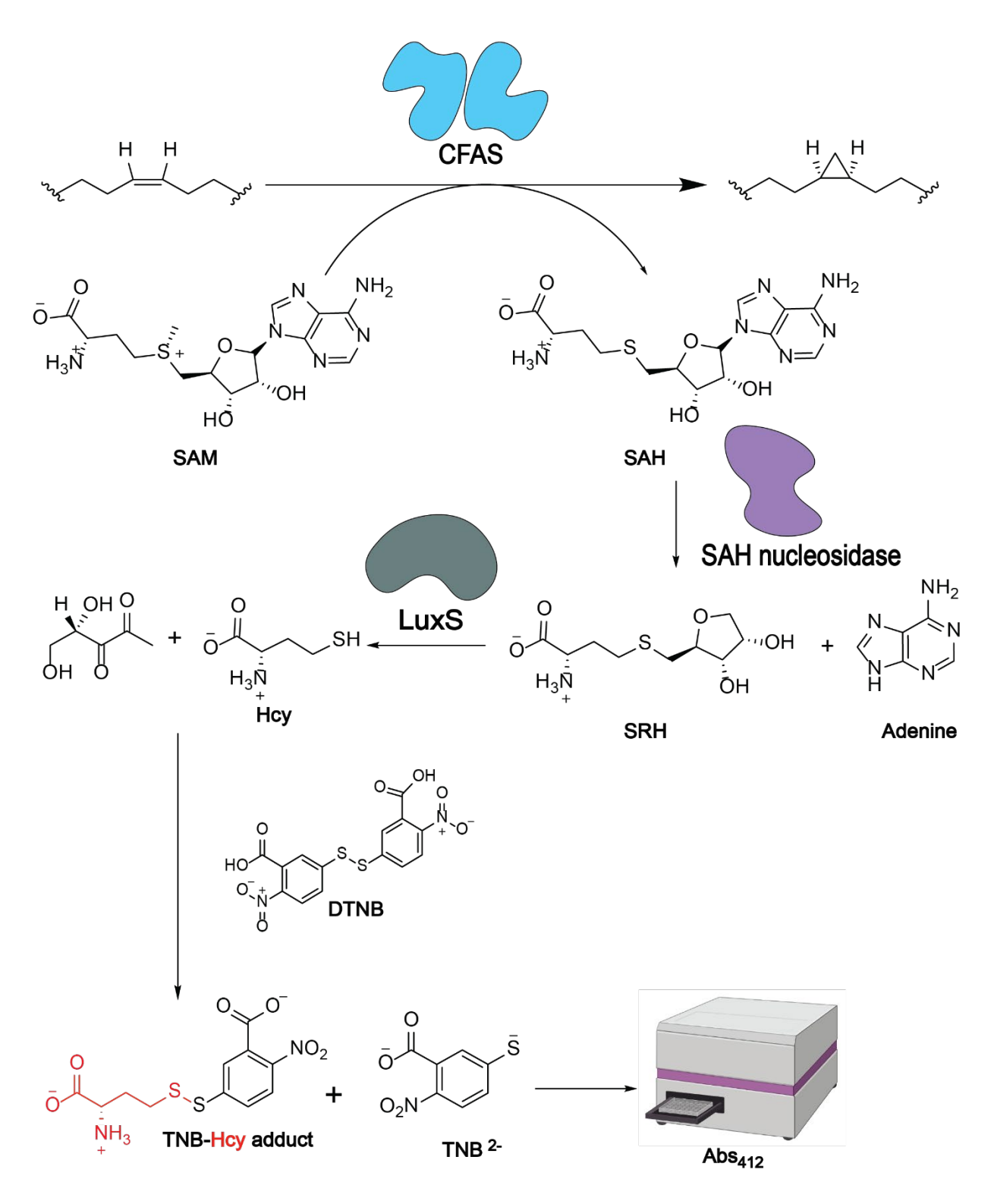


Figure 3.3. Schematic illustration of the colorimetric, coupled enzyme activity assay for CFAS.

SAH nucleosidase and LuxS enzymes were obtained by overexpression in *E. coli* BL21 followed by purification steps similar to those employed for PA-CFAS. Their masses were verified by LC-ESI-MS (Figure 3.4.).

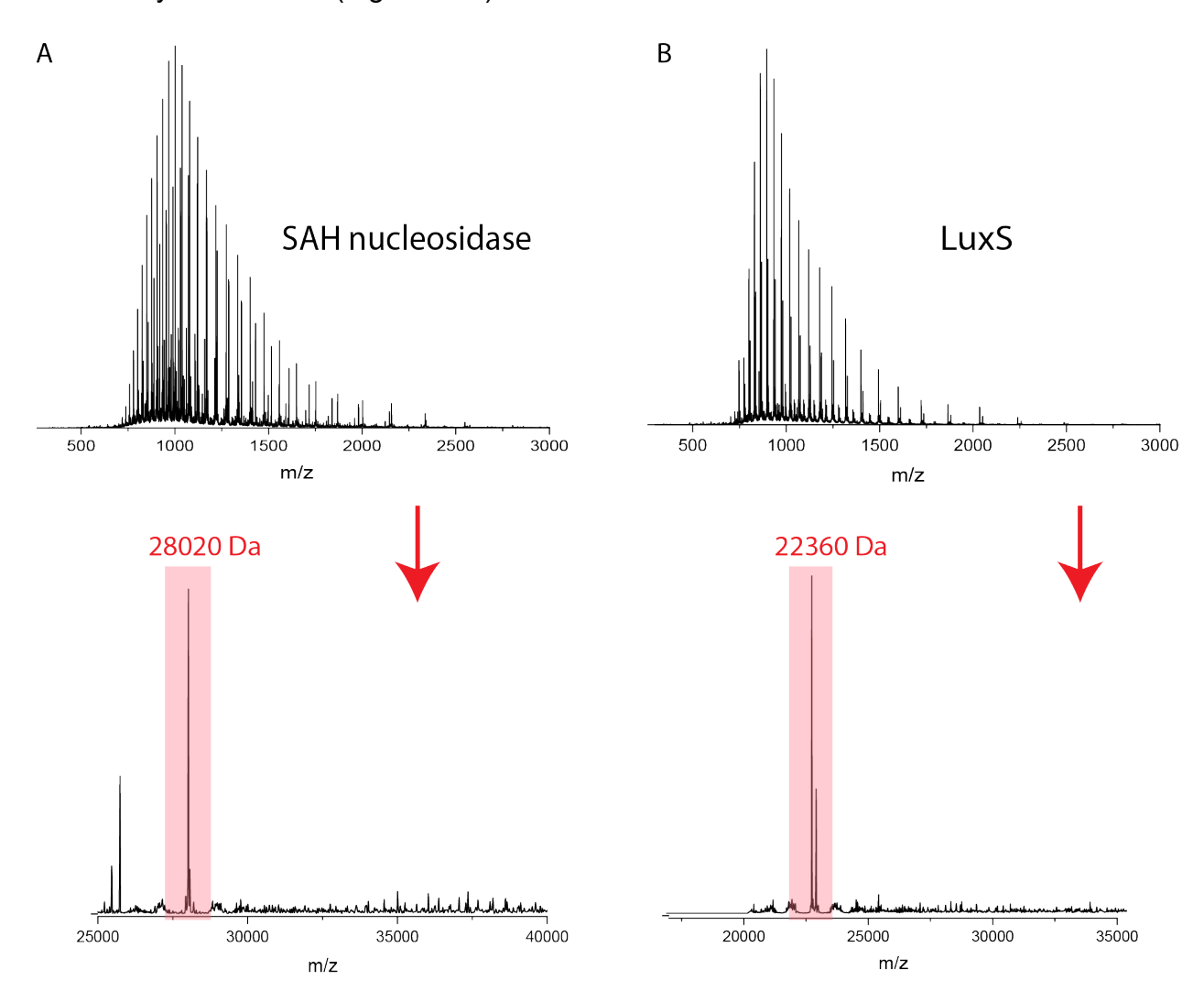


Figure 3.4. LC-ESI-MS spectrum of **A)** SAH nucleosidase (Observed mass = 28020 Da, Expected mass = 28025 Da) and **B)** LuxS (Observed mass = 22360 Da, Expected mass = 22366 Da) with their corresponding deconvoluted mass spectrum.

To quantify the concentration of Hcy after quenching, L-cysteine (Cys) was used to generate a calibration curve for the determination of Hcy concentration in the assay. Different concentrations of Cys were prepared in 50 mM HEPES, pH 7.5 using serial dilutions and were quenched with buffer containing DTNB. The plot (Figure 3.5.) shows a linear relationship between the concentration of Cys and the absorbance at 412 nm with

a slope of 0.00634 and a R-square value of 0.9996. This indicates that we are able to measure the concentration of Hcy in the range of 2 to 250 μ M in an assay mixture without saturating the plate reader detector.

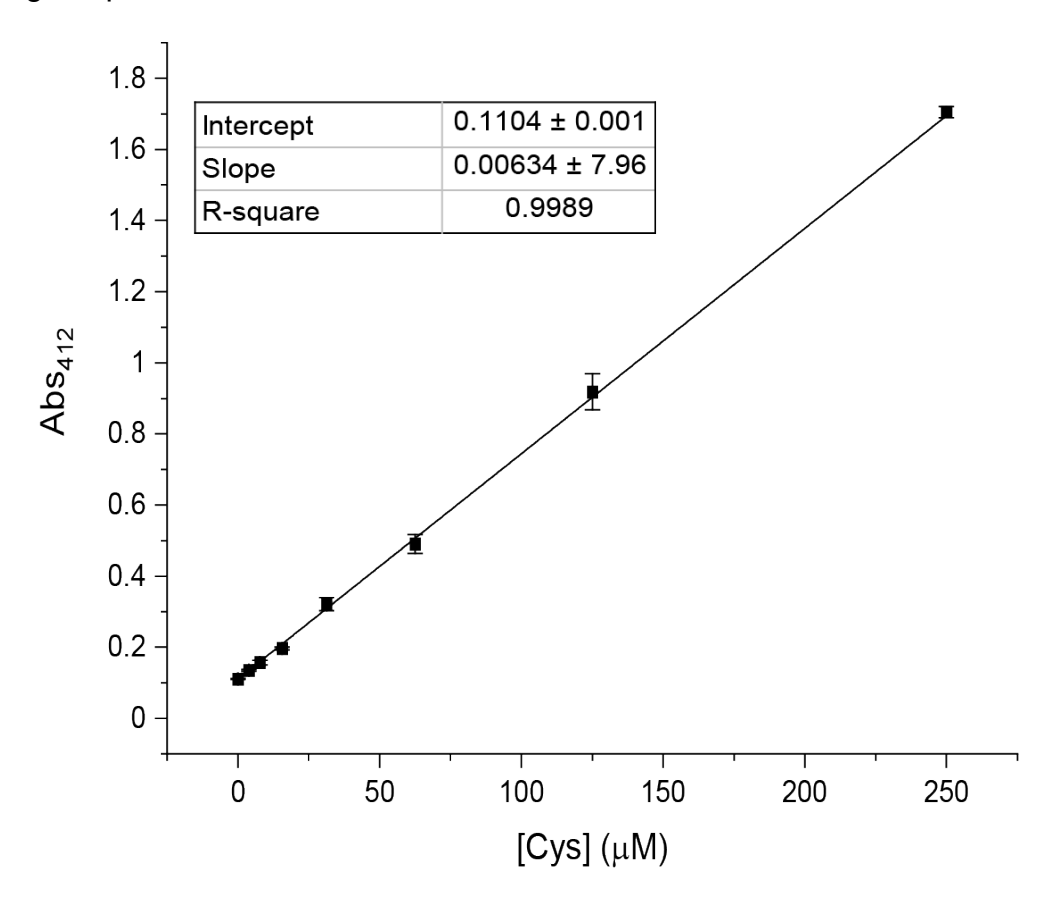


Figure 3.5. Cysteine calibration curve with slope, y-intercept and R-square value indicated. The Cys standards were prepared in CFAS assay buffer.

In order to confirm that the coupled enzymes are working properly, 200 μ M of *S*-adenosyl-L-homocysteine (SAH, the product of the CFAS-catalyzed reaction) was first incubated with 2 μ M of SAH nucleosidase for 5 min at 37 °C and pH 7.5, prior to addition of 10 μ M LuxS. To keep the condition of this control study as close to the real assay as possible, CFAS and liposomes were also included in the mixture to exclude any potential background created by these components. The negative control contained everything except the SAH nucleosidase. The concentration of the Hcy in the assay was calculated by subtracting the absorption reading of the negative control (the background) from the absorption reading of the assay followed by dividing by slope of the Cys calibration curve

(Figure 3.5). The plot shows that within 10 min, nearly all of the 200 μ M of SAH present in the reaction mixture was fully converted into Hcy, with approximately 100 μ M SAH being consumed within a 2 min burst phase (Figure 3.6.). This indicates rapid derivatization of SAH to Hcy under our coupled assay conditions. This result shows that these coupled assay conditions can be used to accurately measure the activity of CFAS as long as the CFAS-catalyzed reaction produces less SAH than the control study within the reaction time.

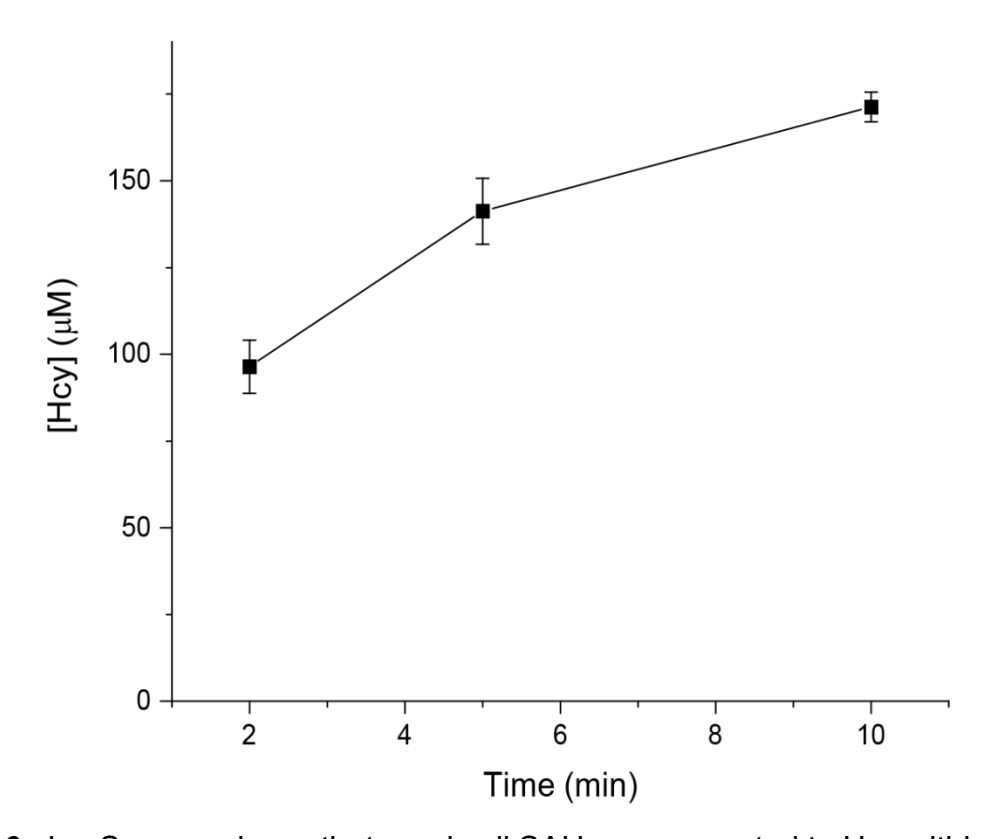


Figure 3.6. LuxS assay shows that nearly all SAH was converted to Hcy within a 10 min derivatization time frame.

3.3.2. CFAS activity depends on pH:

Using this activity assay, we initially tested PA-CFAS activity with conditions very similar to those reported previously for EC-CFAS with a minor modification on the choice of lipid substrate [109]. Instead of using *E. coli* extracted lipids, the assay mixture contained 1 mg/mL of unilamellar vesicles composed of dioleoyl-phosphatidylethanolamine (DOPE) and dipalmitoyl-phosphatidylglycerol (DPPG) in a 6:4 ratio, 1 mM SAM, and 0.5 µM PA-CFAS in 50 mM HEPES (pH 7.5). The EC-CFAS was used as a positive control.

Unfortunately, PA-CFAS was not active under these standard conditions (Table 3.1.), as we did not detect a significant difference between the absorption of the negative control and the assay. On the other hand, EC-CFAS provided an activity of $9.89 \pm 1.13 \text{ min}^{-1}$ which is similar to the previously reported value ($14.62 \pm 0.50 \text{ min}^{-1}$). This result was surprising given the high sequence identity (41%) and structural similarity between the two enzymes.

Table 3.1. Catalytic activity of PA-CFAS depends on pH.

Enzyme	рН	Initial Rate (min ⁻¹)	
P. aeruginosa CFAS	6.5	0.68 ± 0.03	
	7.0	0.70 ± 0.06	
	7.5	0	
	8.0	0	
	8.5	0	
E. coli CFAS (+ control)	7.5	9.89 ± 1.13	

To troubleshoot the activity assay, we first focused on the reaction pH. The pH-rate profile of EC-CFAS was previously studied from pH 5.5 and 9.5 and it was reported that EC-CFAS had a maximum activity at pH 7.5 [112]. We believed that it is possible that PA-CFAS has a different pH preference than EC-CFAS. Therefore, with the aim of finding an optimal condition for PA-CFAS activity, a range of pH values were tested while keeping the liposome composition constant (60:40 DOPE:DPPG). The reaction time was also increased from 20 min to 40 min. As shown in Table 3.1., PA-CFAS is active only at pH 6.5 and 7. The activity measured for PA-CFAS at pH 6.5 is approximately 12-fold less than the activity of the *E. coli* enzyme at pH 7.5. This result is rather unexpected because both EC-CFAS and LA-CFAS function optimally in the pH range 7.5-8.0 [100, 104, 105, 112]. This suggests that PA-CFAS may have some fundamental differences compared to the other enzymes of this family despite their sequence and structural similarity.

3.3.3. PA-CFAS stability test and assay optimization:

Since the initial screen for activity was done using a single time point (40 min for PA-CFAS) and the previous control assay (Section 3.3.1.) only tested the efficiency of the coupled enzymes within the first 10 min, we needed to make sure that the product

formation is linear during the length of the reaction time in order to properly calculate the initial velocity of the CFAS-catalyzed reaction. To test the linearity of the reaction, reactions were quenched at 10, 20, and 40 min. In addition, three different concentrations (1 μ M, 2.5 μ M and 5 μ M) of PA-CFAS were used in order to confirm that the CFAS activity is indeed the rate of product formation in our assay (rather than the coupled enzymes).

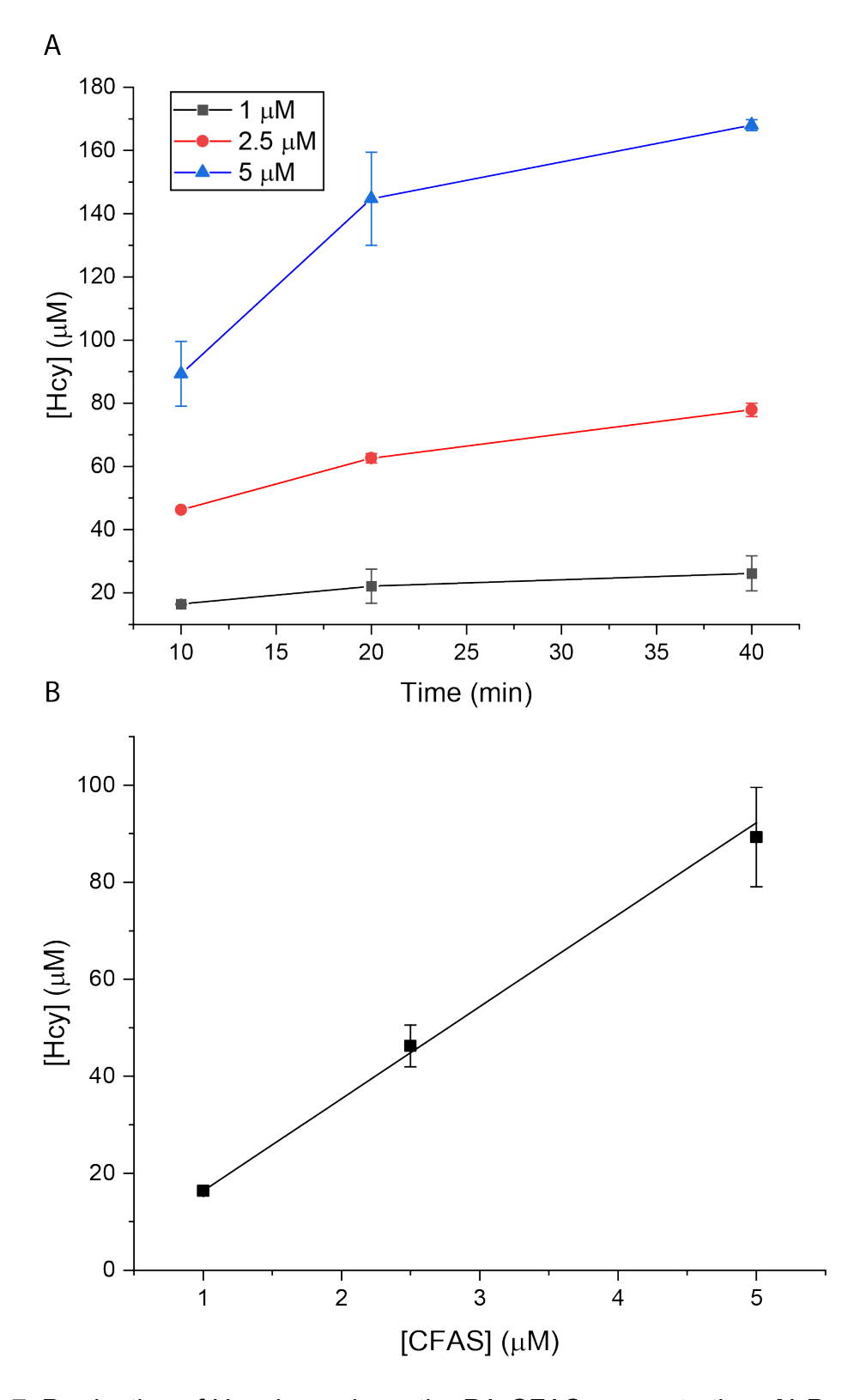


Figure 3.7. Production of Hcy depends on the PA-CFAS concentration. **A)** Production of Hcy over time at various PA-CFAS concentrations (1, 2.5, or 5 μ M). **B)** Production of Hcy

after a 10 min reaction increases linearly with increasing PA-CFAS concentrations. This suggests that CFAS activity is limiting the coupled reaction under these conditions.

After plotting the Hcy formation against the reaction time (Figure 3.7. A), we first observed that increasing the concentration of CFAS from 1 to 5 μ M in the assay led to a proportional increase in Hcy (Figure 3.7. B). This indicates that CFAS is likely the limiting factor in this coupled reaction. To further confirm this finding, we next performed control studies with either double the concentration of SAH nucleosidase (from 2 to 4 μ M) or double the concentration of LuxS (from 10 to 20 μ M) while using 5 μ M of CFAS. A positive control was run in parallel with the standard concentrations of the two coupled enzymes and 5 μ M of CFAS. Because we also observed the flattening of the curve after 10 min at all three CFAS concentrations (Figure 3.7. A), we decided to shorten the total reaction time from 40 min to 10 min using three new time points which are 2 min, 5 min, and 10 min. If the coupled enzymes are indeed limiting the reaction, then by increasing the concentration of individual enzyme should have a positive effect on the overall rate. On the contrary, if CFAS was limiting the reaction, higher concentrations of the coupled enzymes should not change the overall velocity of the product formation.

Figure 3.9. shows that the production of Hcy in this coupled assay is linear over 10 min and the positive control shows an initial velocity of $9.87 \pm 1.08 \,\mu\text{M}$ min⁻¹. By doubling the concentration of SAH nucleosidase, the initial rate of Hcy production was nearly identical $(8.54 \pm 0.64 \,\mu\text{M} \,\text{min}^{-1})$. Similarly, doubling the concentration of LuxS also had only a minor influence on the rate $(7.75 \pm 1.08 \,\mu\text{M} \,\text{min}^{-1})$. These results suggest that the CFAS concentration is the rate limiting factor under our assay conditions (Figure 3.8.).

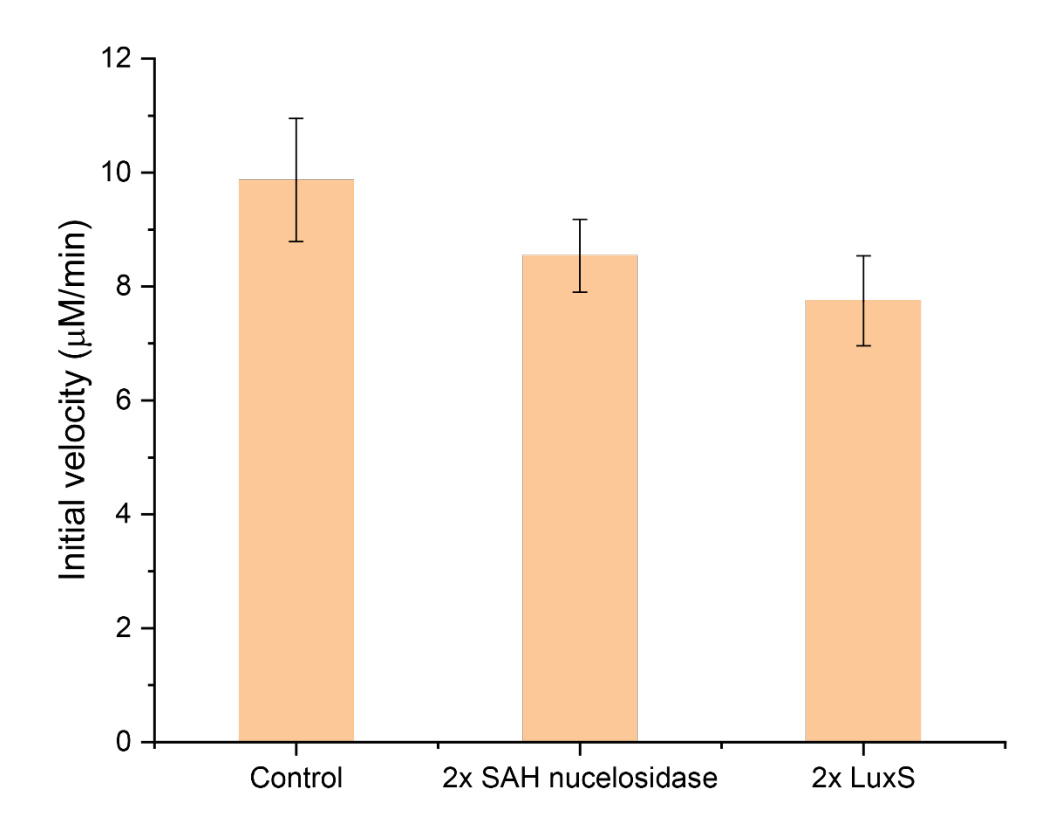


Figure 3.8. The concentrations of SAH nucleosidase and LuxS are not the limiting factors. Control contains the standard concentrations of SAH nucleosidase (2 μ M), LuxS (10 μ M) and PA-CFAS (5 μ M), 2x SAH nucleosidase and 2x LuxS have doubled concentration of the respective enzyme.

Another observation from Figure 3.7. is that the progress curves begin to plateau at all three CFAS concentrations after 10 min. Since the substrates used in the reaction, SAM and liposome, were in great excess compared to the enzyme, the flattening is unlikely caused by the consumption of the substrates. To test whether the loss of activity is caused by denaturation of the enzyme under our assay conditions, PA-CFAS was pre-incubated at 37 °C in pH 6.5 buffer for different length of time (60 min, 120 min and 240 min), before being assayed under standard conditions (Figure 3.9.). Fortunately, no significant differences were observed in the reaction velocity, suggesting that PA-CFAS is stable under these reaction conditions for at least 4 h. The origin of the plateau observed in Figure 3.7. is still not clear.

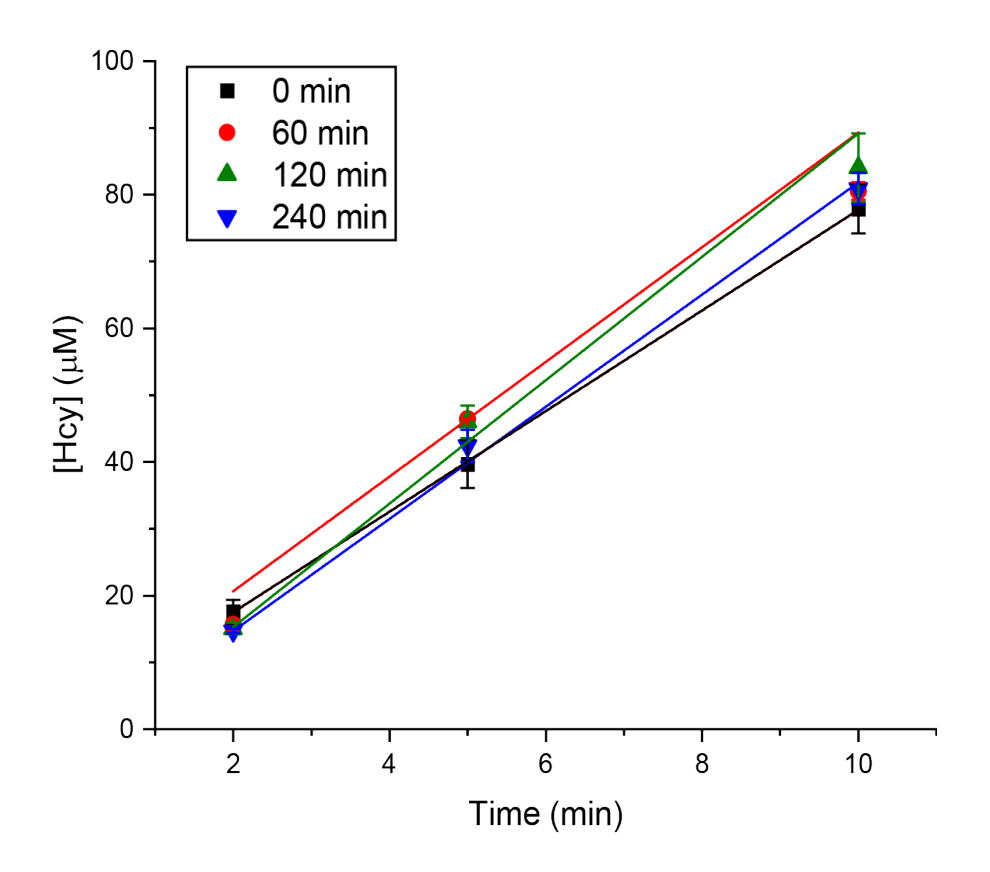


Figure 3.9. Testing the stability of PA-CFAS at 37 °C and pH 6.5. The enzyme was preincubated in 50 mM MOPS, pH 6.5 at 37 °C for 0 min (black), 60 min (red), 120 min (green) and 240 min (blue) before initiating the reaction. The concentration of Hcy produced in each assay is plotted against the reaction time and a linear trend was observed in all preincubation studies with similar slope.

3.3.4. PA-CFAS activity depends on the lipid head groups:

After establishing standard assay conditions for PA-CFAS activity and confirming that the coupled enzyme activity assay is performing as desired, we tested the effects of the lipid head groups on the activity of CFAS. In fact, no previous studies on the effect of lipid head group were reported on other CFAS enzymes such as EC-CFAS and LA-CFAS. Phosphatidylethanolamine (PE) and phosphatidylglycerol (PG) are the two most abundant lipids in most bacterial membranes [79]. In order to measure the lipid headgroup dependence of CFAS activity, the lipids of choice must have identical fatty acyl chains – both in terms of acyl chain length and the degree of unsaturation. In previous assays, DOPE and DPPG were used in a 6 to 4 ratio. DOPE has one double bond on both of its C18-oleoyl chains, while DPPG contains two fully saturated C16-palmitoyl chains. By

varying the ratio of these lipids, the amount of unsaturated fatty acyl chains and the ratio of C18:C16 acyl chains would also change. For this reason, we chose to use 1-palmitoyl-2-oleoyl-PE (POPE) and 1-palmitoyl-2-oleoyl-PG (POPG) lipids, as these each contain one C16-palmitoyl chain and one C18-oleoyl chain (Figure 3.10. A). Using different combinations of these lipids, the initial rate of PA-CFAS activity was measured at pH 6.5 over a 10 min time interval. The activity yielded a bell-curve shaped profile with the highest velocity observed in vesicles containing anywhere from 30-70% POPE, and with noticeable reductions in CFAS activity at higher concentrations of either POPE or POPG Note, we could not make vesicles containing only POPE because precipitation was observed when buffer was added to hydrate the dried lipid film.

After observing this lipid preference of PA-CFAS at pH 6.5, it made us wonder whether the same lipid preference will be observed at pH 7.5. In fact, the cytoplasmic pH of P. aeruginosa is around pH 7.5 during exponential phase [113], which means that CFAS, in theory, should function at a pH close to this range. After performing the same experiments as previously described, we observed a completely different preference profile at PH 7.5. When the same vesicles compositions were used at pH 7.5, the activity profile shifted to have a maximum at 85% POPG. POPG is an anionic lipid, whereas POPE has a zwitterionic head group; however, the p K_a of the primary amine moiety of PE is approximately 9.6 in aqueous buffer [114], suggesting that the mole fraction of the anionic PG lipids will dominate the surface charge on our vesicles at both pH 6.5 and 7.5. Thus, as the pH is changed from 6.5 to 7.5, PA-CFAS seems to have an increased preference for anionic membranes (maximal activity at 30-70% POPG at pH 6.5 and near 85% at pH 7.5). Curiously, PA-CFAS is predicted to be an acidic protein with an isoelectric point of approximately 6.02 and a net negative charge at both pH 6.5 and 7.5. On the basis of these observations, it does not seem like the surface charge of the phospholipid vesicles plays a major role in PA-CFAS activity.

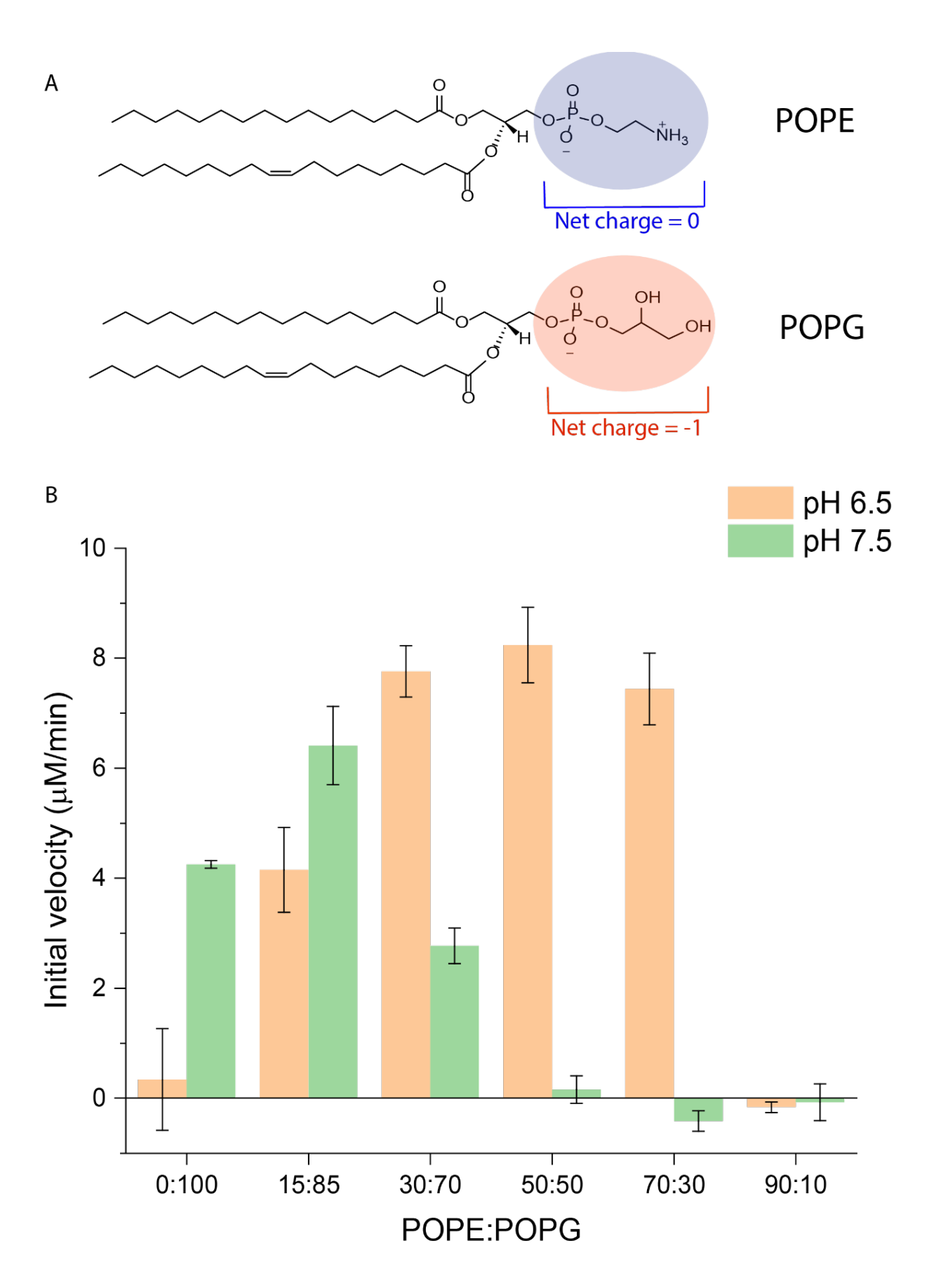


Figure 3.10. PA-CFAS activity depends on POPE:POPG ratio. **A)** The chemical structure of 1-palmitoyl-2-oleoyl-sn-glycero-3-phosphoethanolamine (POPE) and 1-palmitoyl-2-oleoyl-sn-glycero-3-phospho-(1'-rac-glycerol) (POPG). POPE is zwitterionic and POPG is anionic at the pH values used in this study. **B)** The initial velocity of the PA-CFAS catalyzed reaction depends on the POPE:POPG ratio at pH 6.5 (50 mM MOPS) and 7.5 (50 mM HEPES).

3.3.5. Testing CFAS activity using *P. aeruginosa* lipid extracts:

The *P. aeruginosa* plasma membrane is composed of a combination of many different lipids containing different headgroups and fatty acyl chains of different lengths. In contrast, the synthetic liposomes used in the activity assays discussed above were constructed using only the two most abundant lipids species, PE 16:0-18:1 and PG 16:0-18:1. We hypothesized that this overly simplified system may lack essential components that exist in the *P. aeruginosa* membrane such as lipids with low abundance and the variety of fatty acyl chain lengths, which might be important for high level CFAS activity.

To test this hypothesis, we made liposomes directly from lipids extracted from P. aeruginosa cells. Because CFAs are mainly observed in bacteria entering stationary phase, it was important to harvest the membranes from exponentially growing P. aeruginosa cultures, such that the relative abundance of membrane lipids with unsaturated acyl chains (the substrates of CFAS) would be optimal for CFAS activity. To extract membrane lipids, a small overnight culture was first grown, and a larger culture was then inoculated with a 1000-fold dilution of the overnight culture. Once the bacteria had reached optical density at 600 nm (OD₆₀₀) ~0.7, which indicates that the cells have entered the exponential phase, the culture was centrifuged, and the cell pellet was collected. Lipid extraction was performed using the Bligh and Dyer method [115] with a minor modification. Chloroform and methanol (1:2 v/v) were first mixed with the cell pellet and the sample was vortexed to extract total lipids. This organic extract was then mixed with an aqueous phase containing 1 M NaCl to induce phase separation and to improve lipid recovery [116]. In this mixture, the top aqueous layer contains the polar compounds such as small metabolites and salts, while the lower organic phase contains the extracted lipids. Cell debris and proteins precipitate and remain at the interface of the two phases. Accordingly, the chloroform layer was collected and dried under nitrogen to form a lipid

film. The dried lipids were then rehydrated and extruded as described above to create liposomes (unilamellar vesicles). The activity of PA-CFAS was then tested using these extracted lipids at both pH 6.5 and pH 7.5.

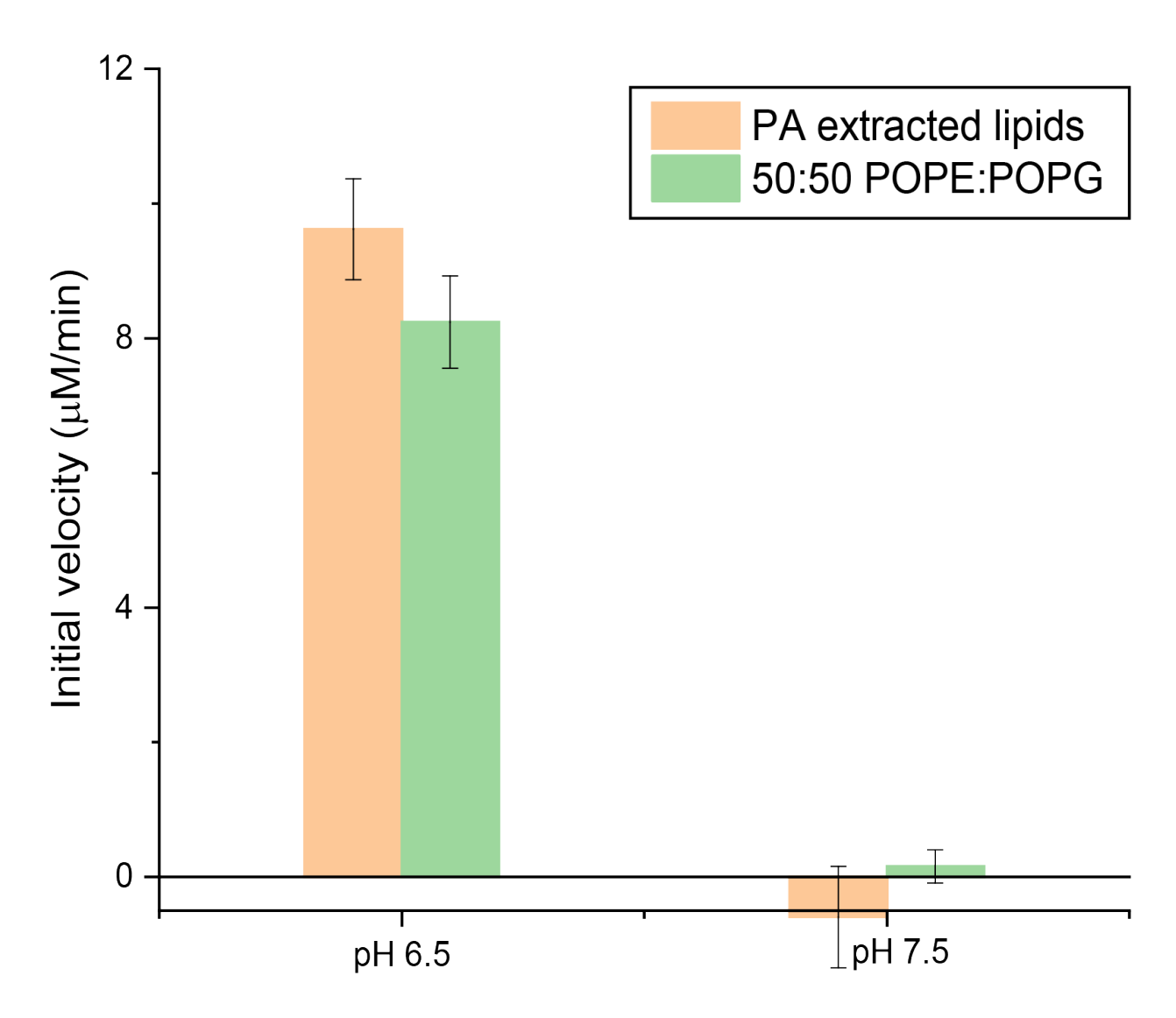


Figure 3.11. PA-CFAS activity assay using *P. aeruginosa* extracted lipid from exponential phase vs. using 50:50 POPE:POPG.

The result shows that PA-CFAS was active at pH 6.5 with an initial velocity similar to the value measured with the 50:50 POPE:POPG vesicles in the previous section (Figure 3.11.). This data suggests that the synthetic vesicles are indeed a good mimic of the natural CFAS membrane substrate. However, no activity was again measured at pH 7.5.

Thus, the vesicles prepared from both purified lipids and PA membrane extracts gave similar results. From these results, the exact lipid composition of the liposomes is unlikely to be responsible for the lower PA-CFAS activity measured at pH 7.5 in our assay. It should be noted that the current extraction method allows for the extraction of total lipids from both the OM and IM of PA. Since PA-CFAS is a cytoplasmic enzyme that modifies lipids within IM, it is possible that our lipid extracts contain components that inhibit PA-CFAS activity. Therefore, the next step would be to repeat the assays using lipids isolated specifically from the IM.

3.3.6. Attempted optimization of PA-CFAS activity at pH 7.5:

The consistently undetectable activity of PA-CFAS at pH 7.5 was not expected, as this is the reported pH of the *P. aeruginosa* cytoplasm [113]. Thus, we made several additional attempts to boost PA-CFAS activity at pH 7.5. Previously, we tested enzyme activity in HEPES buffer at pH 7.5. We additionally tested for PA-CFAS activity using native liposomes at pH 7.5 in MOPS (buffering range pH 6.5 to 7.9) and TAPS (buffering range pH 7.7 to 9.1) [117], but no enhancement in activity was observed with any of these buffers (Figure 3.12.).

CFAS activity is known to be dependent upon bicarbonate (HCO₃-), which binds to the active site and may either electrostatically stabilize or deprotonate the protonated cyclopropane transition state (Figure 1.7.) [104, 118]. It was previously shown that the use of potassium bicarbonate (KHCO₃-) buffer enhances the activity of EC-CFAS by nearly 3-fold and the removal of HCO₃- renders this enzyme completely inactive [118]. Furthermore, similar to pH, salt concentration is also a solution condition that can play a crucial role in enzyme activity [119]. Low concentration of NaCl and KCl are often added to enzymatic assays for this purpose. Potassium ion (K+) is a major intracellular cation in most bacteria and one of its many important roles is to activate intracellular enzymes [120]. Although there was no prior evidence showing a K+ binding site in the CFAS family, we were nevertheless curious to see whether potassium ions play a role in activating PA-CFAS. For these reasons, we decided to introduce potassium bicarbonate (KHCO₃) to the assay as it is a source of both K+ and HCO₃-. We tested the effect of KHCO₃ in two different concentrations, 10 mM and 100 mM. We also introduced KCl as an additive to

the assay to a final concentration of 100 mM to test if there is any effect on CFAS activity. The assay was performed in buffer containing 50 mM HEPES, pH 7.5 and synthetic liposomes composed of 60:40 POPE:POPG, which is close to the native PE:PG ratio in *P. aeruginosa* inner membranes [121]. A control assay was performed in parallel using 50 mM MOPS, pH 6.5 with no additives. Unfortunately, none of these additives increased PA-CFAS activity at pH 7.5. We can thus conclude that the low activity of PA-CFAS at pH 7.5 using a 60:40 POPE:POPG liposomes is not due to the lack of K⁺ or HCO₃⁻.

PA-CFAS is a soluble, cytoplasmic protein which interacts with lipids from the inner membrane. Although it was not previously reported with EC-CFAS, considering the significant difference in lipid and pH preference between EC and PA-CFAS, we thought that there may exist unknown co-factors in the cytosol of *P. aeruginosa* which could assist the function of PA-CFAS. We reasoned that adding PA cell lysates to *in vitro* PA-CFAS reaction mixtures might help to stimulate PA-CFAS activity. However, lysates prepared from neither log phase nor stationary phase PA had any significant stimulatory effect on PA-CFAS activity at pH 7.5 (Figure 3.12.). In fact, addition of log phase lysate to the pH 6.5 assay completely inactivated PA-CFAS activity. The reasons for this inhibition are not known.

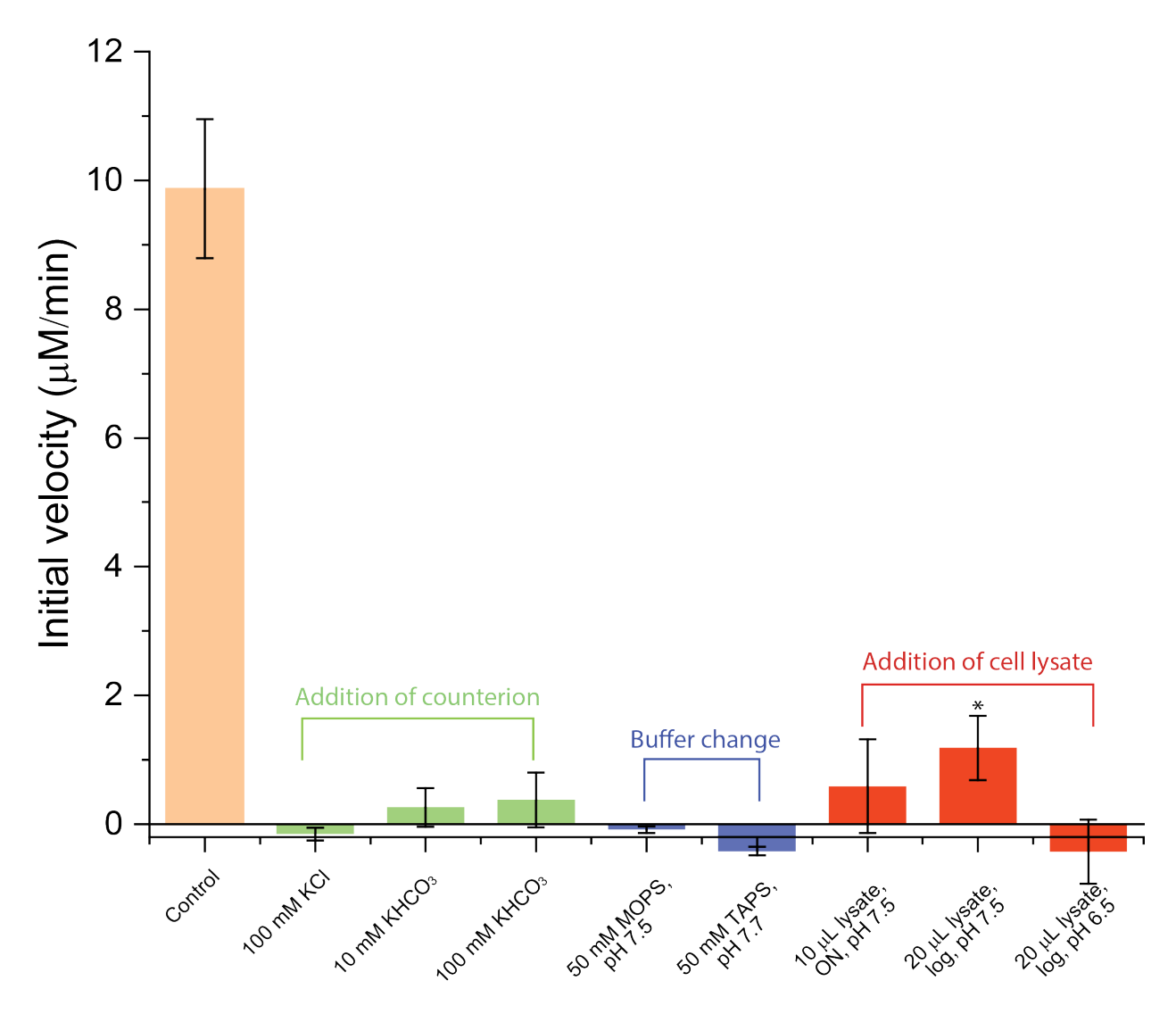


Figure 3.12. Attempted optimization of PA-CFAS activity at pH 7.5. The control assay was conducted at pH 6.5 using lipids extracted from exponential phase PA cells. Results of addition of bicarbonate and potassium ion are colored in green; buffer changes are colored in blue; and the addition of cell lysate are colored in red.

3.3.7. Determination of kinetic parameters for PA-CFAS:

Prior to determining the steady state kinetic parameters of PA-CFAS, we first wanted to employ our colorimetric assay to reproduce the previously reported kinetic parameters for the EC-CFAS, which were determined by an HPLC-based method [100, 118]. The EC-CFAS has a reported $K_{\rm M}$ of 89.4 ± 12.8 μ M for SAM and a $k_{\rm cat}$ of 7.31 min⁻¹ when assayed in HEPES buffer. Using our colorimetric assay, we obtained similar kinetic parameters

for EC-CFAS in HEPES buffer ($K_{\rm M}$ = 67.7 ± 7.9 μ M, $k_{\rm cat}$ = 12.6 ± 0.72 min⁻¹, Table 3.2.). Thus, our colorimetric assay appears to be robust.

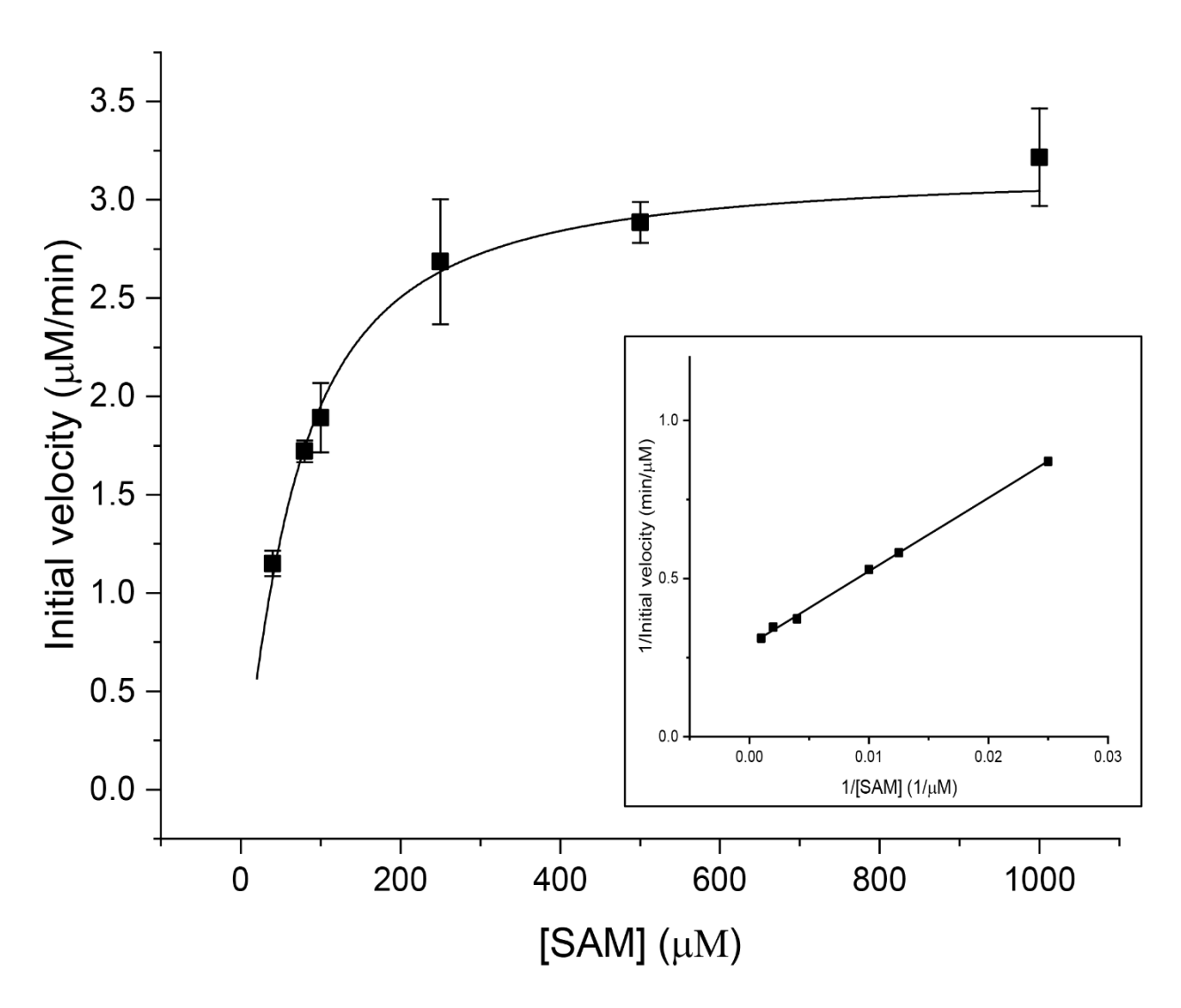


Figure 3.13. Michaelis-Menten kinetics and the corresponding Lineweaver-Burk plot (inset) for EC-CFAS with varied SAM concentrations. Assays were performed in triplicate at 50 mM HEPES, pH 7.5 with 1 mg/mL of 60:40 DOPE:DPPG liposomes, 20-1000 μ M SAM, 0.25 μ M EC-CFAS, 2 μ M SAH nucleosidase and 10 μ M LuxS.

After validating our assay on EC-CFAS, the kinetic parameters for PA-CFAS were determined. Since PA-CFAS performs differently at pH 6.5 and pH 7.5, we employed vesicles composed of POPE:POPG (30:70) as the lipid headgroup ratio because these vesicles were PA-CFAS substrates at both pH values (Figure 3.10). The Michaelis-

Menten and Lineweaker-Burk plots for PA-CFAS at pH 6.5 and pH 7.5 are shown in Figure 3.14 and the kinetic parameters are listed in Table 3.2. Both the K_m for SAM and the k_{cat} double at pH 6.5, leading to a similar catalytic efficiency (k_{cat}/K_m) at each pH. Relative to the EC-CFAS enzyme at pH 7.5, the PA-CFAS suffers an approximately 10 fold decrease in k_{cat} , but the K_m for SAM for the two enzymes is similar. As a control, we also tested the activity of EC-CFAS at pH 7.5 using 30:70 POPE:POPG to mimic the condition of PA-CFAS. Under saturating concentrations of SAM, 0.6 µM EC-CFAS has an k_{cat} of 10.5 ± 0.35 min⁻¹ which is nearly identical to what we observed using 60:40 DOPE:DPPG. This result suggests that despite the difference in liposome compositions used for EC- and PA-CFAS, it is unlikely that the low k_{cat} observed for PA-CFAS arises from the difference in the choice of lipid. Furthermore, in previously reported cases, EC-CFAS has shown similar activity with different lipid substrates ranging from extracted E. coli phospholipids to single lipid types such as 1-stearoyl-2-oleoyl-PG (SOPG,18:0-18:1 PG)[100]. Combined with our result, EC-CFAS appears to be more tolerant to different lipid substrates compared to PA-CFAS, which appears to prefer phosphatidyl glycerol lipids under our conditions.

Table 3.2. Kinetic parameters of EC- and PA-CFAS with SAM.

Enzyme	рН	K _M	V _{max}	K cat	Kcat Km ⁻¹
		(μ M)	(µM/min)	(min ⁻¹)	(µM ⁻¹ min ⁻¹)
EC-CFAS*	7.5	67.7 ± 7.9	3.15 ± 0.18	12.6 ± 0.72	0.1861
PA-CFAS**	6.5	156.3 ± 24.3	4.62 ± 0.20	2.01 ± 0.09	0.0129
-	7.5	79.4 ± 10.1	2.85 ± 0.14	0.95 ± 0.05	0.0120

^{*}Assayed with vesicles composed of 60:40 DOPE:DPPG

^{**}Assayed with vesicles composed of 30:70 POPE:POPG

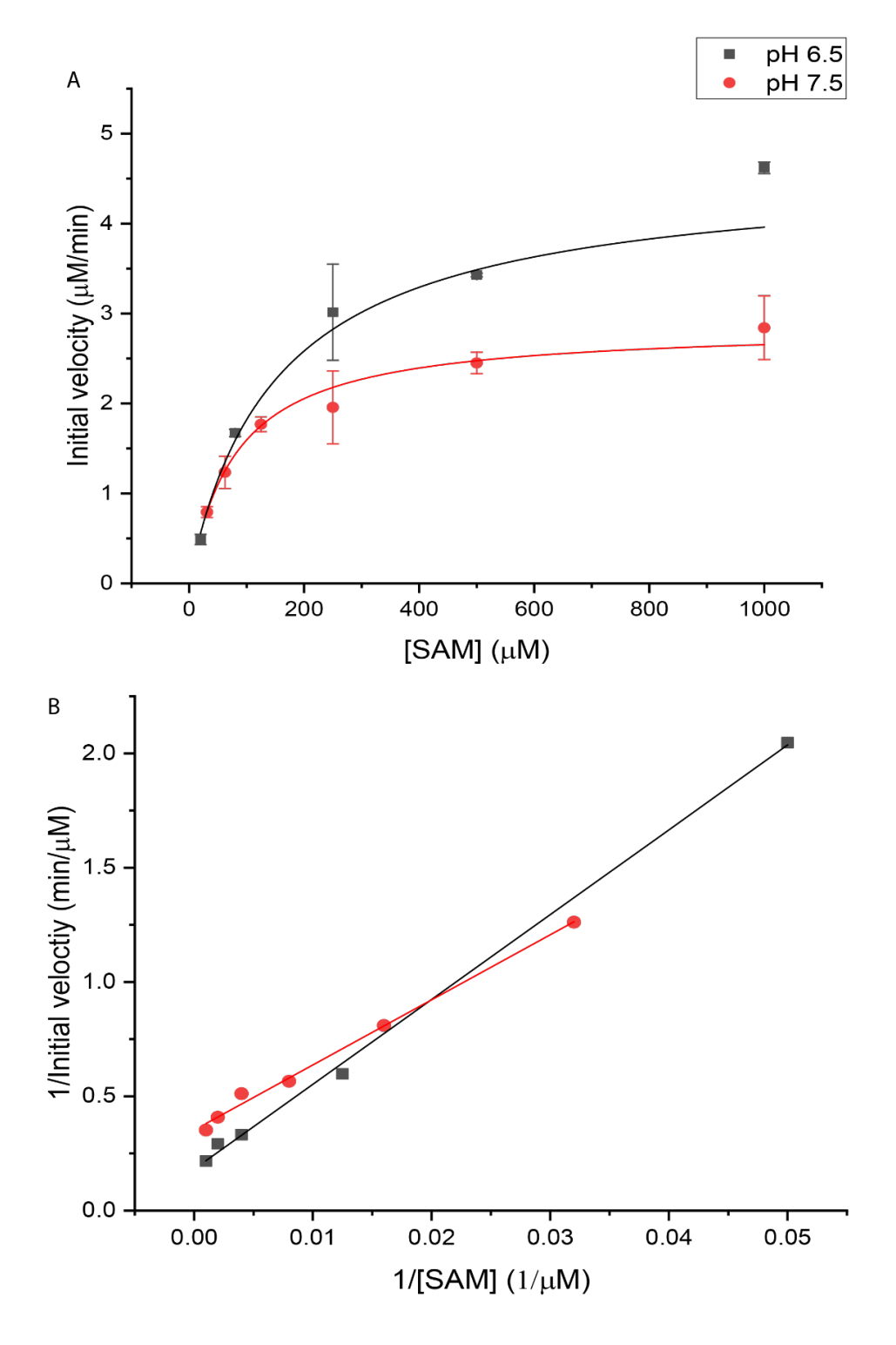


Figure 3.14. Michaelis-Menten kinetics and the corresponding Lineweaver-Burk plot of PA-CFAS with varied SAM concentrations. Assays were performed in triplicate in 50 mM HEPES, pH 7.5 or 50 mM MOPS, pH 6.5 with 1 mg/mL of 30:70 POPE:POPG liposomes, variable SAM (31-2000 μ M), 2.3 (pH 6.5) or 3 μ M (pH 7.5) PA-CFAS, 2 μ M SAH nucleosidase and 10 μ M LuxS.

3.4. Structural analysis of P. aeruginosa CFAS:

3.4.1. Native mass spectrometry (Native MS):

The EC-CFAS crystal structure showed that the enzyme exists in solution as a dimer and functional studies have shown that the dimerization is crucial for enzyme activity [104]. Similarly, PA-CFAS is predicted to be a dimer by AlphaFold (Figure 3.1. B). To validate this *in silico* structural prediction, we characterized PA-CFAS by native electrospray ionization mass spectrometry (ESI-MS). This technique allows us to study intact protein complexes by utilizing a nanoelectrospray ionization (nanoESI) system. The nanoESI emitter generates very small droplets which permit fast and soft ionization of the protein ions. This gentle system provides a non-denaturing condition which preserves protein complexes in a near native state because it does not require excessive heating for desolvation and employs lower voltages for ionization [122, 123].

The PA-CFAS sample was buffer exchanged into ammonium acetate solution in preparation for native MS. The use of this volatile electrolyte allows the protein to experience a similar solvation as in physiological condition while being able to easily desolvate during the ionization process. This can generate cleaner MS data with less adduct formation. The sample was then loaded into a platinum-coated borosilicate emitter and subjected to gentle nanoESI. Two clusters of multiply charged ions of PA-CFAS were obtained under the gentle nanoESI conditions. The bimodal charge state distributions suggest the existence of two separate CFAS conformations. The lower charge states (18-21⁺) could be identified in the range of m/z 4200-5300 while the higher charged states span the lower m/z region. The MaxEnt1 function of MassLynx was used to separately deconvolute each set of ions. The m/z value measured for the 18-22+ charge states were determined to be 93,030 Da, which is very close to the expected molecular weight of the PA-CFAS dimer (92,972 Da). The small mass difference is likely due to incomplete desolvation of the PA-CFAS dimer under these gentle ionization conditions. When the deconvolution was performed on the more highly charged set of ions (charge states 31-40⁺) the measured mass was 92,970 Da, which is nearly identical to the expected mass and is consistent with complete desolvation of the protein ions during nanoelectrospray.

We next calculated the solvent accessible surface area from the bimodal charge state distribution using an established empirical relationship [124-126]. Using the 20-22+ and 33-35+ charge states, we calculated surface areas for the two CFAS conformations of 34,800 ± 130 Ų and 86,590 ± 51 Ų, respectively. The theoretical surface area calculated for the Alpha Fold model of the PA-CFAS dimer was 32,823 Ų, in excellent agreement with the surface area calculated for the 20-22+ ions. This data strongly suggests that the PA-CFAS dimer exists in a near native conformation under our native MS conditions. Interestingly, despite the apparent partial unfolding of the CFAS dimer into a more open and more highly charged conformation, the dimer nevertheless remains intact. This suggests that the protein-protein interactions to form the dimer are relatively strong. Moving forward, native MS may prove to be a useful technique for characterizing the structural properties of the enzyme.

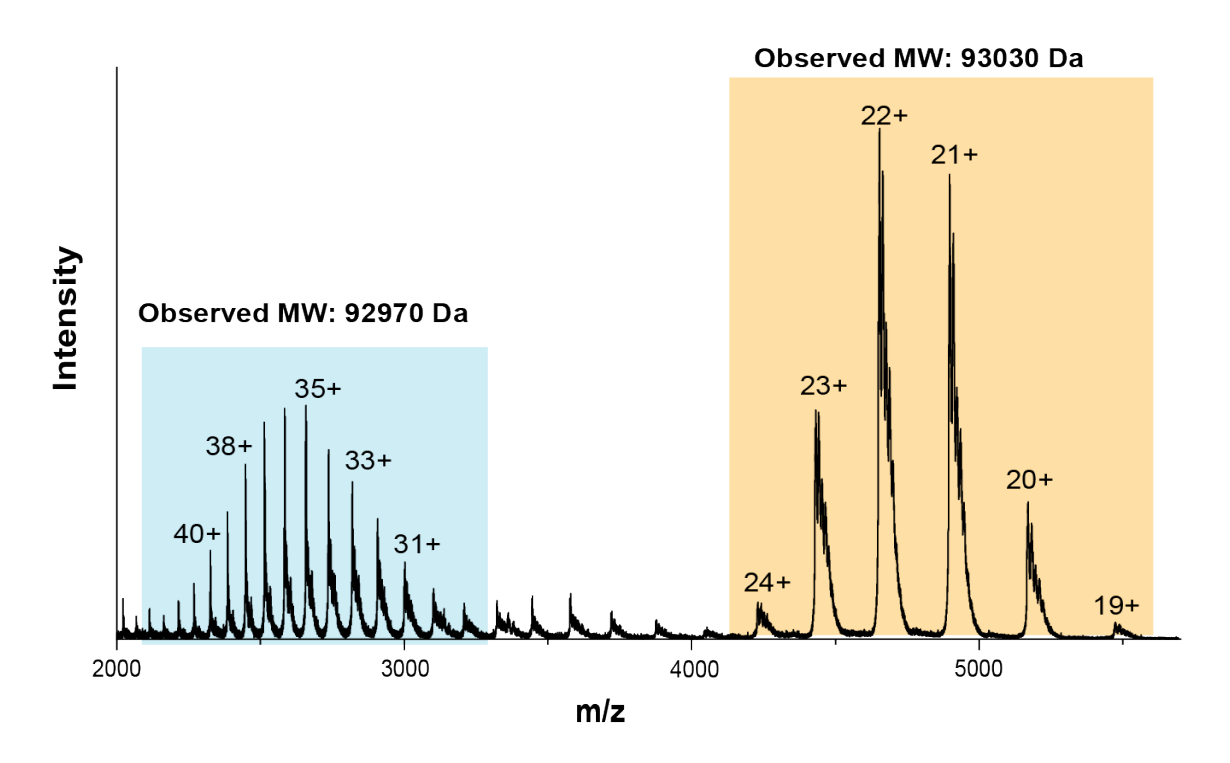


Figure 3.15. Native mass spectrometry studies of the PA-CFAS dimer. Two conformations of the PA-CFAS dimer are observed. A more compact conformation (charge states 19-24+) with a calculated solvent accessible surface area of 34,800 Å² and an apparently partially unfolded conformation (charge states 30-42+) with a calculated solvent accessible surface area of 86,590 Å². The theoretical molecular weight of the PA-CFAS dimer is 92,972 Da.

3.4.2. Biophysical characterization of PA-CFAS using hydrogen-deuterium exchange mass spectrometry (HDX-MS):

Crystal structures of EC- and LA-CFAS allowed us to visualize the folding of these enzymes and revealed the binding pocket for the lipid substrate and bicarbonate ion [104, 105]. Functional studies on EC-CFAS showed that the unstructured linker between the N- and C-domains is important for enzyme activity and was proposed to function as a hinge to facilitate substrate binding and release. This indicates that CFAS may very well be a structurally dynamic enzyme and needs to undergo different conformational changes to fulfill its catalytic cycle. Meanwhile, crystal structures only capture snapshots of static enzymes without providing any information on how CFAS moves to interact with membrane, to extract lipid and feed it to C-domain for catalysis [127]. In fact, it has been previously shown that crystalized enzymes can sometimes look very different from those in solution [127, 128]. To better understand how PA-CFAS functions in solution and to find potential allosteric regulation sites, we decide to use HDX-MS which is a powerful tool to study protein conformational dynamics in solution.

The general workflow starts with incubation of undeuterated protein sample in deuterated buffer. At desired time points, the exchange reaction is guenched by decreasing the pH to 2.5 (a detailed protocol is described in Section 4.4.). At this low pH, deuterated backbone amide undergoes very slow back exchange while deuterated amino acid side chains rapidly back exchanged to protons (with the exception of the guanidine side chains of Arg residues) [129] (Figure 3.16.). This property of the technique allows us to quantify the rate of exchange of amide protons from the protein's backbone with solvent deuterium using MS. The rate of HDX can be affected by multiple factors. For instance, when a region is less protected by hydrogen bonding, or when a region is more exposed to the solvent, deuterium is more easily accessible resulting in a faster HDX and vice versa. HDX is also enhanced in regions with higher flexibility. Enzymes are especially interesting to study by HDX because they very often contain dynamic structural elements that are important for function. During substrate binding and catalysis, enzymes often change conformation in order to complete these reactions. Upon these conformational changes, the HDX rate can be altered by the changes in local structures such as disrupting the intramolecular hydrogen bonds and exposing the backbone amides to deuterated solvent.

HDX-MS is ideal to capture these changes and resolve them with a peptide level resolution [130]. In the case of PA-CFAS, our aim is to establish an HDX-MS workflow to gain information on PA-CFAS conformational dynamics upon lipid binding.

Figure 3.16. Deuterium exchange with backbone amide hydrogen. Hydrogen bonding (dashed line) protects the hydrogen from HDX. Side chain HDX is not illustrated.

We aimed to establish an appropriate HDX-MS workflow to study PA-CFAS. The general bottom-up HDX-MS workflow involves deuterium labelling of the enzyme over a desired incubation period before quenching and freezing. These protein samples are then digested into peptides by pepsin on an HPLC column that is coupled directly to the LC-ESI-MS. Files of the mass spectra are then uploaded to ProteinLynx Global Server (PLGS) which identifies CFAS-derived peptides by matching the observed m/z of a specific peptide to the expected m/z predicted by *in silico* pepsin digestion of the CFAS protein in protonated buffer. PLGS output containing the data of all the peptides and raw MS data for deuterated samples are then uploaded to DynamX 3.0 (Waters) to quantify the amount

of deuterium uptake. Detailed methods for the HDX-MS workflow are described in Section 5.4.

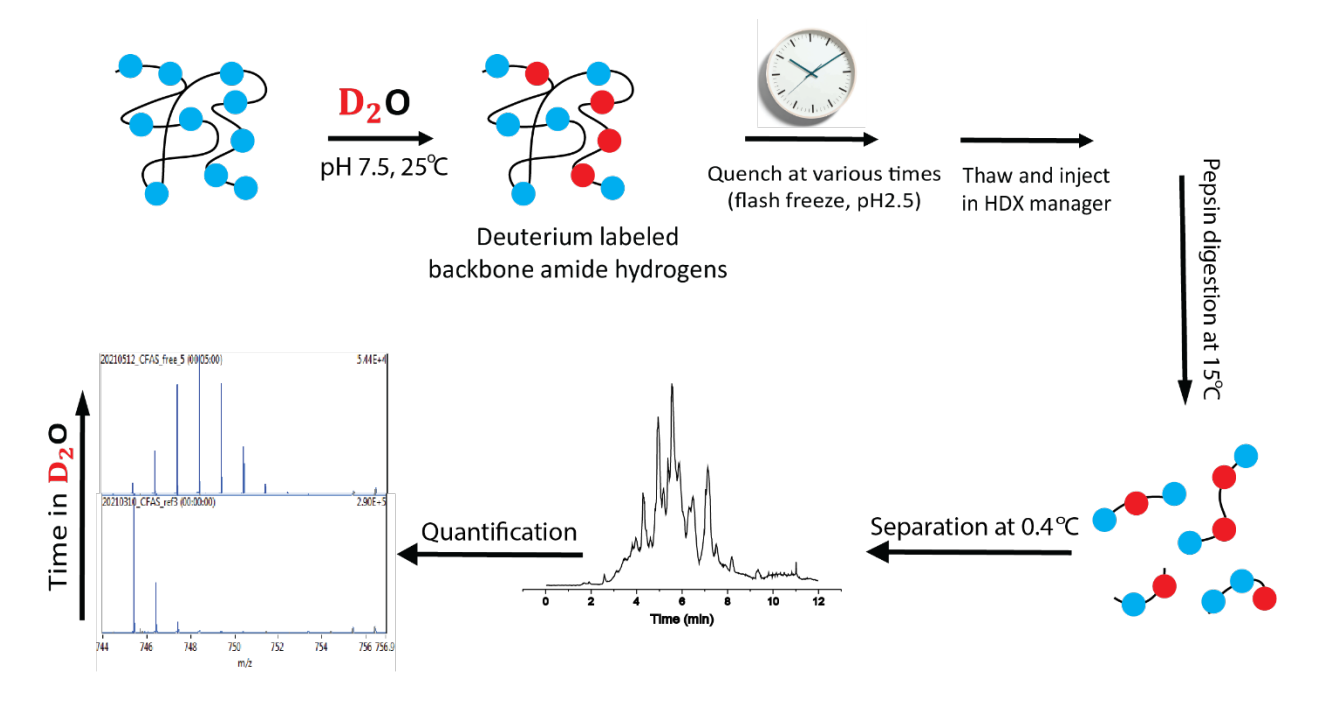
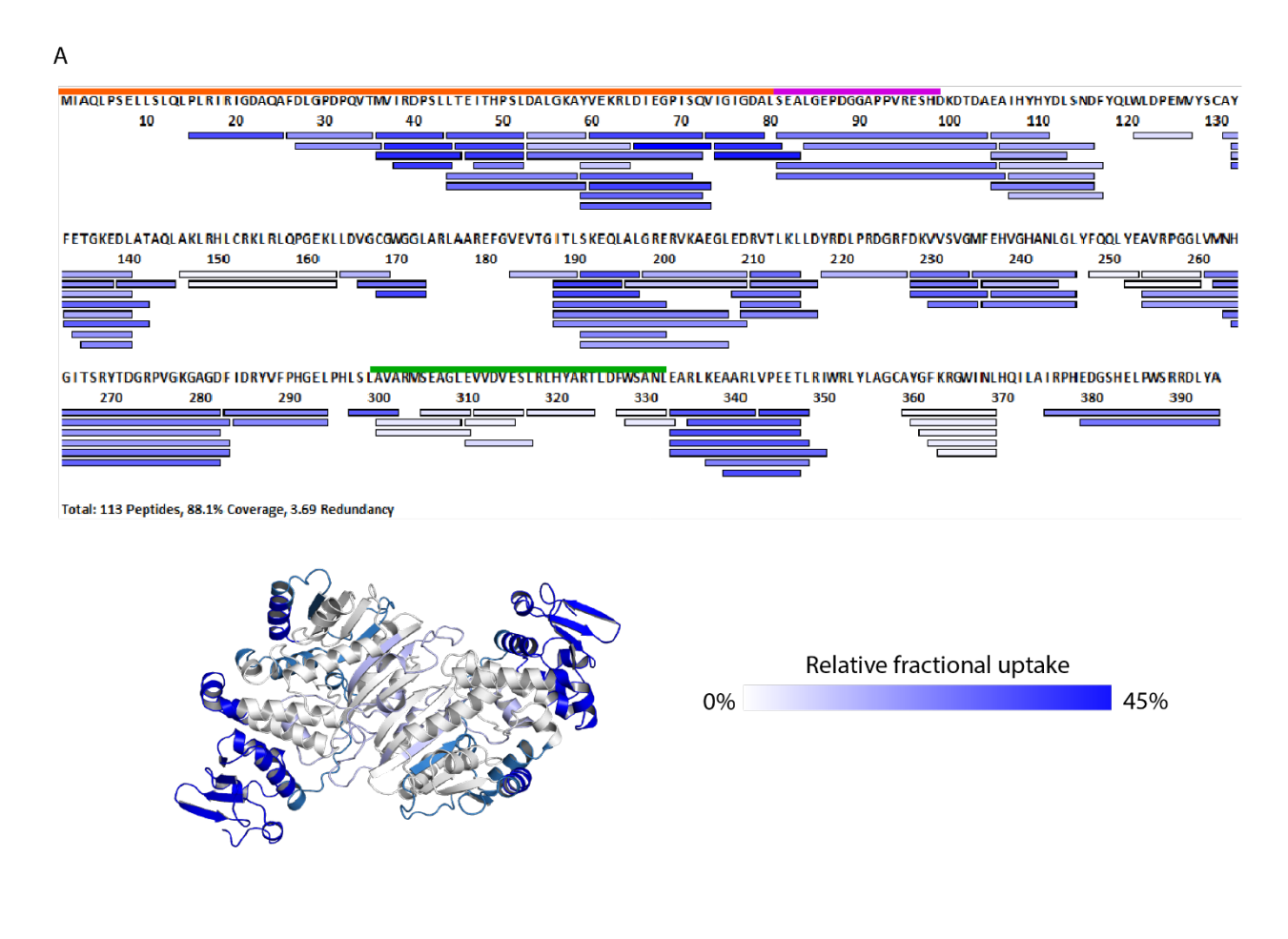


Figure 3.17. General scheme for a bottom-up HDX-MS workflow.

We first tried to generate the peptide map of PA-CFAS using the HDX-MS experimental protocol previously established by our group for HalM2 studies. This method was able to produce over 200 HalM2-derived peptides covering around 90 % of the enzyme sequence with very high reproducibility [131]. As a preliminary study, the deuterium uptake of free PA-CFAS was determined over a 5 min exchange reaction in HEPES buffer at pD 7.1. After data collection by LC-ESI-MS and data processing by PLGS and DynamX 3.0, the results showed a total of 113 peptides spanning 88.1 % of PA-CFAS with 3.69 redundancy (Figure 3.18. A). These peptides cover the important regions such as *N*-terminal lipid binding domain, the linker between *N*- and *C*-terminal domains, the active site of the catalytic domain, and the dimer interface. Moreover, the relative fractional deuterium uptake data suggest that the enzyme contains some conformationally dynamic regions in the absence of lipid substrate. Among these, the entire *N*-terminal domain (indicated by orange bar) is more dynamics with higher deuterium uptake. Since we are only testing free enzyme in this experiment, it is possible that this region needs to be more

dynamic in order to bind membranes and to extract the lipid substrate from the bilayer. The N-C linker (indicated by magenta bar) also has a good amount of deuterium uptake which suggests that it is moderately flexible. Interestingly, Glu333-lle352, a region in the catalytic domain, also appears to have high deuterium uptake. After mapping this region to the AlphaFold model of PA-CFAS, it is observed that this region directly interacts with the N-domain. As conformational dynamics is observed in the N-domain, it is possible that this property is also affecting the N-C interface. The dimer interface (indicated by green bar) remained highly structured during the 5 min of exchange reaction with very low deuterium uptake. Supporting the Native MS data described in the previous section, the protein-protein interaction for dimerization in this enzyme is indeed very strong. This is unsurprising as enzyme activity was proven to be directly related to the formation of a functional dimer in both EC-CFAS and LA-CFAS [104, 105].



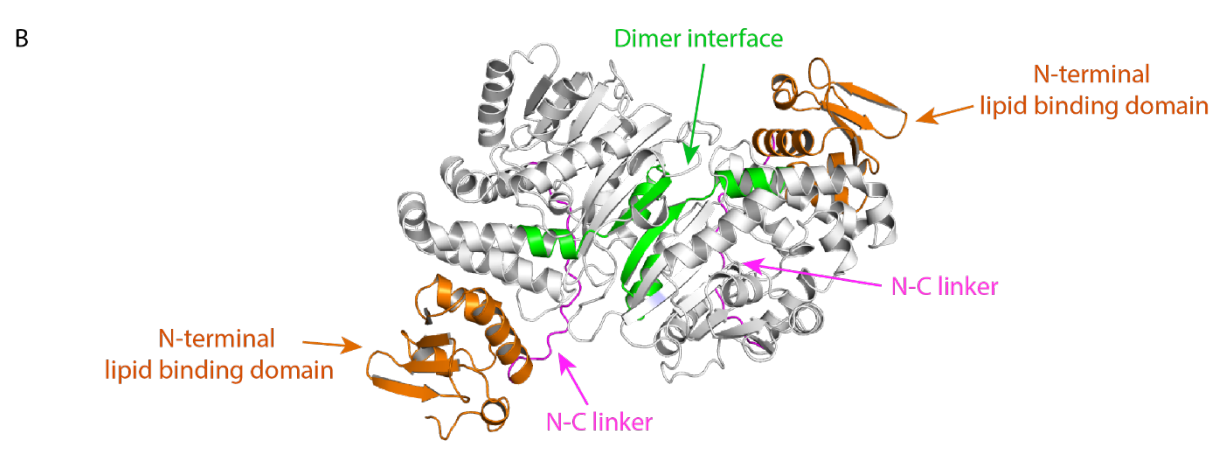


Figure 3.18. Solvent deuterium exchange properties of PA-CFAS. **A)** PA-CFAS coverage map where each bar represents a PA-CFAS derived peptide detected by MS and the coloring reflects their relative fractional uptake of deuterium. A visual representation of PA-CFAS dimer with deuterium uptake mapping. **B)** Critical regions important for enzyme activity previously reported for EC-CFAS are mapped on PA-CFAS dimer.

Since PA-CFAS exhibits maximal activity at pH 6.5 with liposomes composed of 30:70 POPE:POPG, we are curious to see if there are any pH-dependent changes in their conformational dynamics under HDX-MS. As shown in Figure X, the HDX rate decreases as pH decreases from pH 7.5 (or pD 7.1) to pH 6.5 (or pD 6.1) [132]. Due to this exchange rate differences, we need to prolong the HDX reaction time by 10 fold. For an equivalent of 5 min HDX reaction in pD 7.1, 50 min is needed to have the same amount of amide hydrogen exchanged in pD 6.1. After performing HDX-MS of free PA-CFAS with this new pD, data shows a similar pattern than pD 7.1. Dynamic regions such as N-domain and the linker remained flexible in pD 6.1, and dimer interface remained highly structured. The relative deuterium uptake in pD 6.1 is also close to pD 7.1 with this prolonged reaction time. This suggests that the overall enzyme dynamics did not change depending on pH during this HDX reaction window.

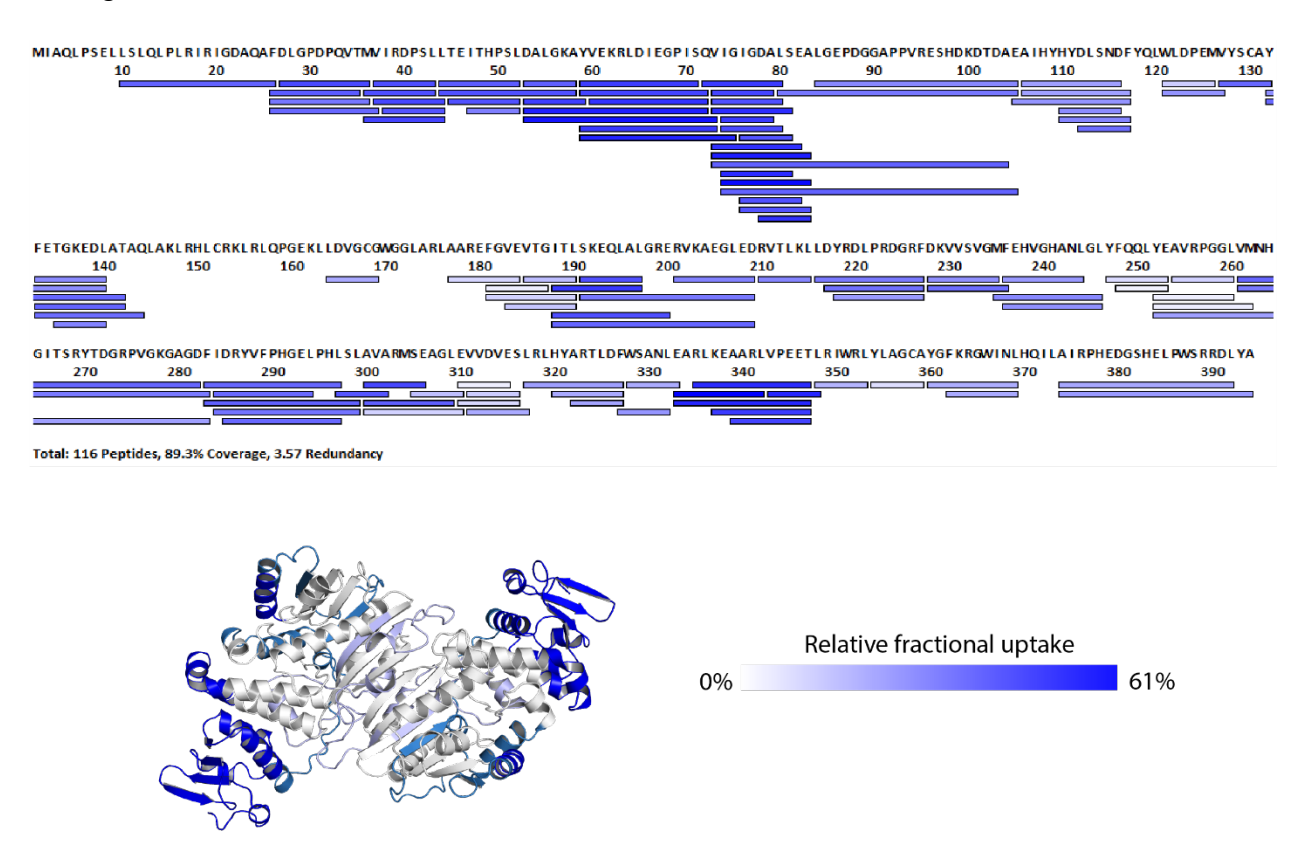


Figure 3.19. Solvent deuterium exchange properties of PA-CFAS at pD 6.1. PA-CFAS coverage map where each bar represents a PA-CFAS derived peptide detected by MS and the coloring reflects their relative fractional uptake of deuterium. A visual representation of PA-CFAS dimer with deuterium uptake mapping.

We have previously confirmed in section 3.3.3 that this enzyme still shows activity after 4 h of 37 °C incubation using the biochemical assay. In parallel, we also conducted HDX-MS to study the stability of PA-CFAS through its conformational dynamics. After a 4h preincubation at pH 6.5, the enzyme was subjected to HDX at pD 6.1 for an hour as mentioned above. After the data were processed, regions with significant HDX were determined via Deuteros 2.0. This software performs statistical tests in order to determine peptides with significant deuterium uptake differences at the 99 % confidence interval. Results showed that no peptides exhibit a significant HDX change between the freshly thawed and pre-incubated enzymes. This data confirms that PA-CFAS is indeed stable at pH 6.5 under our conditions for at least 5 h with no disruption in its overall folding. This result suggests that extensive future HDX-MS studies of PA-CFAS will be feasible.

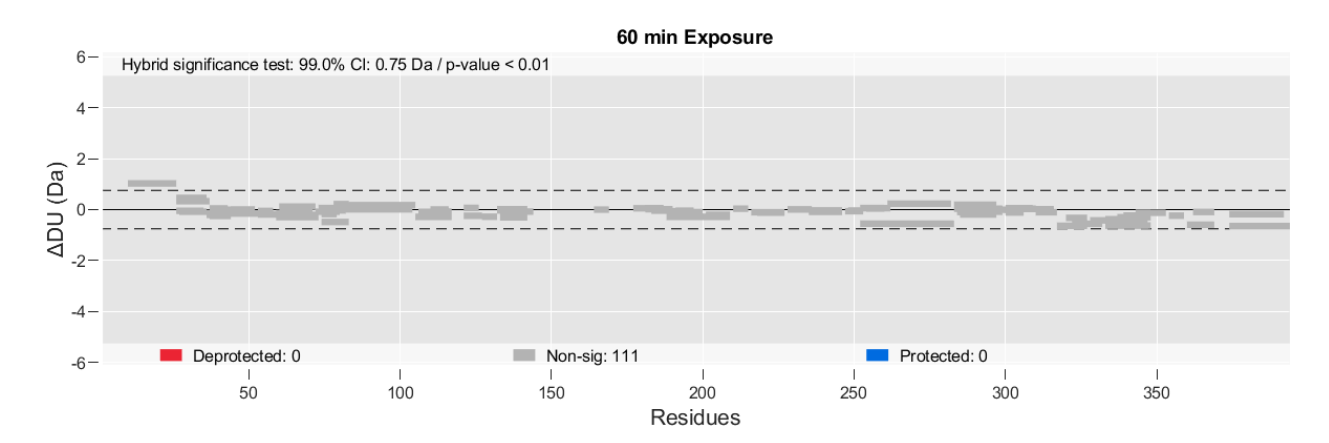


Figure 3.20. Wood plot for PA-CFAS HDX peptides that undergo significant changes (p-value <0.01) in deuterium uptake after 4 h of pre-incubation at 37 °C. No significant peptides are detected after 60 min of exposure at pD 6.1.

We then aimed to study the conformational dynamics of PA-CFAS in the presence of liposomes composed of 30:70 POPE:POPG. SAM is not included in the experiment because we want to investigate the lipid binding dependent conformational dynamics of PA-CFAS under equilibrium conditions without the interference of catalysis. We attempted to perform continuous HDX reactions of PA-CFAS at pD 6.1. Although the reaction mixture remained translucent during the HDX reaction, significant precipitation was observed upon quenching the HDX reaction. We tried to perform these reactions at a higher pD 7.1, and we also used EC-CFAS. Unfortunately, precipitates formed in all the

experiments after quenching, suggesting that the lipids are triggering precipitation at lower pH. We initially thought to remove the precipitates by centrifuging the samples prior to injection for HDX-MS analysis. However, the precipitation appears to remove the majority of the enzyme as evidenced by the weak ion signal intensity in the resulting total ion chromatogram of the LC-MS analysis (data not shown).

We then thought to alter the composition of the quench buffer to increase the solubility of the protein-lipid complex after quenching. Among the tested conditions, reactions performed at pD 7.1 have the lowest level of precipitation. For this reason, we decided to use HDX reactions at pD 7.1 for solubility optimization. The original quench buffer designed contains 0.8 M guanidine hydrochloride (GdmHCl) [131]. Luckily, by removing this component, the amount of visual precipitation in the quenched sample was significantly reduced. Aside from dropping the pH to 2.5, back exchange is also prevented by flash freezing samples in liquid nitrogen. It was observed that even though the quenched solution was clear prior to freezing, it became cloudy after the thawing step. To fully solubilize liposomes, it is possible to add a small amount of MS-compatible detergent such as dodecylmaltoside (DDM) or dodecanoyl sucrose (DDS). DDM is a mild non-ionic detergent often used to stabilize membrane protein for MS studies [133]. To determine its ability to solubilize PA-CFAS, increasing concentrations of DDM were tested. With a final concentration of 0.035% w/v DDM, the quenched reaction became fully clear. Samples containing 0.035% and 0.05% w/v DDM were subjected to HDX-MS. The intensity of TIC indeed increased and the mass spectra have peaks corresponding to peptides compared to previous results with no detergent additive. Between these two conditions, the samples with 0.05 % w/v DDM appeared to have more peptide peaks with better intensities.

Table 3.3. Effect of guench buffer conditions on PA-CFAS-liposome precipitation

Quench buffer components 100 mM KPO ₄ H + 0.8 M GdmHCl	DDM concentration (% w/v)	Precipitation		
		before freeze-thaw	After freeze-thaw	
	0	heavy	heavy	
		mild	heavy	
•	0.012	none	mild	

100 mM NaPO₄H	0.035	none	none
only	0.050	none	none

Although the addition of DDM solves the solubility issue, another problem arises when we analyze larger batch (over 20) of HDX samples containing DDM. We noticed that the intensity of the TIC starts to drop gradually as more samples are being analyzed by MS. The TIC intensity of the last sample (28th) is 10-fold lower than the first sample (Figure 3.21.). A possible explanation to this observation is due to the loss of pepsin column's performance with increasing loading of detergent [133]. However, we did not see a large peak corresponding to non-digested protein caused by this drop in pepsin activity. Therefore, it is more plausible that the accumulation of DDM somehow interferes with the ionization process resulting in poor signal intensity.

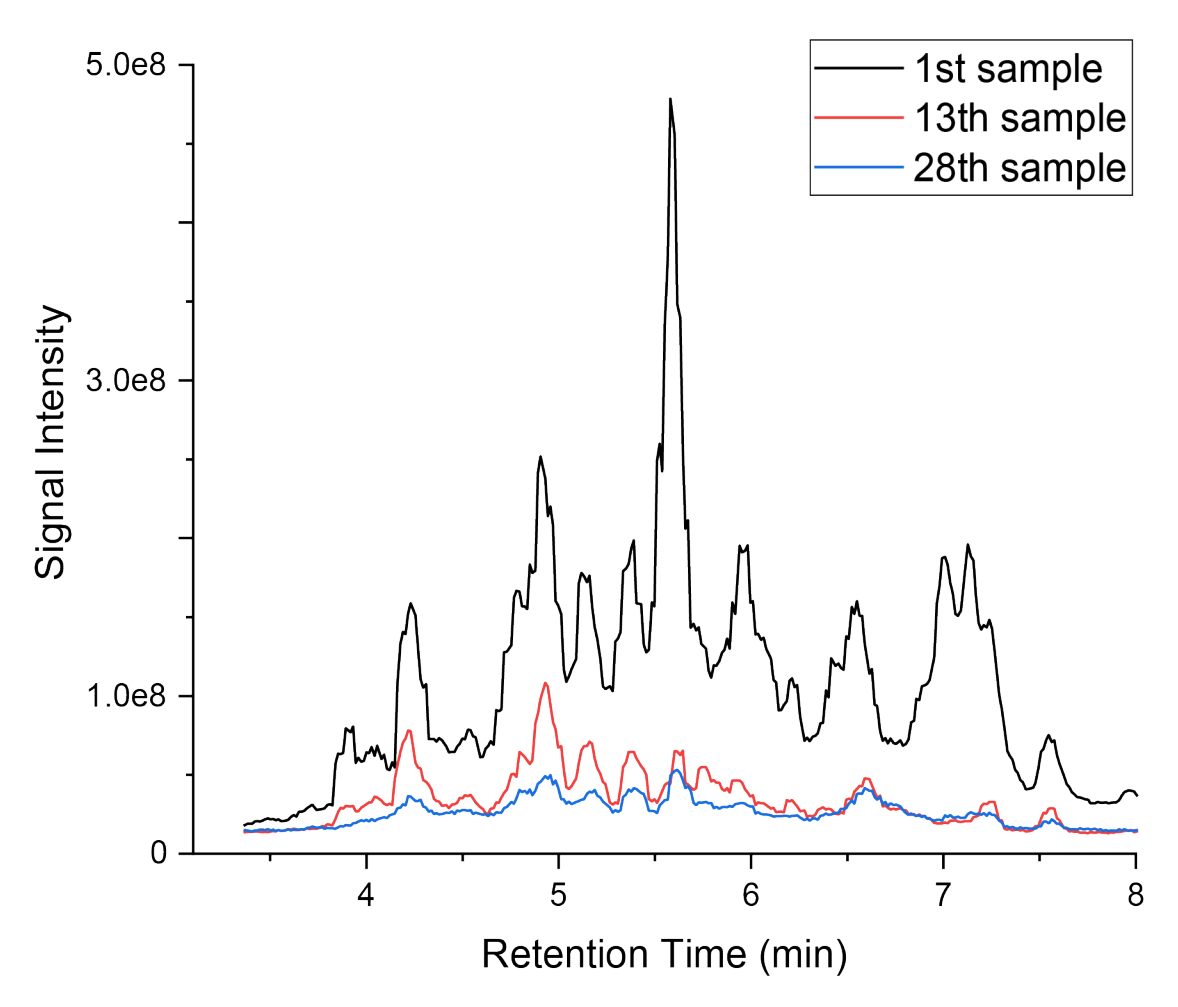


Figure 3.21. Total ion chromatograms of HDX-MS samples containing 0.05% (w/v) DDM, showing the decrease in signal intensity after many injections.

Overall, we were able to perform HDX-MS on free PA-CFAS using the traditional protocol established by our group and partially succeeded in troubleshooting the solubility issue caused by the addition of liposomes. Some future optimizations of the HDX workflow for these samples include testing other MS-compatible detergent such as DDS or using ZrO₂ HybridSPE-Phospholipid beads to remove liposomes prior to MS injections [134].

3.5. Proteomics studies of *P. aeruginosa*:

Expression of the *cfa* gene is controlled by the RpoS sigma factor and its expression is only seen in bacteria entering stationary phase [83]. Inactivation of *cfa* in different strains of bacteria leads to a reduced tolerance towards different environmental stressors. In the case of *P. aeruginosa*, Dr. Nguyen has shown that disrupting the expression of *cfa* results in increased membrane permeability. In addition, they noticed that CFAS disruption led to an increase in the expression of certain enzymes, including outer membrane porins. The exact mechanism by which the removal of CFAs from the inner membrane leads to an alteration of protein expression is not clear, but the data suggest that perturbation of CFAS activity may have a much broader effect on cell physiology. It is possible that removal of CFAs from membranes alters the biophsycial properties of the membrane (such as membrane fluidity), and that this perturbation is somehow sensed by membrane associated enzymes that then trigger a physiological response. Additionally, the altered membrane properties may affect the activity of membrane-embedded transport enzymes, leading to a perturbation of the enzymes present in the periplasm and outer membrane.

To gain a more complete understanding of the effects of CFAS deletion on cell physiology, we aimed to study the change of total protein expression in *P. aeruginosa* caused by the inactivation of *cfa* via proteomic approach. WT and *cfa* KO *P. aeruginosa* grown to exponential and stationary phases were sent as frozen pellets by Dr. Nguyen's group. Using a filter-aided protein extraction protocol [135], we subjected the extracted protein samples to trypsin digestion, followed by a bottom-up LC-ESI-MS analysis. Proteins in the sample were identified using PLGS as described in Section 5.6. This method allowed us to identify over 800 proteins with confidence from *P. aeruginosa* with high reproducibility.

We first verified the expression of the *cfa* gene in these samples. Our data show that *cfa* gene is consistently detected in all WT samples grown to stationary phase but it is not detected in *cfa* KO mutants or in WT bacteria harvested while in exponential phase. These results align with our expectations as *cfa* is only widely expressed when cells enter the stationary phase.

We then conducted statistical tests to determine significant changes in protein expression using a -log10 P-value of 2.5, which represents a confidence interval of 99.7 %. When we compared WT and cfa KO bacteria grown in stationary phase, dozens of proteins were shown to have altered expression levels (Figure 3.22.). Among these, two outer membrane related proteins were identified. OprD (Uniprot ID: P32722) is the most abundant outer membrane porin in P. aeruginosa and it is also known to be downregulated in multidrug resistant (MDR) strains. We observed a 3.3-fold upregulation of this porin in the cfa KO compared to WT. OprQ (Q91083) which is another OM porin belonging to the OprD superfamily, shows a small 1.5-fold increase in its expression in the *cfa* KO mutants. This porin was previously shown to be involved in the virulence of *P*. aeruginosa and an overexpression of this protein can lead to a sensitivity to antibiotics [136]. On the other hand, no significant changes in OprF (P13794) were observed in the cfa KO strain. Simialrly, while many other porins such as OprE (G3XDA5), OprH (G3XD11), OprM (Q51487), OprG (Q9HWW1) and several outer membrane assembly factors in the Bam family (BamB (Q9HXJ7), BamA (Q9HXY4), BamD (P33641), BamE (O68562) are all detected in this proteomic studies, none of these proteins undergoes a significant change in expression level between the WT and mutant cells.

A previous study has shown that MexS (Q9I0Z1) is involved in antibiotic resistance by promoting the transcription of the *mexAB-oprM* operon, which encodes for an efflux pump [137]. In our study, we observe a significant 6.4-fold downregulation of MexS expression in the *cfa* KO mutants. However, since we did not observe any significant differences in OprM expression, MexS may contribute to antibiotic sensitivity via some other unknown routes. Another protein with significant downregulation is YcaC (Q9I4D6) which is a putative cysteine hydrolase. The precise biological function YcaA remains unclear, but related prokaryotic proteins are thought to be involved in drug resistance [138]. In the *cfa*

KO mutant, this protein has a near 8-fold decrease in its expression. These results suggest that by knocking out *cfa* gene, the upregulation of OprD and OprQ, in combination with the downregulation of YcaC and MexS may play a role in the increased OM permeability and antibiotic susceptibility in *P. aeruginosa*.

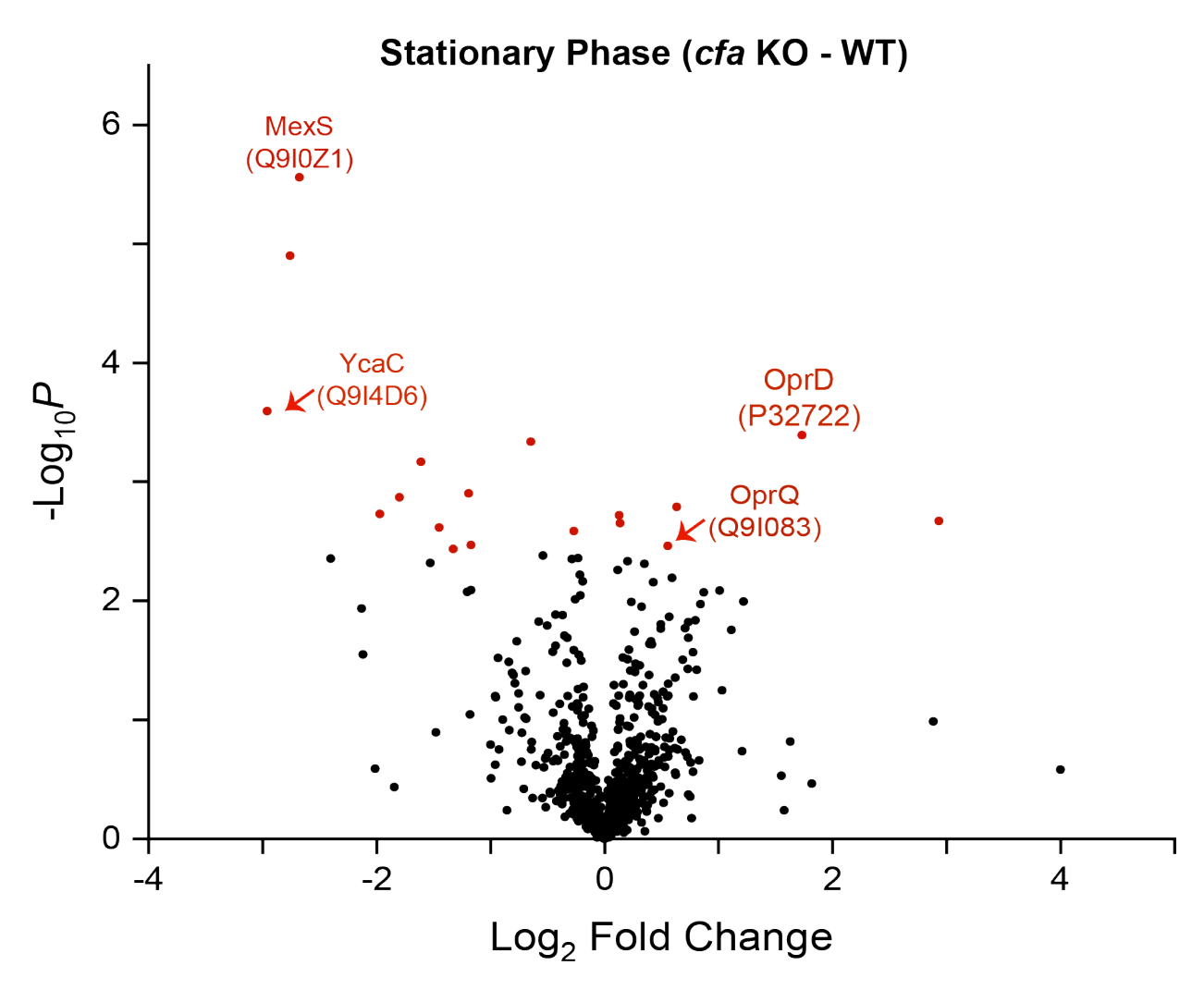


Figure 3.22. Volcano plot of protein expression changes between WT and *cfa* KO *P. aeruginosa* during stationary growth. Each dot represents a detected protein. Red dots represent proteins with significant changes determined by a -Log₁₀ $P \ge 2.5$. A positive fold-change indicates an upregulation of protein expression in the *cfa* KO strain and a negative fold-change indicates a downregulation.

When we compared bacteria grown in exponential phase, the results showed an opposite trend where OprD expression was significantly downregulated in *cfa* KO compared to WT (9.8-fold). This is quite surprising as we did not expect the gene KO to have an impact on

exponentially growing bacteria. LptF (Q9HXU8), which is an OmpA-like OM protein also shows a small downregulation (near 2-fold) in the mutant bacteria. This protein was previously shown to play a role in the resistance of oxidative stress[139]. On the opposite end, the cysteine hydrolase YcaC has a 39-fold increase in protein expression in the *cfa* KO strain.

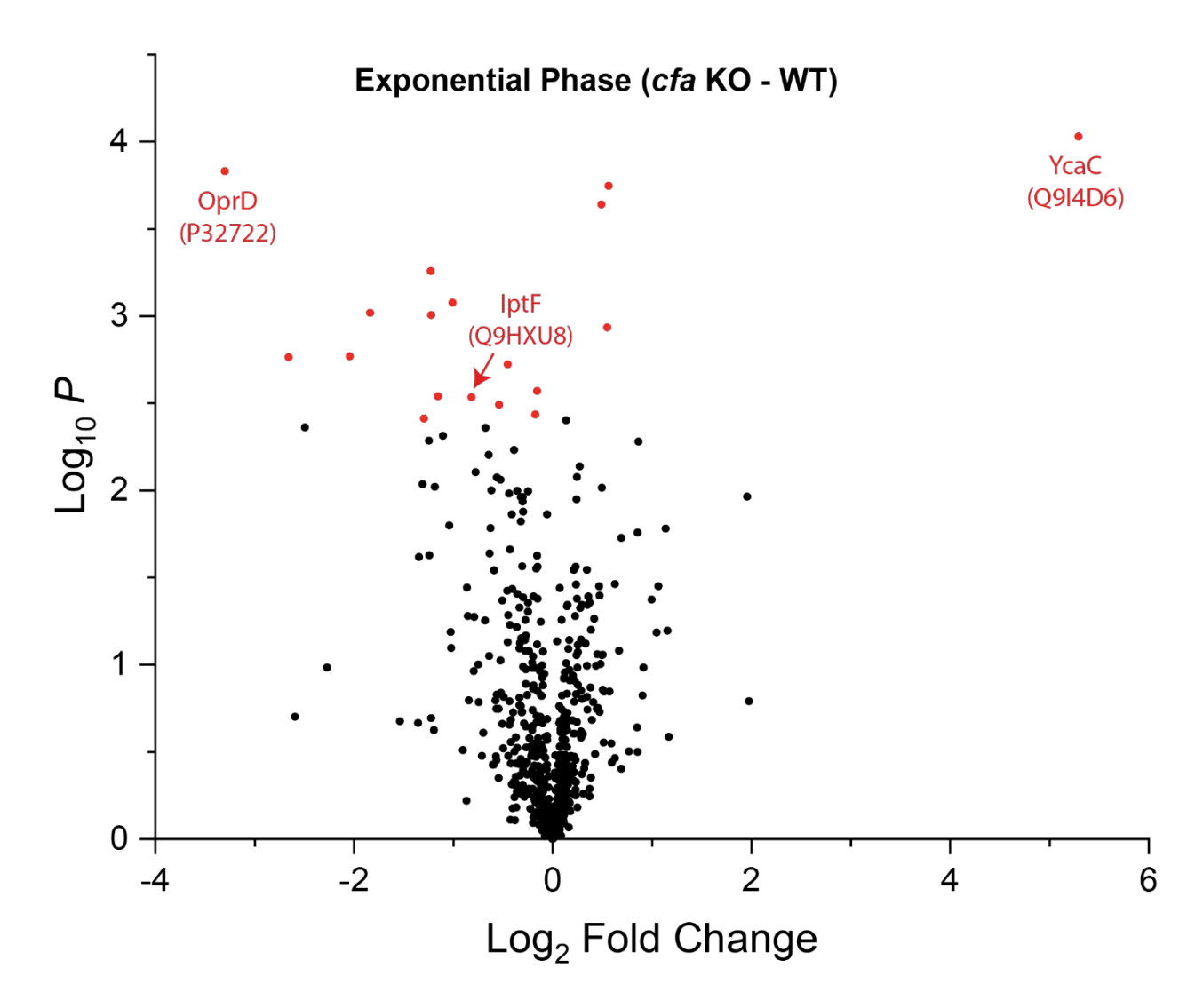


Figure 3.23. Volcano plot of protein expression changes between WT and *cfa* KO *P. aeruginosa* during exponential growth. Each dot represents a detected protein. Red dots represent proteins with significant changes determined by a $-\text{Log}_{10}P \ge 2.5$. A positive fold-change indicates an upregulation of protein expression in the *cfa* KO strain, and a negative fold-change indicates a downregulation.

In brief, our proteomics data showed that there are indeed differences in the global protein expression between the WT and *cfa* KO strain of *P. aeruginosa*. When cells entered stationary phase, there is upregulation in some of the OM porins (OprD and OprQ) and downregulation in genes promoting efflux pump activity (MexS). The proteomic profile is completely different in bacteria grown in exponential phase indicating the changes that we observed are growth stage specific and likely contribute to the increase membrane permeability phenotype.

3.6. Lipidomics studies of *P. aeruginosa*:

3.6.1. Fatty acid methyl esters (FAMEs) analysis using GC-MS:

Similar to our goal in the proteomics studies, we wanted to study the change in total phospholipid profile between WT and cfa KO P. aeruginosa using lipidomics approaches. P. aeruginosa fatty acids were obtained directly from freeze-dried cell pellet via saponification and were then converted into fatty acid methyl esters (FAMEs) by methylation using a mixture of methanol and acetyl chloride. Gas chromatography mass spectrometry (GC-MS) was used to analyze the fatty acids composition in WT and cfa KO bacteria at stationary growth phase. A total of 8 types of both unsaturated and saturated fatty acids are observed in WT and a total of 6 types are observed in the KO mutant. The complete list of detected FAMEs and their abundance are listed in Table 3.4. Compared to previous studies on planktonic P. aeruginosa, some of the low abundance FAs are not detected in our experiment [79, 140]. Another limitation in our study is that we cannot separate *cis*- and *trans*-isomers of FAs since they have the same retention time. According to our result, saturated C16:0 and unsaturated C18:1 are the two most abundant fatty acids in both WT and cfa KO strains. As proteomics studies confirmed that CFAS protein expression is not detected in the mutants, FAMEs analysis shows that the cyclopropane containing FAs, C17:0cyc(9,10) and C19:0cyc(11,12), are only present in WT. As expected, WT has a slightly lower abundance in C16:1 and C18:1 which are the precursors for C17:0cyc(9,10) and C19:0cyc(11,12), respectively. In addition, a small increase in the abundance of shorter chain FAs, C12:0 and C14:0, is observed in the mutant. Since the FAMEs are derivatized from cell pellet, it is possible that these FAs have origins other than PLs such as lipoproteins and lipopolysaccharides. To obtain a better understanding of the PL profile, we developed an LC-ESI-MS approach.

Table 3.4. Abundance of various fatty acids in WT and *cfa* KO *P. aeruginosa* cells as detected by GC-MS analysis.

Fatty acid	cfa KO	WT
C12:0	1.88%±0.67%	1.34%±0.5%
C14:0	1.37%±0.38%	0.51% <u>+</u> 0.17%
C16:1	8.5% ±0.34%	5.6% ±0.4%
C16:0	39.2% ±1.4%	$37.8\% \pm 0.93\%$
C18:1	47.6% ±0.6%	43.5% ±1.6%
C18:0	1.5% ±0.5%	0.8% ±0.07%
C17:0 cyc (9,10)	0%	1.5% ±0.2%
C19:0 cyc (11,12)	0%	9.1% ±1.1%

3.6.2. Phospholipid profile analysis using LC-ESI-MS:

The total PLs were extracted from cell pellets of WT and *cfa* KO mutant using the Bligh and Dyer protocol and the lipid film was then resuspended in solvent A containing 60 % acetonitrile (ACN), 40 % 10 mM ammonium formate, 0.1% formic acid for LC-ESI-MS analysis. We attempted to perform some preliminary lipidomics studies in positive ion mode. Using a previously reported list of phospholipids from *P. aeruginosa* [79, 121], we manually searched for the [M+H]⁺ ion corresponding to each lipid and quantified their abundance from the chromatographic peak area using the QuanLynx function of MassLynx. As an initial result, we were able to identify the large majority of phosphatidyl ethanolamine (PE) and phosphatidyl choline (PC) lipids with various lengths of fatty acyl chains (Table 3.5.). PG lipids were not detected in this initial study because they carry a net negative charge and will only be detected when negative ion mode is applied. PLs are denoted as C:U where C is the total number of carbon atoms in the aliphatic chains and U is the amount of unsaturation. An unsaturation can be due to the presence of a double bond or a cyclopropane ring. Thus, more than one isomer can exist with the same m/z value. The exact configuration of these isomers can be verified using MS/MS, but as

an initial study, it was not used in this experiment. Although MS/MS is not used, we can still determine whether multiple species exist with the same m/z by extracting the chromatogram of a specific m/z value. Among the detected lipids, there are several with potential cyclopropanated species. For example, PE 36:2 (m/z 744.48) can either contain two C18:1 chains or a combination of C17:0cyc and C19:0cyc. When we extracted the chromatogram with the m/z value of 744.48, two peaks appeared in the WT lipid extract whereas only one peak was observed in the *cfa* KO strain (Figure 3.24.). Out of the two peaks, the one with a retention time of 20.87 min is common in both samples which suggests that it is the isomer with two C18:1 fatty acyl chains. In contrast, the species that eluted at 21.27 min is unique to the WT sample, suggesting it could be a cyclopropanated lipid. Using this method, we were able to identify several peaks that are present in the WT but that are absent in the *cfa* KO strain (Table 3.5.).

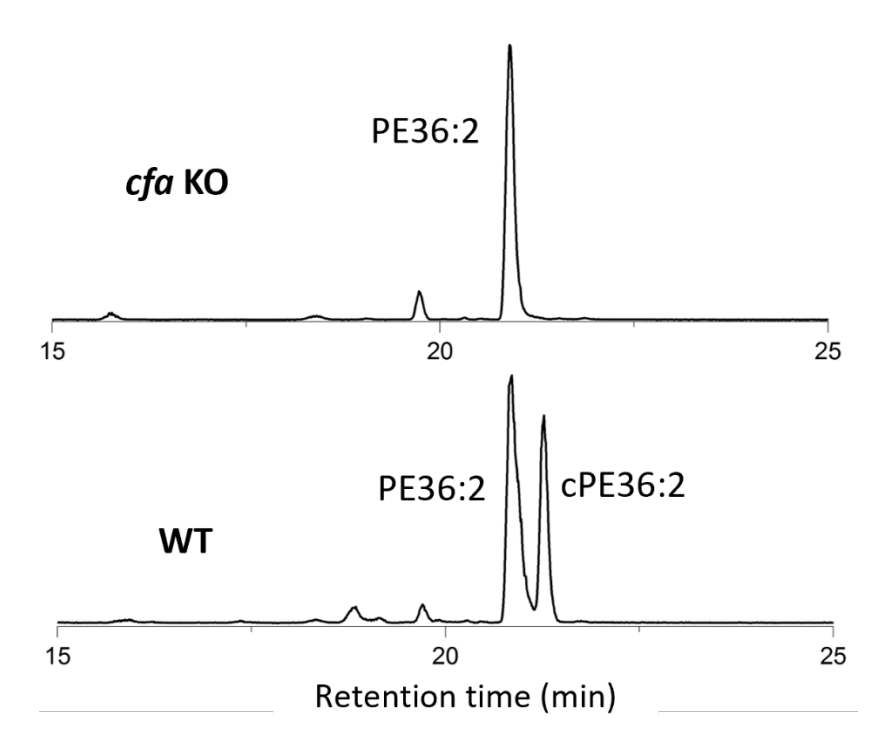


Figure 3.24. Example of an extracted ion chromatogram for 744.48 m/z. WT shows two peaks at the same m/z value while *cfa* KO shows only one peak suggesting the non-overlapping peak is potentially a cyclopropanated species.

In terms of other lipid species, there aren't any significant changes between these two samples. For unsaturated lipids that are precursors of cyclopropanated species, we obtained mixed result. PE 32:1, PE 35:1 and PE 34:1, which are potential precursors for cPE 33:1, cPE 36:1 and cPE 35:1 respectively, shows a greater abundance in the *cfa* KO strain compared to WT. While PC 34:1 and PE 34:2, which are potential precursors for cPC 35:1 and cPE 36:2 showed a decreased abundance in the *cfa* KO strain.

Table 3.5. Abundance of PC and PE with various lengths in WT and *cfa* KO *P. aeruginosa* cells.

PL	[M+H] ⁺	retention	Potential fatty acid	WT	cfa KO
	m/z	time (min)	combination (sn1 + sn2)	(%)	(%)
PC 32:1	732.47	19.3	16:0 + 16:1	5.6	3.9
			14:0 + 18:1		
PC 32:0	734.49	20.36	16:0 + 16:0	2.6	3.04
			14:0 + 18:0		
PC 34:2	758.49	19.42	16:1 + 18:1	12.8	15.1
PC 34:1	760.5	20.44	16:1 + 18:0	14.0	10.9
			16:0 + 18:1		
PC 34:0	762.5	21.36	16:0 + 18:0	0.5	0.8
cPC 35:1*	774.54	21.12	16:0 + 19:0cyc	4.7	0.2
PC 36:2	786.5	20.49	18:1 + 18:1	1.0	1.0
PE 30:1		17.7	14:0 + 16:1	0.06	0.28
PE 32:1	690.51	19.8	16:0 + 16:1	7.7	15.1
			14:0 + 18:1		
PE 32:0	692.52	20.73	16:0 + 16:0	1.1	2.1
			14:0 + 18:0		
PE 33:1	704.52	20.26	CH3-16:0 + C16:1	0.97	0.90
cPE 33:1*		20.47	16:0 + 17:00:0	1.4	0
			16:0 + 17:0cyc		
PE 34:2	716.52	19.91	16:1 + 18:1	8.2	5.8
PE 34:1	718.54	20.83	16:1 + 18:0	14.8	18.7
			16:0 + 18:1		
PE 34:0	720.55	21.87	16:0 + 18:0	0.15	0.78

cPE 35:2*	730.54	20.54	16:1 + 19:0cyc	7.4	0.4
			17:0cyc + 18:1		
PE 35:1	732.55	19.3	CH3-16:0 + 18:1	7.2	12.2
cPE 35:1*	732.55	21.5	16:0 + 19:0cyc	3.7	0.18
PE 36:2	744.48	20.87	18:1 + 18:1	2.8	5.5
cPE 36:2*	744.48	21.27	17:0cyc + 19:0cyc	1.6	0
PE 36:1	746.49	19.95	18:0 + 18:1	0.96	1.8
cPE 36:1*	746.49	20.12	CH3-16:0 + 19:0cyc	0.93	0

Overall, we were able to observe some interesting changes in the PL profile of the *cfa* KO strain of *P. aeruginosa* using GC-MS and LC-ESI-MS. The most obvious change is the absence of cyclopropanated species in the KO strain compared to WT. Some minor changes caused by the loss of CFAs production include an increase of monounsaturated fatty acid precursors C16:1 and C18:1. In terms of total lipid change, similar to FAMEs study, those PLs potentially containing the CFAs in one or both chains significantly disappear in the KO strain which confirms the loss of CFAS function. Interestingly, a very low level of some potential CFAs containing lipids (cPC 35:1, cPE 35:1 and cPE 35:2) are still detected in the *cfa* KO mutant. This may be due to incomplete gene KO or they represent completely different lipid species. This implies that MS/MS analysis is required to determine the identity of these peaks in future studies. Lastly, negative ion mode also needs to be used down the line to detect negatively charged lipids such as PG.

4.0. Conclusion and future perspective:

In this study, the CFAS enzyme from P. aeruginosa was characterized using an $in\ vitro$ colorimetric assay and its structural information was revealed using native MS and HDX-MS methods. Using lipids extracted from PA cells, the PA-CFAS exhibited maximal activity at pH 6.5 while at pH 7.5, PA-CFAS activity is completely abolished. The attempts to optimize enzymatic activity at pH 7.5 were all unsuccessful which suggest that with native lipids, the PA-CFAS strongly prefers a lower pH compared to other characterized CFAS homologs such as EC-CFAS and LA-CFAS [105, 112]. Using different ratios of POPE:POPG, we were able to determine the effect of lipid headgroups on the activity of PA-CFAS. At pH 6.5, PA-CFAS has maximal activity from 30-70% POPE. However, this trend of headgroup preference shifts towards membranes with less POPE at pH 7.5 (maximal activity at 15% POPE). At pH 7.5, no activity is detectable with membranes containing more than 50% POPE. The kinetic parameters reveal that both K_m and k_{cat} doubled at pH 6.5 compared to pH 7.5 which makes the overall catalytic efficiency (k_{cat}/K_m) the same at each pH. Compared to EC-CFAS and LA-CFAS, PA-CFAS is roughly 14-fold slower than the former and 4-fold slower than the latter.

In the case of structural analysis, PA-CFAS is predicted to have a similar fold and dimer structure as compared to EC-CFAS using the AlphaFold server. Active site residues involved in stabilization of the putative carbocationic transition state are also conserved. Native MS confirms that PA-CFAS forms a dimer in solution and shows that the dimerization is strong enough to survive the desolvation process in the MS instrument. HDX-MS analysis of the free PA-CFAS reveals that the dimer interface is well protected from the solvent with a low level of exchange, while the N-domain and the N-C linker are very flexible in the absence of lipid binding. These flexible regions may become more rigid once the enzyme interacts with its lipid substrate, or as conformational changes occur during catalysis. Precipitation presented a challenge to the HDX workflow, but the problem was partially solved by including an MS-compatible detergent, DDM, in the quenched HDX reaction mixtures. The drop in MS signal intensity over time indeed requires further efforts to trouble shoot before the HDX-MS workflow will be viable. The

use of an alternative detergent such as DDS or of phospholipid beads to remove lipids prior to quenching may be considered in the future optimization of the HDX workflow.

In addition, the effect of cfa gene KO on the overall proteome and lipidome change in P. aeruginosa was investigated using LC-ESI-MS and GC-MS approaches. We have established a robust protocol for proteomic studies which reveals some significant changes in protein expression between WT and the KO strains. During stationary phase, the cfa KO strain shows an upregulation of two outer membrane porins and genes potentially involved in drug resistance are downregulated which supports the observation from Dr. Nguyen's group described in Section 1.5.4. Interestingly, these changes are phase specific as the trend is not observed in exponential phase. Fatty acid methyl ester (FAME) analysis by GC-MS and phospholipid (PL) analysis by LC-MS are the two routes we used to study total lipidome changes. As expected, a significant loss of potential cyclopropanated species and an increase in their unsaturated precursors are observed in the cfa KO strain using both approaches. Although FAMEs analysis showed no detectable level of CFAs in the KO strain, PL profile has small peaks corresponding to potential CFA-containing lipids. To confirm whether these are indeed CFA-containing lipids and to distinguish PL isomers, MS/MS will be incorporated into the workflow in future work. Negative ion mode of LC-ESI-MS will also be applied in parallel to positive ion mode to detect negatively charged phosphatidyl glycerol lipids. In brief, we provided some insights to why the loss of cfa potentiates membrane permeability and offered more confidence in validating PA-CFAS as a potential drug target.

As a final note, we are the first group to study the PA-CFAS *in vitro* and demonstrated that, despite some challenges, HDX-MS can be a great tool to study conformational dynamics of this soluble enzyme and understand how it interacts with its hydrophobic substrate. From this point on, motifs with significant alterations in deuterium uptake may be investigated by site-specific mutagenesis. Gaining additional structural insights of this target can eventually facilitate the downstream drug discovery and development for treating *P. aeruginosa* related infections.

5.0. Methods:

5.1. Protein Expression:

- **5.1.1. Expression of** *P. aeruginosa* and *E. coli* CFAS enzyme: 3 L of Luria-Bertani (LB) broth was first prepared and autoclaved. A 30 mL overnight culture was grown using *E. coli* C43 containing the plasmid pET16b with the gene of *P. aeruginosa* or *E. coli* CFAS enzyme and 100 µg/mL ampicillin. This culture was allowed to grow for 18 h at 37 °C with shaking. The following morning, fresh ampicillin stock and the 30 mL overnight culture were added to the 3 L LB broth. This large-scale bacterial culture was allowed to grow at 37 °C with shaking until bacteria reached exponential phase. When the OD600 reached ~ 0.7 , protein expression was induced by the addition of isopropyl β-D-1-thiogalactopyranoside (IPTG) to a final concentration of 0.5 mM. The culture was allowed to grow for 3 h at 30 °C after IPTG induction. The cells were collected using a floor centrifuge at $5000 \times g$ for 30 min at 4 °C and stored at -80 °C for future purification.
- **5.1.2. Expression of** *E. coli* **SAH nucleosidase enzyme:** A 20 mL overnight culture was grown using *E. coli* BL21 containing pET16b with SAH nucleosidase gene and 100 μ g/mL ampicillin. This culture was allowed to grow for 18 h at 37 °C with shaking. A large-scale culture was grown by inoculating the 20 mL overnight culture in 2 L of LB broth with fresh ampicillin and it was allowed to grow until OD₆₀₀ reached ~ 0.7. IPTG was added to a final concentration of 0.5 mM to induce protein expression. This culture was allowed to grow for 18 h at 18 °C before collecting the cells at 4 °C using a floor centrifuge at 5000 x g for 30 min. Cells were stored at -80 °C.
- **5.1.3. Expression of** *E. coli* LuxS enzyme: A 40 mL overnight culture was grown using *E. coli* C43 containing the plasmid pET22b-LuxS and 100 μ g/mL ampicillin. This culture was allowed to grow for 18 h at 37 °C with shaking. A large-scale culture was grown by inoculating the 40 mL overnight culture in 4 L of LB broth with fresh ampicillin and it was allowed to grow until OD₆₀₀ reached ~ 0.7. IPTG was added to a final concentration of 0.1 mM to induce protein expression. This culture was allowed to grow for 5 h at 30 °C before collecting the cells at 4 °C using a floor centrifuge at 5000 x *g* for 30 min and stored at -80 °C.

5.2. Protein Purification:

- 5.2.1. Purification of P. aeruginosa (Uniprot: Q9HT28) and E. coli CFAS enzyme (Uniprot: P0A9H7): The frozen pellet was first resuspended in 100 mL lysis buffer (50 mM Tris, pH 8.0, 100 mM NaCl, 10 % glycerol, 20 mM Imidazole) and 0.1 mg/mL of lysozyme and was mixed for 10 min at 4 °C. The mixture was then sonicated for 15 min (4.4 s pulse, 8.8 s between pulses) and was centrifuged at 15,000 rpm for 45 min to remove the cell debris from the supernatant. The supernatant was loaded on a HisTrap FF column pre-equilibrated with the lysis buffer and was washed with 10 column volume of the lysis buffer. The protein was eluted with a linear gradient of elution buffer (50 mM Tris, pH 8.0, 100 mM NaCl, 10 % glycerol, 300 mM Imidazole) from 0 to 100 % in 60 min using a BioRad NGC Quest 10 Fast Protein Liquid Chromatography (FPLC) instrument with a flow rate of 1.5 mL/min. Fractions of 5 mL containing the protein were pooled together, concentrated and further purified using size exclusion chromatography with a HiLoad 16/600 Superdex 200 prep grade gel filtration column. Proteins were eluted isocratically in gel filtration buffer (50 mM HEPES, pH 7.5, 100 mM NaCl, 10 % glycerol, 1 mM DTT) at a flow rate of 1 mL/min. Final protein fractions were aliquoted, flash frozen with liquid nitrogen and stored at -80 °C. Protein concentration was determined by loading 2 μL of the protein sample to the nanodrop. The concentration was then calculated by using the calculated extinction coefficient of the protein at 280 nm.
- **5.2.2. Purification of** *E. coli* **SAH nucleosidase enzyme:** The purification method followed the protocol described in the previous section with the following modifications. The lysis buffer contained 50 mM sodium phosphate, pH 7.5, 20 mM imidazole. The elution buffer contained 50 mM sodium phosphate, pH 7.5, 250 mM imidazole. The gel filtration buffer contained 50 mM HEPES, pH 7.5, 300 mM KCl and 10 % glycerol.
- **5.2.3. Purification of** *E. coli* **LuxS enzyme:** The purification method followed the protocol described in the section 5.2.1. with the following modifications. The lysis buffer contained 20 mM Tris, pH 8.0, 500 mM NaCl, 5 mM imidazole. The elution buffer contained 20 mM Tris, pH 8.0, 500 mM NaCl, 5 mM imidazole. The gel filtration buffer contains 20 mM HEPES, pH 7.5, 300 mM KCl and 10 % glycerol.

5.2.4. Verification of protein mass using LC-ESI-MS: All samples were analyzed on a Waters Synapt G2-Si instrument. An aliquot of the frozen protein was gently thawed on ice and diluted to 2 µM in solvent A (water with 0.1 % formic acid). 10 µL of the sample was injected into an ACQUITY UPLC Protein C4 column (300 Å x 1.7 µM x 150 mm) preequilibrated in 5 % solvent B (ACN with 0.1 % formic acid) for chromatographic separation. Protein was eluted with a linear gradient of 10 to 100 % B over 20 min with a flow rate of 50 μL/min. The sample was then ionized by electrospray ionization (ESI) using a capillary voltage of 3 kV, a sampling cone voltage of 40 V, a source offset voltage of 80 V and a source temperature of 100 °C. The mass spectrometer was initially calibrated using 3 mg/mL of NaI in 50:50 v/v water:isopropanol. The mass spectra were collected in positive ion sensitivity mode in the range of 100-2000 m/z with 1 scan per second. [Glu-1]fibrinopeptide B (GluFib) was used as an external standard. The mass of the protein was determined using the MaxEnt1 function of MassLynx software by Waters with the following parameters: resolution was 10.00 Da, uniform gaussian damage model width at half height was 1.00 Da, minimum intensity ratio was 33 % for both left and right. Ions in multiple charge states were deconvoluted to their [M+1]¹⁺ charge state.

5.3. CFAS activity assay:

5.3.1. Liposome preparation: All lipids (either purchased from Avanti polar lipids or extracted from *P. aeruginosa*) were first dissolved in chloroform. Lipids were mixed in the desired molar ratio and the chloroform was removed using a dry nitrogen stream. The remaining solvent was removed under vacuum for at least 2 h. The resulting lipid film was resuspended in water to a final concentration of 10 mg/mL. The lipid mixture was quickly frozen in lipid nitrogen and thawed in a water bath with a temperature higher than the phase transition temperature of the working lipids with occasional vortexing. The freeze/thaw cycle was repeated 5-times to properly hydrate the lipids. Once the lipids were hydrated, the mixture was extruded 21-times using the Avanti Extruder Set through a 100-nm membrane filter. The extruded liposomes are unilamellar vesicles suited for further CFAS biochemical assays.

- **5.3.2.** *P. aeruginosa* membrane lipid extraction: 250 mL of LB broth was first prepared and autoclaved. Then, a 5 mL overnight culture of P. aeruginosa PAO1 dsm19880 was grown at 37 °C. On the following day, 2.5 mL of the overnight culture was used to inoculate the large scale 250 mL culture. The culture was allowed to grow at 37 °C until OD₆₀₀ reached 0.7, indicating the cells had entered exponential phase. The cells were then pelleted for 10 min at 5000 x g using a bench-top centrifuge. The pelleted cells were washed twice using 1 mL of Milli-Q water and membrane lipids were extracted following the Bligh-Dyer lipid extraction protocol [115]. The washed lipid pellets were first resuspended in Milli-Q water to a total volume of 1 mL. We then added 1.25 mL of Chloroform and 3.5 mL of methanol to the cell suspension to obtain a water/chloroform/methanol ratio of 0.8/1/2. The mixture was vortexed for 15 min before the addition of 1.25 mL of chloroform. After vortexing continuously for 10 min, 1.25 mL of 1 M sodium chloride (NaCl) was added to the sample and vortexed for an additional 10 min. The mixture was centrifuged at 4000 x g for 2 min to allow better separation of the organic and aqueous layer. The organic layer, (bottom) layer, was collected. For better yield, the aqueous (top) layer was re-extracted with 1.25 mL of chloroform. The combined organic layer was dried under dry nitrogen stream which resulted in a lipid film.
- **5.3.3.** *P. aeruginosa* **cell lysate preparation:** 5 mL overnight and 10 mL log phase *P. aeruginosa* cultures were prepared and cell pellet was washed in 20 mM HEPES, pH 7.5 twice before the final resuspension in the same buffer. The cell suspension was sonicated for 5 min followed by centrifugation (13000 rpm for 5 min). The supernatant was collected and added directly to the assay mixture.
- **5.3.4. Standard spectrophotometric assay for CFAS:** For measuring the enzymatic activity of CFAS, we adapted the discontinuous colorimetric assay developed by Guianvarc'h et. al. where the *S*-adenosyl-L-homocysteine (SAH) product of the CFAS-catalyzed reaction is enzymatically converted to L-homocysteine (Hcy) via the combined action of *S*-adenosyl-L-homocysteine nucleosidase (SAH nucleosidase) and LuxS [109]. The Hcy is then reacted with Ellman's reagent (5,5'-dithiobis-(2-nitrobenzoic acid), DTNB) to produce 2-nitro-5-thio-benzoate (TNB²⁻), which absorbs strongly at 412 nm. A standard assay mixture contained 50 mM of HEPES, pH 7.5, 1 mg/mL liposome, 1 mM SAM, 2 μM

SAH nucleosidase, and 10 μ M LuxS. Prior to the initiation of the reaction, quench buffer (6 M urea, 0.5 % v/v Triton-X 100, 400 μ M DTNB) was prepared and aliquoted in the wells of Costar clear 96-well plate. The plate was then covered in aluminum foil to prevent photodegradation of DTNB in the quench buffer. The reaction was initiated by adding 5 μ M *P. aeruginosa* CFAS (or 0.5 μ M *E. coli* CFAS) at 37 °C. At 2 min, 5 min and 10 min, 100 μ L aliquots of the reaction mixture were removed, mixed thoroughly with the quench buffer in the 96-well plate, and incubated for 10 min at room temperature. The absorption of the quenched solution was then taken at 412 nm. A control sample containing everything except the liposome was also performed simultaneously with the assay sample using the same method. The absorption of the control sample was subtracted from the assay sample. All measurements were conducted in triplicate.

5.3.5. Steady state kinetic analysis: Steady state kinetic parameters were determined using either 2.5 μ M of *P. aeruginosa* CFAS or 0.25 μ M *E. coli* CFAS and by varying the SAM concentration from 20 to 1000 μ M. At each [SAM], reaction aliquots were collected at 2, 5, and 10 min after addition of CFAS to initiate the reaction. The time points were subjected to linear regression to determine the initial velocity at each [SAM]. To ensure the validity of the steady state assumption, the concentration of [SAM] at the final time point was less than 10% of the total SAM used in the assay. Initial velocities were then plotted as a function of [SAM] and the data were fitted to the Michaelis-Menten equation using non-linear regression in OriginPro software as shown below:

$$v_o = \frac{V_{max}[S]}{K_M + [S]}$$

5.3.6. Cysteine calibration curve: For conversion of the A₄₁₂ readings in our activity assay to Hcy concentrations, we constructed a calibration curve using L-cysteine [141]. To construct the curve, we prepared 100 μ L samples of cysteine solution (0 to 250 μ M) in water in triplicate. These samples were mixed with 100 μ L of quench buffer (6 M urea, 0.5% v/v Triton-X 100, 400 μ M DTNB) in a Costar clear 96-well plate. The absorption of each sample at 412 nm was taken using a microplate reader after 10 min of incubation at room temperature. The absorption was plotted against the concentration of the cysteine

and the data were subjected to linear regression. This linear calibration curve was used to determine the concentration of Hcy in the CFAS assay.

5.3.7. SAH nucleosidase and LuxS activity assay: A standard assay mixture contained 50 mM HEPES, pH 7.5, 1 mg/mL liposome, 200 μ M SAH and 2 μ M SAH nucleosidase. A control assay with everything except SAH nucleosidase was performed alongside the reaction. This pre-mixture was incubated at 37 °C for 10 min to ensure all SAH was converted into S-ribosylhomocysteine (SRH). LuxS (10 μ M) was then added to convert SRH into L-Hcy. At 2 min, 5 min and 10min, 100 μ L of assay mixture was taken out and mixed with 100 μ L of quench buffer. The absorption was read at 412 nm. The absorption of the control sample was subtracted from the assay sample.

5.3.8. Assays to ensure that coupled enzymes are not limiting the CFAS reaction: Additional control experiments were performed to ensure that the activity of the SAH nucleosidase and LuxS coupled enzymes were not limiting the production of Hcy under the derivatization and work-up conditions described in section 5.3.4. The best way to do these experiments is to vary the concentration of SAH nucleosidase and LuxS in the standard CFAS reaction mixture. A standard CFAS reaction was set up containing all components necessary for activity and a saturating amount of SAM (1 mM). In one reaction, 2 μ M of SAH nucleosidase and 10 μ M of LuxS. In the second assay, use 4 μ M SAH nucleosidase and 10 μ M LuxS. In the third reaction, use 2 μ M SAH nucleosidase and 20 μ M LuxS. Data were collected as described in section 5.3.4.

5.4. Hydrogen-Deuterium exchange (HDX) assays:

5.4.1. Standard HDX assays preparation: A standard HDX reaction was performed in 50 mM MOPS, pD 6.1 containing 2 μM of *P. aeruginosa* CFAS at 37 °C. At desired time points, 50 μL of the reaction mixture was mixed with 75 μL of quench buffer containing 100 mM potassium phosphate, 0.8 M GdmHCl, pH 2.1 to reach a final pH meter reading of approximately 2.3. These samples were quickly frozen in liquid nitrogen and stored at -80 °C until ready to analyze with LC-MS. All samples were prepared in triplicate. Reference protein samples were performed following the same method described above with 50 mM MOPS, pH 6.5 or 50 mM HEPES, pH 7.5 in buffer lacking deuterium. For the

HDX reaction performed at pD 7.1, 50 mM HEPES was used and quench buffer pH was adjusted to 1.8. Modification of the quench buffer composition included removal of the GdmHCl, and addition of different concentrations of DDM as described in the Results and Discussion. Aside from these alterations, the HDX reactions were prepared and quenched in an identical manner.

5.4.2. LC-MS conditions for HDX: All samples were analyzed on a Waters Synapt G2-Si instrument. Frozen aliquots (100 µL) were thawed for exactly 70 s and injected into the 40 µL injection loop of the Waters HDX Manager. Exactly 2 min after removal of the aliquot from the -80 °C freezer, the thawed sample was loaded onto an Enzymate pepsin column from Waters™ (300 Å, 5 µm, 2.1 mm x 30 mm) at 15 °C for 3 min. The solvent used was water with 0.1 % formic acid and the flow rate was 100 µL/min. Pepsin is an acid-stable protease which cleaves proteins non-specifically into peptides. These peptides derived from CFAS were then eluted from the pepsin column and trapped onto a C18 guard column at 0.4 °C to minimize back exchange. The peptides were loaded onto a Waters BEH C18 UPLC column (1 x 100 mm) with a flow rate of 40 µL/min and equilibrated in 95 % A (water with 0.1 % formic acid) and 5 % B (ACN with 0.1 % formic acid). The separation was performed with an increasing gradient of B from 5 to 100 % over 10 min. Separated peptides were ionized using the ESI method with a capillary voltage of 2.8 kV, a sampling cone voltage of 30 V, a source offset voltage of 30 V and a desolvation temperature of 175 °C. The mass spectrometer was initially calibrated using 3 mg/mL of Nal in 50:50 v/v water:isopropanol. The mass spectra were collected in positive ion and resolution modes in the range of 100-2000 m/z with 1 scan per second. [Glu-1]fibrinopeptide B (GluFib) was used as an external standard. For HDX sample acquisition, a gas phase separation of peptide ions was also performed using travelling wave ion mobility (TWIM). The following settings were used for TWIM: travelling wave velocity = 650 m/s, wave height = 40 V, IMS bias = 3 V, low trap collision energy = 6 V, high collision energy ramp = 21 to 44 V over 0.4 s. IMS adds another dimension of separation which helps to separate peptides with the same m/z and overlapping C18 elution times. The low energy allows the travelling of peptides as precursor ions, while the high energy fragments them into daughter ions via CID. Alternating between fragmentation and nonfragmentation allows matching of daughter ions to their corresponding precursor ions.

5.4.3. HDX-MS data analysis: Raw MS data obtained for reference samples were first uploaded into ProteinLynx Global Server (PLGS, Waters). This software scans through all the mass spectra and identifies CFAS-derived peptides. PLGS matches the observed m/z of a specific peptide to the expected m/z predicted by *in silico* pepsin digestion of the CFAS protein. Prior to uploading the MS files, a workflow was created to help PLGS score peptides according to pre-set parameters. These settings include the maximum ppm error between the theoretical and observed m/z, the difference in chromatographic retention time and ion mobility drift time of parent and fragment ions, and the number of matched MSMS fragment ions. PLGS output containing the data of all the peptides is then uploaded to DynamX 3.0 (Waters) to further refine the peptide list. Additional parameters filtered out low scoring peptides and allowed only confident peptides to be retained in the list. Peptides needed to be within 5 ppm of the expected m/z, have at least 3 fragment ions and 2 consecutive fragment ions, and they had to be detected in all replicates. Raw MS data for deuterated samples were then uploaded to DynamX 3.0 and the amount of deuterium exchange per peptide was compared to these reference samples.

5.5. Native Mass Spectrometry (native MS):

- **5.5.1. Native MS sample preparation:** An aliquot of the purified enzyme was taken out of the freezer and gently thawed on ice. Buffer exchange was done by using a Micro Bio-Spin 6 column into 200 mM ammonium acetate, pH 7.5 prior to the native MS injection. The process was done by first adding 500 μ L of the 200 mM ammonium acetate buffer to the spin column and centrifuged it at 1 000 x g for 1 min to remove the Tris buffer. This step was repeated three more times to result in >99.9% of buffer exchanged. The enzyme sample (50 μ L) was then applied to the column and centrifuged at 1,000 x g for 4 min to complete the buffer exchange.
- **5.5.2. Native MS conditions:** The buffer exchanged protein (10 μ L) was pipetted into a platinum-coated nanospray emitter (tip diameter was about 1-2 μ m) using an Eppendorf 20 μ L GELoader tip. The emitter was briefly centrifuged to ensure all the liquid was at the tip of the emitter and was assembled onto the ion mobility mass spectrometer equipped with a nanospray ESI source. The ESI source conditions are as follows: capillary voltage

= 1.5 kV, cone voltage = 1 V, source offset = 1 V, source temperature = 35 °C, trap collision energy = 4 V, trap gas flow = 2 mL/min, trap DC bias = 35 V. For ion mobility conditions, IMS gas flow was 90 mL/min, IMS bias was 3 V, IMS wave velocity was 550 m/s, and wave height was 40 V. The equipment was calibrated using 3 mg/mL of NaI in 50:50 v/v water:isopropanol. [Glu-1]-fibrinopeptide B (GluFib) was used as an external standard. Mass spectra were collected in positive ion and sensitivity modes over a range of 100-8000 m/z with a scan rate of 1 s. Raw MS data were deconvoluted to determine the mass of the protein complex using the MaxEnt1 function as described in section 4.2.4.

5.5.3. Native MS data analysis: The native MS data were fitted to determine the solvent accessible area using the established empirical relationship between the charge state distribution and the size of the protein by following this equation [124-126]:

Equation 1:

$$\ln(Z_{avg}) = 0.604 \ln(SA) - 3.285$$

In this equation, SA is the experimental determined surface area of our protein, Z_{avg} is the average number of charges which is determined by calculating the weighted average of the peak areas of the three most abundant charge states of PA-CFAS.

Additionally, we generated an AlphaFold model for the CFAS dimer using default parameters on the Google CoLab server [106, 107]. This AlphaFold model of the CFAS dimer was used to determine the solvent accessible surface area in PyMol using the following commands:

set dot_solvent, on
set dot_density, 4
set solvent_radius, 1.4
get_area PAdimerAlphafold

5.6. Proteomics studies:

5.6.1. Proteomics sample preparation: A 5 mL overnight culture of *P. aeruginosa* (WT or mutants) was used for proteomics studies. Prior to protein extraction, Amicon Ultra -0.5 mL Centrifugal Filter units (30 kDa) and collection tubes were incubated overnight in 250 mL of passivation solution (5 % (v/v) TWEEN-20) with shaking at 170 rpm. On the next day, these filtration units and collection tubes were transferred into a clean container with 500 mL of deionized water and shook for 30 min. This step was repeated once. Cell cultures were centrifuged at 10,000 rpm in non-passivated Eppendorf tubes to remove media. They were washed twice using deionized water and after the final wash, water was discarded, and the cell pellet was used for lysis. Lysis buffer (4 % w/v SDS, 0.2 % w/v deoxycholic acid (DCA), 50 mM TCEP, 100 mM ammonium bicarbonate (ABC), pH 8) (200 µL) was added to each cell pellet for resuspension. This mixture was incubated at 90 °C for 10 min and vortexed occasionally. The lysate was then sonicated for 30 s in three 10 s intervals (17 % intensity, 10 s pulse, 10 s between pulses) and was centrifuged at 14,000 x g to remove cell debris. The supernatant (200 µL) was transferred into a new, non-passivated Eppendorf tube and 500 mM N-ethylmaleimide (NEM) in ethanol was added to a final concentration of 25 mM. The samples were incubated at 37 °C for 1 h with 160 rpm and were quenched by adding 8 µL of 1 M dithiothreitol (DTT) in 100 mM ABC, pH 8.0. The quenched sample (25 µL) was diluted with 200 µL of exchange buffer (8 M urea, 0.2 % w/v DCA, 100 mM ABC, pH 8) and was dispensed onto a passivated filter unit assembled with a non-passivated collection tube. The passivated collection tube was kept for later use. The sample was centrifuged for 10 min at 14,000 x g and the filtrate was discarded. 200 µL of exchange buffer was added to the filter unit and was centrifuged at the same speed and time as previously described. This latter step was repeated twice. Digestion buffer (0.2 % w/v DCA, 50 mM ABC, pH 8) (200 µL) was added to the filter unit and the centrifugation step was repeated. Samples were then washed two additional times with this digestion buffer. After washing, the filter unit was assembled with a passivated collection tube and 100 µL of digestion buffer was added. To cleave proteins into peptides, 1 µL of Promega sequencing grade modified trypsin was mixed with the extracted proteins. The assembled filtration unit was wrapped in parafilm to prevent any evaporation and the proteolytic digestion was performed at 37 °C for 16 h. After the protein digestion was complete, these filtration units were centrifuged, and the filtrate was collected. 50 mM ABC, pH 8 (50 μ L) was added to the filter unit and centrifuged to collect the remaining peptides. This step was repeated once to maximize peptide recovery. DCA was removed by acidification and phase transfer of the peptide sample into ethyl acetate (EA). For this step, EA (200 μ L) was added to the recovered peptides and this mixture was transferred to a 2 mL Eppendorf LoBind tube. Trifluoroacetic acid (TFA) (2.5 μ L) was then added to the mixture and quickly vortexed. 1 mL of EA was added to the acidified sample and sonicated for 10 s at 17 % intensity. After centrifuging at 16,000 x g for 10 min, two phases could be observed, and the upper phase was removed. New EA was added, and the sonication and centrifugation steps were repeated two more times. After the final removal of the upper phase, the samples were allowed to be incubated in the fume hood at 60 °C for 10 min with open lid. This step ensures the complete removal of EA. The aqueous phase was flash frozen with liquid nitrogen and lyophilized.

5.6.2. LC-MS conditions for proteomics: Lyophilized samples were resuspended in 100 μ L of 96.8% water, 3% ACN and 0.2% formic acid. Precipitate was removed by centrifuging at 13,000 rpm for 2 min. The peptide concentration was measured using a nanodrop and the sample absorption at 280 nm. A total of 10 μ g of peptide was loaded on a Waters Acquity UPLC BEH C18 column (130 Å, 1.7 μ m, 2.1 mm x 50 mm) for separation. The column was pre-equilibrated in 95 % A (0.1% formic acid) and 5 % B (100% ACN, 0.1% formic acid) with a flow rate of 50 μ L/min. Peptides were eluted with the following gradient: 5-35 % B over 60 min, 35-85 % B over 2 min and were held at 85 % B for 5 min. The column was re-equilibrated with 85-5 % B over 2 min and held at 5 % B for 10 min. The MS data was collected in positive ion and resolution modes for 60 min. The capillary voltage was 2.8 kV, source temperature was 80 °C, Sampling Cone and Source offset were both 30, desolvation temperature was 175 °C, cone gas flow was 50 L/h and desolvation gas flow was 400 L/h. IMS was also used for proteomics with the following settings to ensure better separation of this complex peptide mixture: wave velocity = 1000 m/s, wave height = 40 V.

5.6.3. Proteomics data processing and analysis: Raw MS data obtained for proteomics samples were uploaded to PLGS and the data were searched for tryptic peptides using the proteome of *P. aeruginosa* strain PAO1 as the library. The general workflow is similar to section 5.4.3. For relative quantitation of proteomic data, protein abundance was assumed to be proportional to the sum of the top three most intense parent peptide ions matched to that protein. This parameter is provided as output for each detected protein by the PLGS software. To perform statistically significant comparisons, only proteins that were detected in all three replicates in both WT and cfa KO mutants were analyzed. Using excel "VLOOKUP" function, proteins that were existed in all samples could be found and the ones that didn't exist in all samples were rejected. The intensity data were transformed to the Log₂ scale and the average and standard deviation of the Log₂ value was calculated for each protein. The fold change was then calculated by subtracting the Log₂ score of the KO strain from the WT strain. Significant differences were then determined using a heteroscedastic, two-tailed t-test as implemented by the T.TEST function in Excel. A Log₁₀ p-value of 2.5 was used as a cutoff for identifying significant protein changes. A volcano plot was graphed by using the Log₂ fold change on the x-axis and Log₁₀ p-value on the y-axis.

5.7. Lipidomics studies:

5.7.1. Preparation of Fatty acid methyl esters (FAMEs): *P. aeruginosa* (WT or mutants) overnight culture (5 mL) was pelleted and freeze-dried. A mixture of 20:1 methanol:acetyl chloride was prepared with caution. Methanol was first added to a glass vial and kept on ice. Acetyl chloride was added dropwise to the methanol until the ratio was reached. Dried cell pellet was transferred to a 10 mL glass vial. A mixture methanol:acetyl chloride (2 mL) and hexane (1 mL) were added to each vial. Samples were heated at 100 °C for 10 min and a single phase should be observed. Mixtures were allowed to cool to room temperature and 2 mL of Milli-Q water and 2 mL of hexane were added sequentially. This step allowed the formation of two phases. The upper hexane phase containing the FAMEs were collected and dried under nitrogen stream. Dried FAMEs were kept in -20 °C.

- 5.7.2. GC-MS conditions for FAMEs analysis and data processing: FAMEs were resuspended into 100 μ L of hexane. A small volume of this sample (1 μ L) was injected to SCION single quad GC-MS instrument equipped with a HP-5MS column (30 m x 0.25 mm x 0.25 μ m) with the following oven conditions: 80 °C for 1 min, 20 °C /min over 6.5 min followed by ramping at 10 °C /min to reach 300 °C. Transfer line temperature was 250 °C and EI source temperature was 200 °C. The MS data was collected in the range of 45 to 800 Da. After identifying each FAME species by matching its fragmentation pattern to the theoretical mass spectrum, the chromatograms were exported and uploaded into Origin software. The area under each FAME peak was determined and the relative abundance was calculated.
- **5.7.3.** Lipid extraction and preparation for lipidomics studies: Lipid extraction was done as described in section 5.3.2. After the lipid film was extracted and dried, it was redissolved in 1 mL of solvent A (60 % ACN, 40 % 10 mM ammonium formate, 0.1% formic acid) and 20 μ L of lipid sample was used for LC-MS injections.
- 5.7.4. LC-MS conditions for lipidomics analysis and data processing: The Acquity UPLC CSH C18 1.7 µm column was pre-equilibrated in 100 % A (0.1% formic acid in water) with a flow rate of 50 µL/min and pre-heated to 50 °C. Lipids were eluted with the following gradient: 0-62 % B (88 % isopropanol, 8 % ACN, 4 % 10 mM ammonium formate, 0.1 % formic acid) over 3 min, 62-70 % B over 5 min and held at 70 % B for 5 min, 70-89 % B over 2 min and held at 89 % B for 6 min, 89-100 % B over 1 min and held for 6 min. The column was re-equilibrated with 100-0 % B over 1 min and held for 6 min. The MS data was collected in positive ion sensitivity mode for 35 min. The capillary voltage was 2.0 kV, source temperature was 120 °C, Sampling Cone was 30 V and Source offset was 50 V, desolvation temperature was 400 °C, cone gas flow was 50 L/h and desolvation gas flow was 600 L/h. For ion mobility conditions, IMS gas flow was 90 mL/min, IMS bias was 3 V, IMS wave velocity was 600 m/s, and wave height was 40 V. The QuanLynx module of MassLynx software (Waters) was used to analyze and quantify the lipidomic data. First, a list of PA lipids was created as the input for the search F1 [121]. The raw data were searched with tolerance windows of 0.02 Da for m/z and 2 min for retention time. The software then ran though MS data of each sample and extracted the

corresponding chromatogram for each lipid. The integrated peak areas for each lipid were manually checked and altered if necessary. The corrected ion peak areas were then used for relative quantitation of lipid abundance.

6.0. References:

- 1. Kerr, K.G. and A.M. Snelling, *Pseudomonas aeruginosa: a formidable and ever-present adversary.* J Hosp Infect, 2009. **73**(4): p. 338-44.
- 2. Jacob, J.S. and J. Tschen, *Hot Tub-Associated Pseudomonas Folliculitis: A Case Report and Review of Host Risk Factors.* Cureus, 2020. **12**(9): p. e10623.
- 3. Laghmouche, N., et al., Successful treatment of Pseudomonas aeruginosa osteomyelitis with antibiotic monotherapy of limited duration. J Infect, 2017. **75**(3): p. 198-206.
- 4. Ramírez-Estrada, S., B. Borgatta, and J. Rello, *Pseudomonas aeruginosa ventilator-associated pneumonia management*. Infect Drug Resist, 2016. **9**: p. 7-18.
- 5. Cole, S.J., et al., *Catheter-associated urinary tract infection by Pseudomonas aeruginosa is mediated by exopolysaccharide-independent biofilms.* Infect Immun, 2014. **82**(5): p. 2048-58.
- 6. Kollef, M.H., et al., *Global prospective epidemiologic and surveillance study of ventilator-associated pneumonia due to Pseudomonas aeruginosa*. Crit Care Med, 2014. **42**(10): p. 2178-87.
- 7. Rello, J., et al., Evaluation of outcome for intubated patients with pneumonia due to Pseudomonas aeruginosa. Clin Infect Dis, 1996. **23**(5): p. 973-8.
- 8. Micek, S.T., et al., *An international multicenter retrospective study of Pseudomonas aeruginosa nosocomial pneumonia: impact of multidrug resistance.* Crit Care, 2015. **19**(1): p. 219.
- 9. World Health, O., Guidelines for the prevention and control of carbapenem-resistant Enterobacteriaceae, Acinetobacter baumannii and Pseudomonas aeruginosa in health care facilities. 2017, Geneva: World Health Organization.
- 10. Flemming, H.-C. and S. Wuertz, *Bacteria and archaea on Earth and their abundance in biofilms*. Nature Reviews Microbiology, 2019. **17**(4): p. 247-260.
- 11. Costerton, J.W., P.S. Stewart, and E.P. Greenberg, *Bacterial Biofilms: A Common Cause of Persistent Infections*. Science, 1999. **284**(5418): p. 1318-1322.
- 12. Donlan, R.M., Biofilms: microbial life on surfaces. Emerg Infect Dis, 2002. 8(9): p. 881-90.
- 13. Sauer, K., et al., *Pseudomonas aeruginosa displays multiple phenotypes during development as a biofilm.* J Bacteriol, 2002. **184**(4): p. 1140-54.
- de Kievit, T.R., et al., *Role of the Pseudomonas aeruginosa las and rhl quorum-sensing systems in rhll regulation.* FEMS Microbiology Letters, 2002. **212**(1): p. 101-106.
- 15. Miller, M.B. and B.L. Bassler, *Quorum sensing in bacteria*. Annu Rev Microbiol, 2001. **55**: p. 165-99.
- 16. Davies, D.G., et al., *The Involvement of Cell-to-Cell Signals in the Development of a Bacterial Biofilm.* Science, 1998. **280**(5361): p. 295-298.
- 17. Sauer, K., et al., *The biofilm life cycle: expanding the conceptual model of biofilm formation*. Nature Reviews Microbiology, 2022. **20**(10): p. 608-620.
- 18. Chang, C.S. and C.Y. Kao, *Current understanding of the gut microbiota shaping mechanisms*. J Biomed Sci, 2019. **26**(1): p. 59.
- 19. Prieto-Barajas, C.M., E. Valencia-Cantero, and G. Santoyo, *Microbial mat ecosystems: Structure types, functional diversity, and biotechnological application.* Electronic Journal of Biotechnology, 2018. **31**: p. 48-56.
- 20. Bjarnsholt, T., et al., *Pseudomonas aeruginosa biofilms in the respiratory tract of cystic fibrosis patients.* Pediatr Pulmonol, 2009. **44**(6): p. 547-58.
- 21. Hall-Stoodley, L. and P. Stoodley, *Biofilm formation and dispersal and the transmission of human pathogens*. Trends Microbiol, 2005. **13**(1): p. 7-10.
- 22. Kragh, K.N., et al., *The Inoculation Method Could Impact the Outcome of Microbiological Experiments*. Applied and Environmental Microbiology, 2018. **84**(5): p. e02264-17.

- 23. Gilbertie, J.M., et al., Equine or porcine synovial fluid as a novel ex vivo model for the study of bacterial free-floating biofilms that form in human joint infections. PLoS One, 2019. **14**(8): p. e0221012.
- 24. Secor, P.R., et al., Entropically driven aggregation of bacteria by host polymers promotes antibiotic tolerance in Pseudomonas aeruginosa. Proc Natl Acad Sci U S A, 2018. **115**(42): p. 10780-10785.
- 25. Dorken, G., et al., *Aggregation by depletion attraction in cultures of bacteria producing exopolysaccharide.* J R Soc Interface, 2012. **9**(77): p. 3490-502.
- 26. Dastgheyb, S., et al., *Effect of biofilms on recalcitrance of staphylococcal joint infection to antibiotic treatment.* J Infect Dis, 2015. **211**(4): p. 641-50.
- 27. Maurice, N.M., B. Bedi, and R.T. Sadikot, *Pseudomonas aeruginosa Biofilms: Host Response and Clinical Implications in Lung Infections*. Am J Respir Cell Mol Biol, 2018. **58**(4): p. 428-439.
- 28. Mulcahy, L.R., V.M. Isabella, and K. Lewis, *Pseudomonas aeruginosa biofilms in disease*. Microb Ecol, 2014. **68**(1): p. 1-12.
- 29. Reygaert, W.C., *An overview of the antimicrobial resistance mechanisms of bacteria*. AIMS Microbiol, 2018. **4**(3): p. 482-501.
- 30. Eng, R.H., et al., *Bactericidal effects of antibiotics on slowly growing and nongrowing bacteria*. Antimicrob Agents Chemother, 1991. **35**(9): p. 1824-8.
- 31. Conlon, B.P., et al., *Persister formation in Staphylococcus aureus is associated with ATP depletion.* Nat Microbiol, 2016. **1**: p. 16051.
- 32. Stewart, P.S., et al., *Contribution of stress responses to antibiotic tolerance in Pseudomonas aeruginosa biofilms*. Antimicrob Agents Chemother, 2015. **59**(7): p. 3838-47.
- 33. Gefen, O., et al., *TDtest: easy detection of bacterial tolerance and persistence in clinical isolates by a modified disk-diffusion assay.* Sci Rep, 2017. **7**: p. 41284.
- 34. Levin-Reisman, I., et al., *Epistasis between antibiotic tolerance, persistence, and resistance mutations.* Proceedings of the National Academy of Sciences, 2019. **116**(29): p. 14734-14739.
- 35. Stewart, P.S. and M.J. Franklin, *Physiological heterogeneity in biofilms*. Nat Rev Microbiol, 2008. **6**(3): p. 199-210.
- 36. Nguyen, D., et al., *Active starvation responses mediate antibiotic tolerance in biofilms and nutrient-limited bacteria*. Science, 2011. **334**(6058): p. 982-6.
- 37. Martins, D., et al., Superoxide dismutase activity confers (p)ppGpp-mediated antibiotic tolerance to stationary-phase <i>Pseudomonas aeruginosa</i>. Proceedings of the National Academy of Sciences, 2018. 115(39): p. 9797-9802.
- 38. Häussler, S. and T. Becker, *The pseudomonas quinolone signal (PQS) balances life and death in Pseudomonas aeruginosa populations.* PLoS Pathog, 2008. **4**(9): p. e1000166.
- 39. Martins, D., et al., Sublethal Paraquat Confers Multidrug Tolerance in Pseudomonas aeruginosa by Inducing Superoxide Dismutase Activity and Lowering Envelope Permeability. Front Microbiol, 2020. **11**: p. 576708.
- 40. Anderl, J.N., M.J. Franklin, and P.S. Stewart, *Role of antibiotic penetration limitation in Klebsiella pneumoniae biofilm resistance to ampicillin and ciprofloxacin.* Antimicrob Agents Chemother, 2000. **44**(7): p. 1818-24.
- 41. Levin-Reisman, I., et al., *Antibiotic tolerance facilitates the evolution of resistance.* Science, 2017. **355**(6327): p. 826-830.
- 42. Raetz, C.R. and W. Dowhan, *Biosynthesis and function of phospholipids in Escherichia coli.* J Biol Chem, 1990. **265**(3): p. 1235-8.
- 43. Joseleau-Petit, D., et al., *Unstable Escherichia coli L forms revisited: growth requires peptidoglycan synthesis.* J Bacteriol, 2007. **189**(18): p. 6512-20.
- 44. Typas, A., et al., From the regulation of peptidoglycan synthesis to bacterial growth and morphology. Nat Rev Microbiol, 2011. **10**(2): p. 123-36.

- 45. Vollmer, W., D. Blanot, and M.A. de Pedro, *Peptidoglycan structure and architecture*. FEMS Microbiol Rev, 2008. **32**(2): p. 149-67.
- 46. Silhavy, T.J., D. Kahne, and S. Walker, *The bacterial cell envelope*. Cold Spring Harb Perspect Biol, 2010. **2**(5): p. a000414.
- 47. Brown, L., et al., *Through the wall: extracellular vesicles in Gram-positive bacteria, mycobacteria and fungi.* Nature Reviews Microbiology, 2015. **13**(10): p. 620-630.
- 48. Mazgaeen, L. and P. Gurung, *Recent Advances in Lipopolysaccharide Recognition Systems*. International Journal of Molecular Sciences, 2020. **21**(2): p. 379.
- 49. Mathelié-Guinlet, M., et al., *Lipoprotein Lpp regulates the mechanical properties of the E. coli cell envelope.* Nature Communications, 2020. **11**(1): p. 1789.
- 50. Fadl, A.A., et al., *Murein lipoprotein is a critical outer membrane component involved in Salmonella enterica serovar typhimurium systemic infection.* Infect Immun, 2005. **73**(2): p. 1081-96.
- 51. Cowan, S.W., et al., *Crystal structures explain functional properties of two E. coli porins.* Nature, 1992. **358**(6389): p. 727-33.
- 52. Benz, R., A. Schmid, and R.E. Hancock, *Ion selectivity of gram-negative bacterial porins*. J Bacteriol, 1985. **162**(2): p. 722-7.
- 53. Masi, M., et al., *Mechanisms of envelope permeability and antibiotic influx and efflux in Gramnegative bacteria*. Nature Microbiology, 2017. **2**(3): p. 17001.
- 54. Arora, A., et al., *Refolded Outer Membrane Protein A of Escherichia coliForms Ion Channels with Two Conductance States in Planar Lipid Bilayers**. Journal of Biological Chemistry, 2000. **275**(3): p. 1594-1600.
- 55. Du, D., et al., *Structure, mechanism and cooperation of bacterial multidrug transporters*. Curr Opin Struct Biol, 2015. **33**: p. 76-91.
- 56. Li, X.Z., P. Plésiat, and H. Nikaido, *The challenge of efflux-mediated antibiotic resistance in Gram-negative bacteria*. Clin Microbiol Rev, 2015. **28**(2): p. 337-418.
- 57. Nikaido, H. and Y. Takatsuka, *Mechanisms of RND multidrug efflux pumps*. Biochimica et Biophysica Acta (BBA) Proteins and Proteomics, 2009. **1794**(5): p. 769-781.
- 58. Chevalier, S., et al., *Structure, function and regulation of Pseudomonas aeruginosa porins.* FEMS Microbiol Rev, 2017. **41**(5): p. 698-722.
- 59. Huang, H. and R.E. Hancock, *Genetic definition of the substrate selectivity of outer membrane porin protein OprD of Pseudomonas aeruginosa*. J Bacteriol, 1993. **175**(24): p. 7793-800.
- 60. Richardot, C., et al., *Carbapenem resistance in cystic fibrosis strains of Pseudomonas aeruginosa as a result of amino acid substitutions in porin OprD.* Int J Antimicrob Agents, 2015. **45**(5): p. 529-32.
- 61. Biswas, S., et al., *Structural insight into OprD substrate specificity*. Nature Structural & Molecular Biology, 2007. **14**(11): p. 1108-1109.
- 62. Rawling, E.G., F.S. Brinkman, and R.E. Hancock, *Roles of the carboxy-terminal half of Pseudomonas aeruginosa major outer membrane protein OprF in cell shape, growth in low-osmolarity medium, and peptidoglycan association.* J Bacteriol, 1998. **180**(14): p. 3556-62.
- 63. Cassin, E.K. and B.S. Tseng, *Pushing beyond the Envelope: the Potential Roles of OprF in <i>Pseudomonas aeruginosa</i> Biofilm Formation and Pathogenicity*. Journal of Bacteriology, 2019. **201**(18): p. e00050-19.
- 64. Bouffartigues, E., et al., *The absence of the Pseudomonas aeruginosa OprF protein leads to increased biofilm formation through variation in c-di-GMP level.* Front Microbiol, 2015. **6**: p. 630.
- 65. Yoon, S.S., et al., *Pseudomonas aeruginosa anaerobic respiration in biofilms: relationships to cystic fibrosis pathogenesis.* Dev Cell, 2002. **3**(4): p. 593-603.
- 66. Fito-Boncompte, L., et al., *Full virulence of Pseudomonas aeruginosa requires OprF.* Infect Immun, 2011. **79**(3): p. 1176-86.

- 67. Nestorovich, E.M., et al., *Pseudomonas aeruginosa porin OprF: properties of the channel.* J Biol Chem, 2006. **281**(24): p. 16230-7.
- 68. Bellido, F., et al., Reevaluation, using intact cells, of the exclusion limit and role of porin OprF in Pseudomonas aeruginosa outer membrane permeability. J Bacteriol, 1992. **174**(16): p. 5196-203.
- 69. Jaouen, T., et al., *Pore size dependence on growth temperature is a common characteristic of the major outer membrane protein OprF in psychrotrophic and mesophilic Pseudomonas species.* Appl Environ Microbiol, 2004. **70**(11): p. 6665-9.
- 70. Klein, S., et al., Adaptation of Pseudomonas aeruginosa to various conditions includes tRNA-dependent formation of alanyl-phosphatidylglycerol. Mol Microbiol, 2009. **71**(3): p. 551-65.
- 71. Staubitz, P., et al., MprF-mediated biosynthesis of lysylphosphatidylglycerol, an important determinant in staphylococcal defensin resistance. FEMS Microbiology Letters, 2004. **231**(1): p. 67-71.
- 72. Cronan, J.E., *Phospholipid modifications in bacteria*. Current Opinion in Microbiology, 2002. **5**(2): p. 202-205.
- 73. Schweizer, H.P. and K.-H. Choi, *Pseudomonas aeruginosa aerobic fatty acid desaturase DesB is important for virulence factor production.* Archives of Microbiology, 2011. **193**(3): p. 227-234.
- 74. Aguilar, P.S. and D. De Mendoza, *Control of fatty acid desaturation: a mechanism conserved from bacteria to humans.* Molecular Microbiology, 2006. **62**(6): p. 1507-1514.
- 75. Zhu, K., et al., *Two aerobic pathways for the formation of unsaturated fatty acids in Pseudomonas aeruginosa*. Molecular Microbiology, 2006. **60**(2): p. 260-273.
- 76. Keweloh, H. and H.J. Heipieper, *Trans unsaturated fatty acids in bacteria.* Lipids, 1996. **31**(2): p. 129-137.
- 77. Heipieper, H.J., et al., *Effect of Environmental Factors on the trans/cis Ratio of Unsaturated Fatty Acids in Pseudomonas putida S12.* Applied and Environmental Microbiology, 1996. **62**(8): p. 2773-2777.
- 78. Benamara, H., et al., *Impact of the biofilm mode of growth on the inner membrane phospholipid composition and lipid domains in Pseudomonas aeruginosa*. Biochimica et Biophysica Acta (BBA) Biomembranes, 2011. **1808**(1): p. 98-105.
- 79. Benamara, H., et al., Characterization of membrane lipidome changes in Pseudomonas aeruginosa during biofilm growth on glass wool. PLoS One, 2014. **9**(9): p. e108478.
- 80. Le Sénéchal, C., et al., *Phospholipid Content of Pseudomonas aeruginosa PAO1 Is Modulated by the Growth Phase Rather Than the Immobilization State.* Lipids, 2019. **54**(9): p. 519-529.
- 81. Le Sénéchal, C., et al., Analysis of the Phospholipid Profile of the Collection Strain PAO1 and Clinical Isolates of Pseudomonas aeruginosa in Relation to Their Attachment Capacity. Int J Mol Sci, 2021. **22**(8).
- 82. Chang, Y.-Y. and J.E. Cronan, *Membrane cyclopropane fatty acid content is a major factor in acid resistance of Escherichia coli.* Molecular Microbiology, 1999. **33**(2): p. 249-259.
- 83. Wang, A.-Y. and J.E. Cronan Jr, The growth phase-dependent synthesis of cyclopropane fatty acids in Escherichia coli is the result of an RpoS(KatF)-dependent promoter plus enzyme instability. Molecular Microbiology, 1994. **11**(6): p. 1009-1017.
- 84. Storvik, K.A. and P.L. Foster, *RpoS, the stress response sigma factor, plays a dual role in the regulation of Escherichia coli's error-prone DNA polymerase IV.* J Bacteriol, 2010. **192**(14): p. 3639-44
- 85. Atkinson, G.C., T. Tenson, and V. Hauryliuk, *The RelA/SpoT homolog (RSH) superfamily:* distribution and functional evolution of ppGpp synthetases and hydrolases across the tree of life. PLoS One, 2011. **6**(8): p. e23479.

- 86. Bianco, C.M., K.S. Fröhlich, and C.K. Vanderpool, *Bacterial Cyclopropane Fatty Acid Synthase mRNA Is Targeted by Activating and Repressing Small RNAs*. Journal of Bacteriology, 2019. **201**(19): p. e00461-19.
- 87. Shrivastava, R. and S.S. Chng, *Lipid trafficking across the Gram-negative cell envelope.* J Biol Chem, 2019. **294**(39): p. 14175-14184.
- 88. Okuda, S., et al., *Lipopolysaccharide transport and assembly at the outer membrane: the PEZ model.* Nat Rev Microbiol, 2016. **14**(6): p. 337-45.
- 89. Okuda, S. and H. Tokuda, Lipoprotein sorting in bacteria. Annu Rev Microbiol, 2011. 65: p. 239-59.
- 90. Shrivastava, R., X. Jiang, and S.S. Chng, *Outer membrane lipid homeostasis via retrograde phospholipid transport in Escherichia coli*. Mol Microbiol, 2017. **106**(3): p. 395-408.
- 91. Chong, Z.S., W.F. Woo, and S.S. Chng, *Osmoporin OmpC forms a complex with MlaA to maintain outer membrane lipid asymmetry in Escherichia coli*. Mol Microbiol, 2015. **98**(6): p. 1133-46.
- 92. Shabala, L. and T. Ross, Cyclopropane fatty acids improve Escherichia coli survival in acidified minimal media by reducing membrane permeability to H+ and enhanced ability to extrude H+. Research in Microbiology, 2008. **159**(6): p. 458-461.
- 93. Pini, C.V., et al., *Cyclopropane fatty acids are involved in organic solvent tolerance but not in acid stress resistance in Pseudomonas putida DOT-T1E.* Microb Biotechnol, 2009. **2**(2): p. 253-61.
- 94. Jiang, X., et al., *The Cyclopropane Fatty Acid Synthase Mediates Antibiotic Resistance and Gastric Colonization of Helicobacter pylori.* J Bacteriol, 2019. **201**(20).
- 95. Karlinsey, J.E., et al., *Cyclopropane Fatty Acids Are Important for Salmonella enterica Serovar Typhimurium Virulence*. Infect Immun, 2022. **90**(1): p. e0047921.
- 96. Grogan, D.W. and J.E. Cronan, Jr., *Cyclopropane ring formation in membrane lipids of bacteria*. Microbiol Mol Biol Rev, 1997. **61**(4): p. 429-41.
- 97. Tran, T.T., et al., Whole-Genome Analysis of a Daptomycin-Susceptible Enterococcus faecium Strain and Its Daptomycin-Resistant Variant Arising during Therapy. Antimicrobial Agents and Chemotherapy, 2013. **57**(1): p. 261-268.
- 98. Poger, D. and A.E. Mark, *A Ring to Rule Them All: The Effect of Cyclopropane Fatty Acids on the Fluidity of Lipid Bilayers.* The Journal of Physical Chemistry B, 2015. **119**(17): p. 5487-5495.
- 99. Guerard, C., et al., Synthesis and evaluation of analogues of S-adenosyl-L-methionine, as inhibitors of the E. coli cyclopropane fatty acid synthase. Bioorg Med Chem Lett, 2004. **14**(7): p. 1661-4.
- 100. Iwig, D.F., et al., Isotope and elemental effects indicate a rate-limiting methyl transfer as the initial step in the reaction catalyzed by Escherichia coli cyclopropane fatty acid synthase. Biochemistry, 2004. **43**(42): p. 13510-24.
- 101. Guangqi, E., D. Lesage, and O. Ploux, *Insight into the reaction mechanism of the Escherichia coli cyclopropane fatty acid synthase: isotope exchange and kinetic isotope effects.* Biochimie, 2010. **92**(10): p. 1454-7.
- 102. Huang, C.-c., et al., *Crystal Structures of Mycolic Acid Cyclopropane Synthases from Mycobacterium tuberculosis **. Journal of Biological Chemistry, 2002. **277**(13): p. 11559-11569.
- 103. Kozbial, P.Z. and A.R. Mushegian, *Natural history of S-adenosylmethionine-binding proteins*. BMC Struct Biol, 2005. **5**: p. 19.
- 104. Hari, S.B., R.A. Grant, and R.T. Sauer, *Structural and Functional Analysis of E. coli Cyclopropane Fatty Acid Synthase.* Structure, 2018. **26**(9): p. 1251-1258 e3.
- 105. Ma, Y., C. Pan, and Q. Wang, *Crystal structure of bacterial cyclopropane-fatty-acyl-phospholipid synthase with phospholipid.* The Journal of Biochemistry, 2019. **166**(2): p. 139-147.
- 106. Evans, R., et al., *Protein complex prediction with AlphaFold-Multimer.* bioRxiv, 2021: p. 2021.10.04.463034.
- 107. Jumper, J., et al., *Highly accurate protein structure prediction with AlphaFold.* Nature, 2021. **596**(7873): p. 583-589.

- 108. Reva, B.A., A.V. Finkelstein, and J. Skolnick, *What is the probability of a chance prediction of a protein structure with an rmsd of 6 A?* Fold Des, 1998. **3**(2): p. 141-7.
- 109. Guianvarc'h, D., et al., *Identification of new inhibitors of E. coli cyclopropane fatty acid synthase using a colorimetric assay.* Biochim Biophys Acta, 2006. **1764**(8): p. 1381-8.
- 110. Pei, D. and J. Zhu, *Mechanism of action of S-ribosylhomocysteinase (LuxS)*. Curr Opin Chem Biol, 2004. **8**(5): p. 492-7.
- 111. Riener, C.K., G. Kada, and H.J. Gruber, *Quick measurement of protein sulfhydryls with Ellman's reagent and with 4,4'-dithiodipyridine.* Analytical and Bioanalytical Chemistry, 2002. **373**(4): p. 266-276.
- 112. Courtois, F., et al., *Escherichia coli cyclopropane fatty acid synthase*. Eur J Biochem, 2004. **271**(23-24): p. 4769-78.
- 113. Arce-Rodriguez, A., et al., *Non-invasive, ratiometric determination of intracellular pH in Pseudomonas species using a novel genetically encoded indicator.* Microb Biotechnol, 2019. **12**(4): p. 799-813.
- 114. Tsui, F.C., D.M. Ojcius, and W.L. Hubbell, *The intrinsic pKa values for phosphatidylserine and phosphatidylethanolamine in phosphatidylcholine host bilayers*. Biophys J, 1986. **49**(2): p. 459-68.
- 115. Bligh, E.G. and W.J. Dyer, *A rapid method of total lipid extraction and purification*. Can J Biochem Physiol, 1959. **37**(8): p. 911-7.
- 116. Ranjith Kumar, R., P. Hanumantha Rao, and M. Arumugam, *Lipid Extraction Methods from Microalgae: A Comprehensive Review.* Frontiers in Energy Research, 2015. **2**.
- 117. Ferreira, C.M.H., et al., (Un)suitability of the use of pH buffers in biological, biochemical and environmental studies and their interaction with metal ions a review. RSC Advances, 2015. **5**(39): p. 30989-31003.
- 118. Iwig, D.F., et al., *The activity of Escherichia coli cyclopropane fatty acid synthase depends on the presence of bicarbonate.* J Am Chem Soc, 2005. **127**(33): p. 11612-3.
- 119. Park, C. and R.T. Raines, *Quantitative Analysis of the Effect of Salt Concentration on Enzymatic Catalysis*. Journal of the American Chemical Society, 2001. **123**(46): p. 11472-11479.
- 120. Epstein, W., *The Roles and Regulation of Potassium in Bacteria*, in *Progress in Nucleic Acid Research and Molecular Biology*. 2003, Academic Press. p. 293-320.
- 121. Deschamps, E., et al., *Determination of the collision cross sections of cardiolipins and phospholipids from Pseudomonas aeruginosa by traveling wave ion mobility spectrometry-mass spectrometry using a novel correction strategy.* Anal Bioanal Chem, 2019. **411**(30): p. 8123-8131.
- Tamara, S., M.A. den Boer, and A.J.R. Heck, *High-Resolution Native Mass Spectrometry*. Chem Rev, 2022. **122**(8): p. 7269-7326.
- 123. Weerasinghe, N.W., et al., *Exploring the Conformational Landscape of a Lanthipeptide Synthetase Using Native Mass Spectrometry*. Biochemistry, 2021. **60**(19): p. 1506-1519.
- 124. Kaltashov, I.A. and A. Mohimen, *Estimates of protein surface areas in solution by electrospray ionization mass spectrometry*. Anal Chem, 2005. **77**(16): p. 5370-9.
- 125. Hall, Z. and C.V. Robinson, *Do charge state signatures guarantee protein conformations?* J Am Soc Mass Spectrom, 2012. **23**(7): p. 1161-8.
- 126. Li, J., et al., *Conformational effects in protein electrospray-ionization mass spectrometry*. Mass Spectrometry Reviews, 2016. **35**(1): p. 111-122.
- 127. Acharya, K.R. and M.D. Lloyd, *The advantages and limitations of protein crystal structures.* Trends Pharmacol Sci, 2005. **26**(1): p. 10-4.
- 128. Swaminathan, G.J., et al., *Crystal structures of oligomeric forms of the IP-10/CXCL10 chemokine.* Structure, 2003. **11**(5): p. 521-32.
- 129. Smith, D.L., Y. Deng, and Z. Zhang, *Probing the non-covalent structure of proteins by amide hydrogen exchange and mass spectrometry.* J Mass Spectrom, 1997. **32**(2): p. 135-46.

- 130. Marcsisin, S.R. and J.R. Engen, *Hydrogen exchange mass spectrometry: what is it and what can it tell us?* Anal Bioanal Chem, 2010. **397**(3): p. 967-72.
- 131. Habibi, Y., et al., *Insights into the Dynamic Structural Properties of a Lanthipeptide Synthetase using Hydrogen–Deuterium Exchange Mass Spectrometry.* Journal of the American Chemical Society, 2019. **141**(37): p. 14661-14672.
- 132. Li, J., et al., *Hydrogen-deuterium exchange and mass spectrometry reveal the pH-dependent conformational changes of diphtheria toxin T domain.* Biochemistry, 2014. **53**(43): p. 6849-56.
- 133. O'Brien, D.P., et al., *Hydrogen/Deuterium Exchange Mass Spectrometry for the Structural Analysis of Detergent-Solubilized Membrane Proteins*. Methods Mol Biol, 2020. **2127**: p. 339-358.
- 134. Adhikary, S., et al., *Conformational dynamics of a neurotransmitter:sodium symporter in a lipid bilayer*. Proceedings of the National Academy of Sciences, 2017. **114**(10): p. E1786-E1795.
- 135. Erde, J., R.R.O. Loo, and J.A. Loo, *Enhanced FASP (eFASP) to Increase Proteome Coverage and Sample Recovery for Quantitative Proteomic Experiments*. Journal of Proteome Research, 2014. **13**(4): p. 1885-1895.
- 136. Arhin, A. and C. Boucher, *The outer membrane protein OprQ and adherence of Pseudomonas aeruginosa to human fibronectin.* Microbiology, 2010. **156**(5): p. 1415-1423.
- 137. Uwate, M., et al., Two routes of MexS-MexT-mediated regulation of MexEF-OprN and MexAB-OprM efflux pump expression in Pseudomonas aeruginosa. Microbiology and Immunology, 2013. **57**(4): p. 263-272.
- 138. Grøftehauge, M.K., et al., Crystal Structure of a Hidden Protein, YcaC, a Putative Cysteine Hydrolase from Pseudomonas aeruginosa, with and without an Acrylamide Adduct. Int J Mol Sci, 2015. **16**(7): p. 15971-84.
- 139. Damron, F.H., et al., Lipotoxin F of Pseudomonas aeruginosa is an AlgU-dependent and alginate-independent outer membrane protein involved in resistance to oxidative stress and adhesion to A549 human lung epithelia. Microbiology (Reading), 2009. **155**(Pt 4): p. 1028-1038.
- 140. Chao, J., G.M. Wolfaardt, and M.T. Arts, *Characterization of Pseudomonas aeruginosa fatty acid profiles in biofilms and batch planktonic cultures.* Can J Microbiol, 2010. **56**(12): p. 1028-39.
- 141. Park, S.H., et al., Simple and Novel Assay of the Host-Guest Complexation of Homocysteine with Cucurbit[7]uril. J Microbiol Biotechnol, 2019. **29**(1): p. 114-126.